NASA CR-111952

OPTIMUM RADARS AND FILTERS FOR THE PASSIVE SPHERE SYSTEM

James K. Luers
Charles D. MacArthur
University of Dayton Research Institute

With an Appendix on
Radar Analysis of the AN/FPS-16 Tracking a
Falling Sphere by

Aaron Soltes
Raytheon Company

Prepared by
University of Dayton Research Institute
Dayton, Ohio

for NASA Langley Research Center
Under NASA Contract NASI-10329

NASA CR-111952

OPTIMUM RADARS AND FILTERS FOR THE PASSIVE SPHERE SYSTEM

James K. Luers

Charles D. MacArthur

University of Dayton Research Institute

With an Appendix on

Radar Analysis of the AN/FPS-16 Tracking a

Falling Sphere by

Aaron Soltes

Raytheon Company

Prepared by

University of Dayton Research Institute

Dayton, Ohio

for NASA Langley Research Center

Under NASA Contract NASI-10329

ABSTRACT

Studies have been conducted to determine the influence of the tracking radar and data reduction technique on the accuracy of the meteorological measurements made in the 30 to 100 kilometer altitude region by the ROBIN passive falling sphere. A survey of accuracy requirements was made of agencies interested in data from this region of the atmosphere. In light of these requirements, various types of radars were evaluated to determine the tracking system most applicable to the ROBIN, and methods were developed to compute the errors in winds and density that arise from noise errors in the radar supplied data. The effects of launch conditions on the measurements were also examined. Conclusions and recommendations have been made concerning the optimum tracking and data reduction techniques for the ROBIN falling sphere system.

TABLE OF CONTENTS

LIST OF FIGURES

LIST OF TABLES

LIST OF SYMBOLS

Symbol	Definition
x	Downrange position coordinate in the rectangular coordinate system.
y	Crossrange position coordinate in the rectangular coordinate system.
z	Vertical position coordinate in the rectangular coordinate system.
$\dot{x}, \dot{y}, \dot{z}$	Components of velocity in the rectangular coordinate system.
$\ddot{x}, \ddot{y}, \ddot{z}$	Components of acceleration in the rectangular coordinate system.
R	Slant range position coordinate in the spherical coordinate system.
E	Elevation angle position coordinate in the spherical coordinate system.
A	Azimuth angle position coordinate in the spherical coordinate system.
$\dot{R}, \dot{E}, \dot{A}$	Components of velocity in the spherical coordinate system.
$\ddot{R}, \ddot{E}, \ddot{A}$	Components of acceleration in the spherical coordinate system.
$\delta x, \delta y, \delta z$	An increment of error in x, y, z.
$\delta R, \delta E, \delta A$	An increment of error in R, E, A.
$\sigma_x, \sigma_y, \sigma_z$	RMS error in x, y, z.
$\sigma_{\dot{x}}, \sigma_{\dot{y}}, \sigma_{\dot{z}}$	RMS error in $\dot{x}, \dot{y}, \dot{z}$.

$\sigma_{\ddot{x}}, \sigma_{\ddot{y}}, \sigma_{\ddot{z}}$	RMS error in $\ddot{x}$, $\ddot{y}$, $\ddot{z}$.
$\sigma_R, \sigma_E, \sigma_A$	RMS error in R, E, A.
$\sigma_{\dot{R}}, \sigma_{\dot{E}}, \sigma_{\dot{A}}$	RMS error in $\dot{R}$, $\dot{E}$, $\dot{A}$.
$\sigma_{\ddot{R}}, \sigma_{\ddot{E}}, \sigma_{\ddot{A}}$	RMS error in $\ddot{R}$, $\ddot{E}$, $\ddot{A}$.
$\sigma_{\dot{R}}^*$	RMS error in $\dot{R}$ obtained from Slant Range Radar.
$\sigma_R^*, \sigma_E^*, \sigma_A^*$	RMS error in Smoothed R, E, A.
$E[q]$	The expected value of the quantity q.
ρ_{ij}	Correlation coefficient between errors in velocity obtained in the slant range radar smoothing technique.
$\Phi_{ij}(\dot{q})$	Correlation factor arising from correlated errors in the quantity q in the range-rate radar smoothing technique.
$\sigma_{\dot{R}_{sr}}$	RMS error in $\dot{R}$ as measured by a slant range radar.
$\dot{R}_D$	Measurement of $\dot{R}$ from a range-rate radar.
$\dot{R}_D^*$	Average value of $\dot{R}_D$ over a given number of points.
$\sigma_{\dot{R}_D}$	RMS error in $\dot{R}_D$.
Q	A number of points over which various quantities are averaged.
ω	Frequency (Hz).
$g(\omega, N), f(\omega, N)$	Frequency response functions.
W_x, W_y	Wind speed in the x and y directions.
σ_{Wx}, σ_{Wy}	RMS error in wind speed in the x and y directions.

ρ	Density.
σ_ρ	RMS error in density.
V	Velocity.
$\{\delta x_r\}$	A set of r errors in the quantity x.
$[M], [N], [P], [Q]$	The matrices "M", "N", "P", "Q".
$[M^2], [N^2]$, etc.	The matrices "M^2", "N^2", "P^2", "Q^2".
r_i	A measurement of a quantity r.
r_i^t	The true value of r_i.
δr_i	An error in the measurement of r_i.
K_1, K_2	Constants.
C	A constant, also the cost rating of a radar.
Δt	The spacing between successive radar data points.
Δt_2	Time spacing between successive computed velocity points.
N	The number of points in the position smoothing interval.
M	The number of points in the velocity smoothing interval.
k, L	Orders of smoothing polynomials.
S	Slide = number of old points discarded and new points acquired in moving a filter ahead in time.
$P_k(i)$	k^{th} order Legendre polynomial in i.
$P_k'(i)$	First derivative of k^{th} order Legendre polynomial in i.
$P_k''(i)$	Second derivative of k^{th} order Legendre polynomial in i.

a_i, b_i	Weighting factors used in the Legendre polynomial fitting.

INTRODUCTION

The passive falling sphere technique of acquiring winds, density, pressure, and temperature from the radar track of a falling sphere has the potential of being a reliable, low-cost system for measuring these meteorological parameters to altitudes of 100 kilometers. There are, however, operational and theoretical problems which remain to be solved before the system becomes an accurate and reliable operational tool for all users. One area of concern is that of the tracking radar. Most all passive sphere flights today are being tracked with the FPS-16 radar. Satisfactory density and wind measurements above 70 kilometers can only be achieved with a high precision radar such as the FPS-16. The purpose of this study is to determine the interrelationships that exist between radar tracking characteristics and wind and density accuracy. Implied in this statement are questions concerning what is the best type radar (slant range, Doppler, accelerometer, gyros, etc.) for tracking passive spheres; is each type economically feasible; will it satisfy the user's needs for wind and density accuracy; under what launch conditions (launch azimuth, elevation, and wind direction) tracking is most desirable; and what filter or filters provide the required accuracies. These are the questions that have been addressed by UDRI in this study contract.

Early in the study it became obvious that only two types of radar were economically feasible - the standard slant range, elevation angle and azimuth angle radar and the Doppler, slant range, elevation angle, azimuth

angle radar. For convenience of notation, throughout this report the first type radar is referred to as a slant range radar, and the second type as a Doppler or range-rate radar. The accuracy requirements of a slant range radar to provide accurate wind and density measurements to 100 kilometers are of the order of those achieved with the present FPS-16 radar. Thus, the study essentially concentrated on the FPS-16 slant range radar and a range-rate radar that would provide commensurate accuracy.

SURVEY OF USER REQUIREMENTS

The University of Dayton Research Institute, in inaugurating the radar filter error study program, undertook a survey of user requirements for wind, density, temperature, and pressure accuracy between 30 and 100 kilometers. It was felt that the study of radar error and filters should be geared toward achieving the accuracies required by those who use the system. By knowing present and future accuracy requirements, combinations of radar accuracies and filters could be determined that satisfy these requirements.

The survey taken by the University consisted of contacting various Governmental agencies where it was believed that requirements would exist for meteorological parameters at altitudes to 100 kilometers. The agencies contacted were NASA, AFCRL, the U.S. Army, and ESSA. A letter was sent to representatives of each agency. The letter requested the requirements of the agency regarding the steady state errors, bias errors, and wavelength structure of the four meteorological parameters wind, density, pressure, and temperature in the altitude range from 30 kilometers to 100 kilometers. Response to the survey was discouraging. Not all agencies responded, and those which did failed to reveal any specific accuracy requirements if such requirements do exist. Consensus of the responders was that there are few programs that demand specific accuracies in meteorological parameters, particularly above 60 kilometers. Application of meteorological parameters

to specific programs such as Apollo, Space Shuttle, etc., is generally limited to altitudes below 60 kilometers and is presently being collected with the required accuracies by operational systems. The need for accurate data above 60 kilometers is most important to the research man studying the structure of the atmosphere.

The researcher desires his data as accurate as possible, but seldom can justify making a statement concerning how accurate his data need be to be useful. In the future, however, the need for accurate meteorological data to prove, disclaim, or hypothesize atmospheric structure theories will increase and may be used to justify accuracy requirement statements of an agency.

An alternate source of agency requirement information is contained in the document "Federal Plan for Upper Air Observation Above 30 Kilometers" (Ref. 1). The document quotes accuracy requirements of meteorological parameters for the AEC, DOC, DOD, and NASA. A common Federal accuracy requirement is also specified which consists of a meshing of the various agency requirements. The requirements stated in this document give a quantitative statement about errror magnitude with no corresponding statement concerning wave structure requirements. Furthermore, justification for the stated accuracy requirements is not satisfactorily explained in the document. Nevertheless, since this is the only source of quantitative accuracy requirements available to UDRI, the common Federal Data Requirement Table as extracted from that document (Table 1) has been used as a general guideline for the radar-filter error study.

TABLE 1. COMMON FEDERAL DATA REQUIREMENTS

Parameter (30 - 100 km)	Accuracy	Firing Frequency
1. Density	(5%)*	237-580/yr
2. Wind	(5mps, 10^{o} direction)	237-580/yr
3. Temperature	(3^{o} C.)	237-580/yr
4. Pressure	(5%)*	237-580/yr

*Tolerances stated are within an estimated 2 sigma.

EVALUATION OF TYPES OF RADAR

To determine the meteorological parameters of wind, density, temperature, and pressure, it is critical to be able to accurately measure the acceleration and velocity of the sphere. The position of the sphere is important only insofar as assigning an altitude to the point where the meteorological measurements are made. It is velocity, and of even more importance, acceleration, that requires precise accuracy - particularly above 70 kilometers. The natural question is: what type radar will best measure velocity and accleration. With a standard spherical coordinate (range, elevation, azimuth) radar, velocities and accelerations are obtained by numerical differentiation of the spherical coordinates. It is worth investigating whether other types of radars that directly measure velocity and acceleration could provide more accurate meteorological data, and if so, at what relative expense can these radars be obtained. Mr. Aaron Soltes of Raytheon was asked by UDRI to act as a radar consultant in order to provide an answer to this question. A questionnaire which requested a cost ranking of different type radar measurements of several specified accuracies was submitted to Mr. Soltes. The accuracies specified were to be maintained under geometric conditions typical of an 80^{o} launch, 125-kilometer apogee ROBIN trajectory. The type radar measurements considered were:

a) Range measurement
b) Range-rate by Doppler
c) Azimuth and elevation angles

d) $\dot{A}$ and $\dot{E}$ by gyros and otherwise

e) $\ddot{A}$ and $\ddot{E}$ by accelerometers and otherwise

The accuracies specified by UDRI were those that were estimated to provide density and wind errors of the magnitude outlined in the Federal Accuracy Requirements (Table 1). Table 2 shows the cost ratings and time constants produced by Soltes. The time constant, as described by Soltes, "...is the observation time over which individual measurements are averaged." The cost rating column is based on a 1-10 scale with "1" representing the cheapest radar components. An FPS-16 radar would rate about in the middle at "5". Some entries in Table 2 are subject to constraints and proper interpretation which Soltes points out in comments about each type component.

Slant Range. --Soltes comments that the sharp rise in cost rating in going from five-meter to one-meter accuracy is because of a variety of residual errors that are close to their irreducible ultimate limits.

Range-Rate.--Soltes comments that the accuracy and longest allowable time constant for Doppler frequency measurements are dependent upon the R.F. wavelength used by the radar. The requirements of direct, simultaneous, unambiguous measurements of slant range and Doppler may or may not be compatible, depending upon the maximum magnitudes of R and $\dot{R}$ that must be measured and upon the R.F. wavelength.

Azimuth and elevation (A and E). --"The cost and time constant ratings shown are for electro-mechanically steered antennas. The 0.1-milliradian accuracy requirement is achieved with 'Cadillac-quality'

TABLE 2

Matrix of Cost Ratings and Time Constants

vs

Type of Measurement

Type Measurement	Accuracy RMS	Cost Rating (1-10)				Time Constant (seconds)	
2. Slant Range	1 meter	10				0.1	
	5 meter	3				0.1	
	15 meter	1				0.1	
3. Range Rate (Doppler)	1/3 met/sec	4				0.1	
	1 met/sec	3				0.1	
	5 met/sec	2				0.1	
4. Azimuth (A) and Elevation (E)	.1 mils	5				0.1	
	.5 mils	3				0.1	
	1.0 mils	2				0.1	
		Servo	Gyro	Servo	Gyro		
5. $\dot{A}$ and $\dot{E}$ (Gyros) or otherwise	.005 mils/sec	10	10	10	1		
	.01 mils/sec	10	10	4	0.1		
	.1 mils/sec	5	10	0.3	0.1		
	.5 mils/sec	2		0.1			
	1.0 mils/sec	1		0.1			
6. $\ddot{A}$ and $\ddot{E}$ (accelero-meters) or otherwise	.001 mils/sec^2	?				?	
	.01 mils/sec^2	?				?	
	.1 mils/sec^2	?				?	
	.5 mils/sec^2	10				?	
	1.0 mils/sec^2	5				?	

mechanical components and is close to the best that has been claimed to date (0.05-milliradians). To maintain 0.1-milliradian rated accuracy in the field requires meticulous attention to and corrections for a variety of error sources including solar heating, dynamic deflections, target dynamics, etc., and frequent calibration and boresighting."

$\dot{A}$ and $\dot{E}$. --$\dot{A}$ and $\dot{E}$ can be measured by several methods. The two for which cost ratings and time constants are given are for the angle velocity data derived from angle tracking servo and rate gyros. These types appear most practical for the falling sphere technique. The angle tracking servo method may be the simplest, but it requires sufficiently fine-grain angle position data. The rate gyros yield a direct analog output that is more accurate, but very complex "care and feeding" of the gyros is required.

$\ddot{A}$ and $\ddot{E}$. --Soltes comments: the inability of an electromechanically steered antenna to move smoothly while it follows a target creates even more noise in the second derivative of its motion than in the first derivative that is not related to true target motion. Consequently, unless a large time constant can be tolerated, it is self-defeating to attempt to measure $\ddot{A}$ and $\ddot{E}$ directly to the higher accuracies cited in Table 2.

In order to apply the results of Table 2 to a projected radar design, Soltes was asked whether there are any constraints inherent in designing a radar that consists of a combination of the different type measurement components. For example, is it feasible to design a radar with gyros to measure $\dot{A}$ and $\dot{E}$, and a Doppler to measure $\dot{R}$. Soltes' reply is summarized

as follows: the constraints on angular and radial measurements are generally either independent or compatible. Constraints on slant range and Doppler measurements may or may not be directly compatible. If they are not directly compatible, they can be made compatible at some additional expense.

A final question asked of Soltes was "What improvement in the time constant or accuracy can be achieved by a) having a real-time knowledge of an average trajectory of the sphere and b) or programming the radar to anticipate the trajectory of the sphere?" Soltes' answer to part (a) is that an average trajectory is of no value because individual trajectories probably differ too greatly from each other. Soltes answered part (b) as follows: "predicting the motion of a particular sphere in real time from its own past history is definitely useful and the name of the radar tracking game. How much real time computing can be accomplished within the allotted time constant may well determine how accurately the target tracking mechanism can estimate the true target motion from the noise-corrupted radar measurements."

The UDRI has used the answers and other information supplied by Soltes in an effort to determine what is the best and most economical type of radar to be used for tracking the ROBIN sphere. The next section discusses the evaluation of each type radar and the conclusions reached by UDRI.

Comparative Evaluation of Radar Types

The best tracking radar consists of the combination of type components that have the lowest cost rating and will produce the desired accuracy and wave structure in density and winds. The FPS-16 radar is the radar generally used for tracking passive spheres. It is available at all ranges and therefore can be used as a guide to determine if a proposed radar, or radar component, would improve upon accuracy, or be less costly than that presently attained with the FPS-16 radar.

The first analysis of Table 2 consisted of determining whether slant range or Doppler radars had a better cost rating in providing a specified accuracy in $\dot{R}$, and under what conditions each was better. A specifed accuracy consists of an RMS error and a frequency response. Thus, in order for the $\dot{R}$ obtained from differentiating the slant range measurement to have the same accuracy as the $\dot{R}$ from the Doppler, two things are necessary:

1) they must have the same RMS error in $\dot{R}$, and

2) they must have the same frequency response, i.e., the wave structure retained in each $\dot{R}$ measurement is identical.

Consequently, the technique used to compare the slant range and Doppler components is the following:

Given a slant range radar of RMS accuracy $\underline{\sigma_{\dot{x}}}$ m/sec, cost rating of $\underline{C}$, and time constant of $\underline{\Delta t}$ seconds,

a) Define a method of obtaining $\dot{R}$ from the slant range measurement.

b) Determine the RMS error and frequency response of the $\dot{R}$ determined from (a).

c) Define an averaging method to get a smoothed value of $\dot{R}$ from the Doppler measured $\dot{R}$.

d) Find the RMS accuracy of the Doppler radar that will provide, in the smoothed $\dot{R}$, the same RMS error and frequency response as that from the slant range radar (step b).

e) From Table 2, determine the cost rating of the Doppler radar with RMS accuracy specified in step d.

f) Compare cost rating of slant range radar to cost rating of Doppler radar from step e. Since both radars produce the same error and frequency response in $\dot{R}$, the one with the smaller cost rating is the most desirable.

The method of obtaining $\dot{R}$ from the slant range (step a) will be defined as fitting a linear polynomial to N slant range data points and taking the slope as the range velocity at the midpoint of the data. The velocity so defined will be denoted by $\dot{R}_{sr}$. For this differentiating technique, the RMS error in $\dot{R}_{sr}$ and frequency response, step b, are given respectively as:

$$\sigma_{\dot{R}_{sr}} = \left[\frac{12}{N(N^2-1)\Delta t^2} \sigma_R^2 \right]^{1/2} \qquad (1)$$

where

Δt is the time spacing between data points

N is the number of points used in the linear fit

σ_R is the RMS error in slant range - assumed to be normally distributed with mean zero,

and the frequency response as

$$g(\omega, N) = \frac{3}{[\pi(N-1)\Delta t\,\omega]^3} \left\{ \sin[\pi(N-1)\Delta t\,\omega] - \pi(N-1)\Delta t\,\omega \cos[\pi(N-1)\Delta t\,\omega] \right\} \qquad (2)$$

where

ω is the frequency in cycles per second.

The derivation of Equations (1) and (2) can be found in References 2 and 3, respectively.

The method of obtaining a smoothed $\dot{R}$ from the Doppler $\dot{R}$ (step c) is defined as moving averages. That is, Q values of Doppler $\dot{R}$ are averaged and the averaged value of $\dot{R}$ is defined as the smoothed $\dot{R}$ at the midpoint of the data. The Doppler $\dot{R}$ is denoted as $\dot{R}_D$ and the smoothed Doppler $\dot{R}$ as $\dot{R}^*_D$. The RMS error of $\dot{R}^*_D$ (step d) is given as:

$$\sigma_{\dot{R}^*_D} = \frac{\sigma_{\dot{R}_D}}{\sqrt{Q}} \qquad (3)$$

where

Q is the number of Doppler values of $\dot{R}$ averaged, and

$\sigma_{\dot{R}_D}$ is the RMS error in the Doppler $\dot{R}$ - assumed to be normally distributed with mean zero.

The frequency response of $\dot{R}^*_D$ is given as

$$f(\omega, Q) = \frac{1}{Q} \left\{ \frac{\sin (Q \pi \Delta t \, \omega)}{\sin (\pi \Delta t \, \omega)} \right\} \quad . \qquad (4)$$

The derivation of Equation (4) is given in Appendix A. A plot of the two frequency response functions for various values of N and Q, Equations (2) and (4), is shown as Figure 1.

The application of steps (a) through (f) is illustrated by the following example. Consider a slant range radar from Table 2 with RMS accuracy of five meters, cost rating of three, and time constant of 0.1 second. Determine if an equivalent Doppler radar has a higher or lower cost rating.

The RMS error in the $\dot{R}$ from differentiating the slant range is obtained from Equation (1) as:

$$\sigma_{\dot{R}_{sr}} = \left[\frac{30,000}{N(N^2 - 1)} \right]^{1/2} \quad . \qquad (5)$$

The Doppler radar that produces an error in the smoothed Doppler $\dot{R}$, $\dot{R}^*_D$, equivalent to the error in the differentiated $\dot{R}$, $\dot{R}_{sr}$, is determined by equating Equation (5) to Equation (3). That is,

$$\sigma_{\dot{R}_D} = \left[\frac{30,000 \, Q}{N(N^2 - 1)} \right]^{1/2} \quad . \qquad (6)$$

Equation (6) determines the Doppler RMS accuracy required to make $\sigma_{\dot{R}_{sr}} = \sigma_{\dot{R}^*_D}$ for specified values of N and Q.

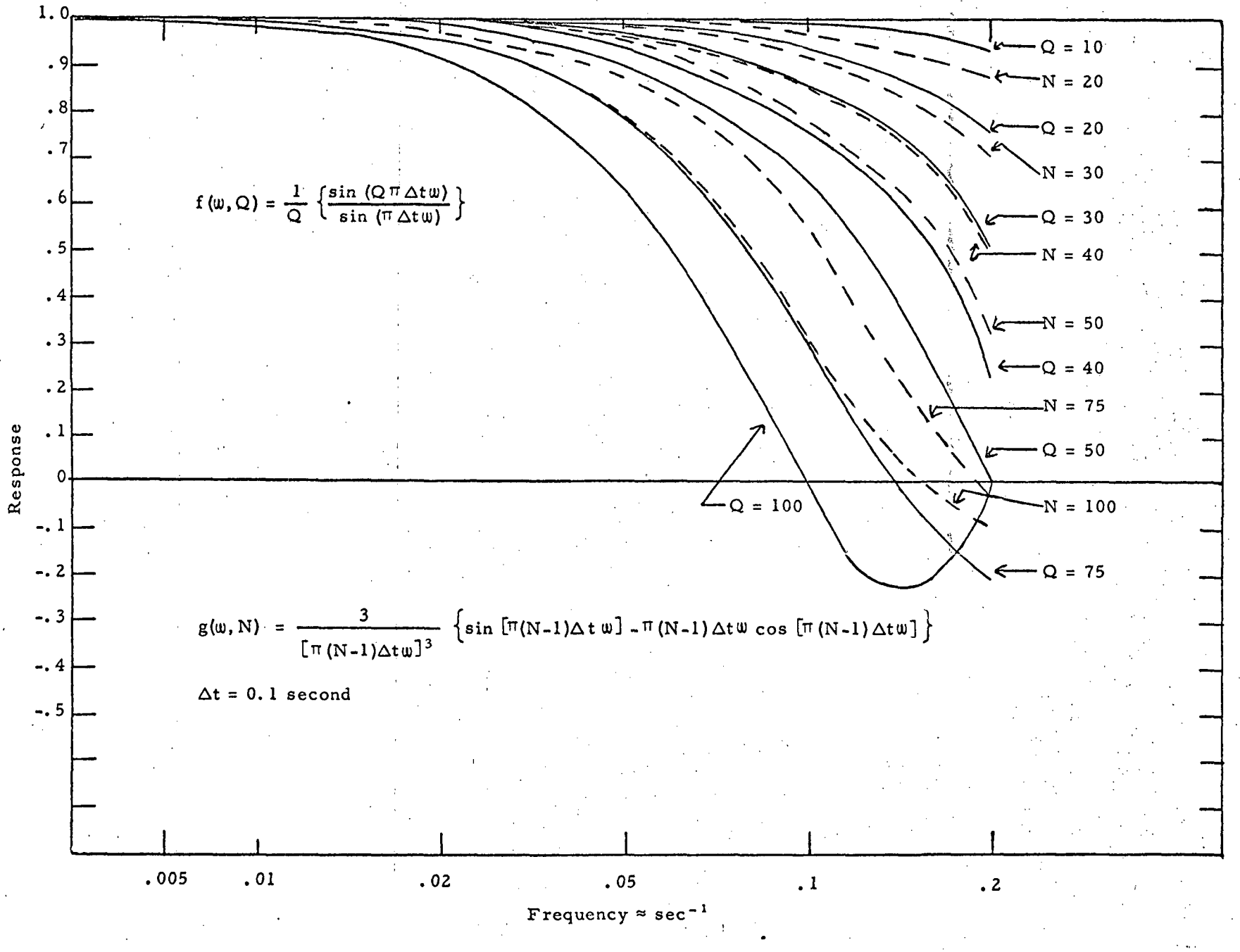

Figure 1. Frequency Response of Averaging and Differentiating Filters.

Since it is also required that the frequency response of $\dot{R}_{sr}$ be the same as the frequency response of $\dot{R}^{*}_{D}$, a constraint will be placed on the relationship that must exist between N and Q.

The two response functions $g(\omega, N)$ and $f(\omega, Q)$ are shown in Figure 1 for various values of N and Q. It is obvious that the two response functions will not be identical over all frequencies, particularly over the higher frequencies. However, when $Q = 3/4N$, it is remarkable how well the two functions agree over the lower frequencies of interest. The response of the two functions differs by less than 2%. When the frequencies are higher, say greater than 0.2, the difference between the two functions is sometimes larger, but this is of little importance since these wavelengths are essentially destroyed by the filters.

A substitution of $Q = 3/4N$ into Equation (6) determines the Doppler RMS accuracy required to make both the RMS errors and frequency response functions equal. That is, $\sigma_{\dot{R}_{sr}} = \sigma_{\dot{R}^{*}_{D}}$ and $g(\omega, N) = f(\omega, Q)$ for $\omega < 0.2$. This substitution yields:

$$\sigma_{\dot{R}_{D}} = \frac{150}{[N^2 - 1]^{1/2}} \tag{7}$$

Equation (7) shows that the Doppler radar equivalent (same RMS and same frequency response) to the specified slant range radar depends upon the number of points, N, used to determine $\dot{R}_{sr}$. The choice of N strongly influences the density and wind accuracy that can be achieved. If N is

chosen too small, for example, a large noise error in density and winds will result which is not indicative of the maximum accuracy in wind and density that could be achieved by choosing the best N. On the other hand, if N is chosen too large, excessive smoothing will result that destroys real oscillations in the data that could otherwise be observed. By considering the present FPS-16 system as a standard, the optimum density accuracy is achieved when N = 91 points. This corresponds to the linear smoothing interval presently used in the High Altitude ROBIN Program.* Substituting N = 91 into Equation (7) gives

$$\sigma_{\dot{R}_D} = 1.65 \text{ m/sec}$$

From Table 2, the cost rating of the Doppler radar with RMS accuracy of 1.65 m/sec is approximately 2.9. To summarize, the following has been accomplished: it has been determined that a Doppler radar with RMS accuracy of 1.65 m/sec is equivalent to a slant range radar with RMS accuracy of five meters and time constant of 0.1 second for N = 91. The cost rating of the Doppler is 2.9 and the slant range radar is 3.0. Consequently, in this case there is a negligible cost advantage of one radar over the other.

The analysis presented in the above example was performed for the slant range radars of the other accuracies specified in Table 2. Table 3 shows the results of this analysis using N = 91 in each case. It should be recalled that an N = 91 represents the smoothing interval used in the

---

*The High Altitude ROBIN Program smooths on 19 one-half second spaced data points. This corresponds to 91 point smoothing of 0.1 second data points.

High Altitude ROBIN Program and as such provides the same frequency response as is presently being operationally achieved. The noise error in $\dot{R}$ resulting from using N = 91 will only be the same as that achieved with the High Altitude Program if the RMS error and time constant of the slant range radar is the same as that of the FPS-16. The noise error in $\dot{R}$ for N = 91 and each accuracy is also given in Table 3.

TABLE 3. FREQUENCY RESPONSE--N FIXED

Time Constant Both Radars	Slant Range Radar			Error in Smoothed Velocity	Equivalent Doppler Radar		
Δt seconds	σ_R meters	N	Cost Rating	$\sigma_{\dot{R}_{sr}} = \sigma_{\dot{R}_D}^*$ m/second	Q	$\sigma_{\dot{R}_D}$ m/sec	Cost Rating
.1	1	91	10	.04	68	.33	4
.1	5	91	3	.20	68	1.65	2.9
.1	15	91	1	.60	68	4.95	2

The results of Table 3 are graphically presented in Figure 2. This figure shows the relative cost ratings of equivalent slant range and Doppler radars. Any point on the curve represents equivalent radars when compared at the frequency response of the ROBIN system. As the curve proceeds to the right, the equivalent radars will provide less noise error in the derived $\dot{R}$. The noise error at which the Doppler radar becomes more economical (crosses the line of equal cost ratings) than the slant range radar is approximately $\sigma_{\dot{R}}$ = 0.20 m/sec. Increasing the accuracy in $\dot{R}$ is relatively insensitive to cost when measured by a range-rate radar, but highly sensitive to cost if measured by a slant range radar. For example, improving the error in $\dot{R}$

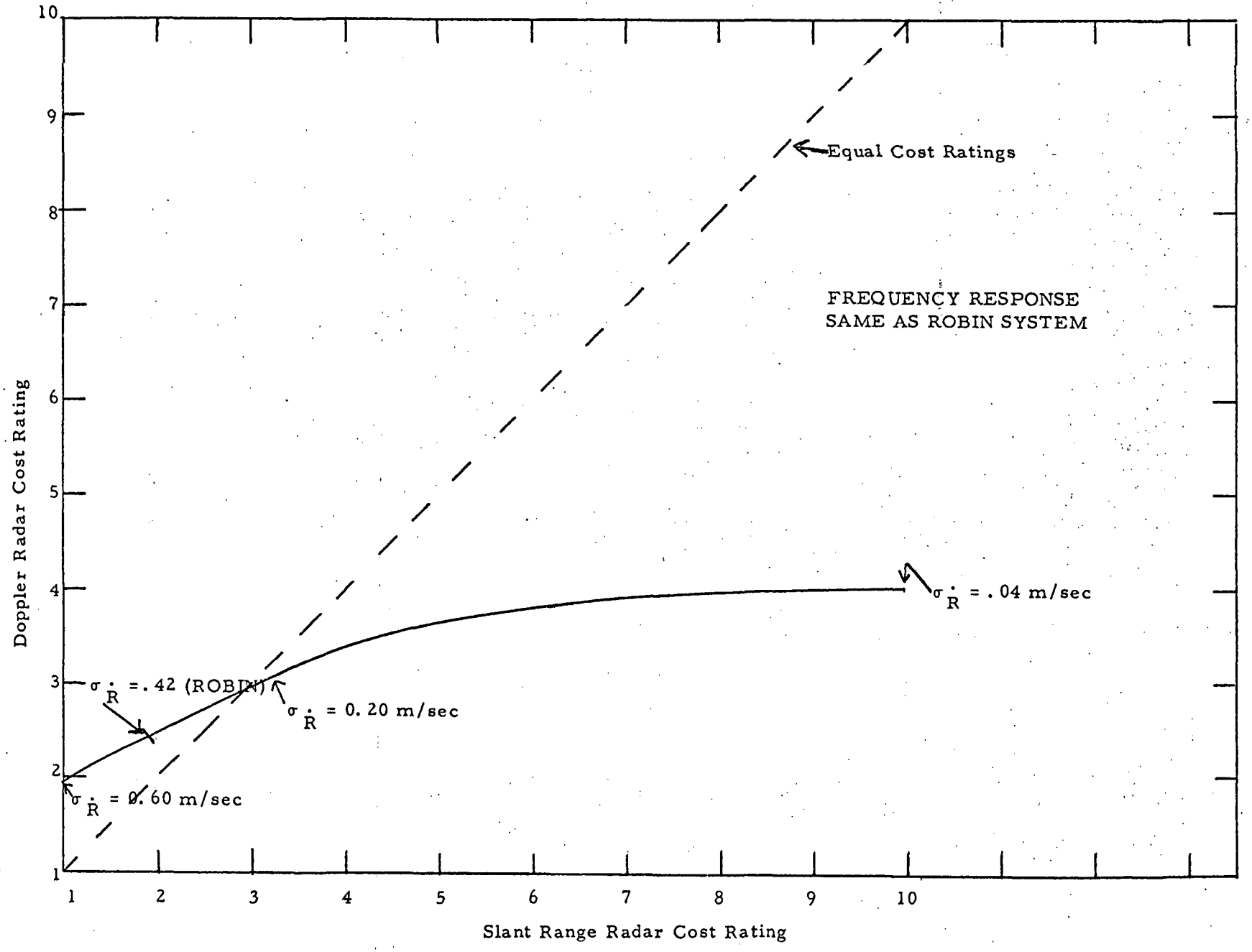

Figure 2. Equivalent Doppler and Slant Range Radars at Fixed Frequency Response.

from $\sigma_{\dot{R}}$ = .2 m/sec to $\sigma_{\dot{R}}$ = .04 m/sec increases the cost rating for a slant range radar from three to ten, but only increases the cost rating for a Doppler radar from three to four. When using the FPS-16 radar and the High Altitude ROBIN Program, the error in $\dot{R}$ is approximately $\sigma_{\dot{R}}$ = 0.42 m/sec. Consequently, from Figure 2, it is seen that to improve upon the accuracy of the present FPS-16 radar, it is more economical to enhance the accuracy of a Doppler rather than that of a slant range radar.

The results of Table 3 and Figure 2 were for a fixed smoothing interval (N = 91) and consequently will all provide the same frequency response in density - that of the High Altitude ROBIN Program. The slant range and Doppler radars can also be compared for a fixed value of the noise error in $\dot{R}$. This fixed value can be chosen as that presently obtained with the FPS-16 radar and the High Altitude ROBIN Program: $\sigma_{\dot{R}}$ = 0.42 meter per second. In this case, the rationale for choosing N is: determine that N which will produce $\sigma_{\dot{R}}$ = 0.42 meter per second. This is easily calculated from Equation (1). Table 4 compares slant range and Doppler radars that provide the noise error presently attained in the High Altitude Program. Figure 3 presents the results of Table 4. For the present ROBIN system the slant range radar has a cost rating of 2.1 and the Doppler radar a rating of 2.7. However, if improved frequency response is needed, Figure 3 shows it is much more economically achieved by a more accurate Doppler radar.

TABLE 4

$\sigma_{\dot{R}}$ = .42 m/sec (High Altitude ROBIN Program)

Time Constant Both Radars	Slant Range Radar			Equivalent Doppler Radar		
Δt seconds	σ_R meters	N	Cost Rating	Q	$\sigma_{\dot{R}_D}$ m/sec	Cost Rating
.1	1	19	10	14	1.6	2.9
.1	5	55	3	41	2.7	2.8
.1	15	114	1	86	3.9	2.5

Comparative evaluation when time constant equals one-half second. -- Since the time constant of 0.1 second is less than that generally achieved by an FPS-16 radar, and furthermore, since actual computation with 0.1 second data is often overwhelming in volume, it is instructive to look at 0.5 second time constant. Cost ratings for this type radar were not available; so we assumed 0.5 second time constant was obtained by averaging five 0.1 second data points. This would in effect decrease the RMS measurement error by a factor of $1/\sqrt{5}$. The comparison was then made between range and range rate radars using the resultant accuracies. Table 5 gives the results which are identical to those of Table 4. This should not be surprising. Averaging of five data points from both a range radar and its equivalent range-rate radar should again provide equivalent accuracies. We conclude from Table 5 only that you can not get something for nothing.

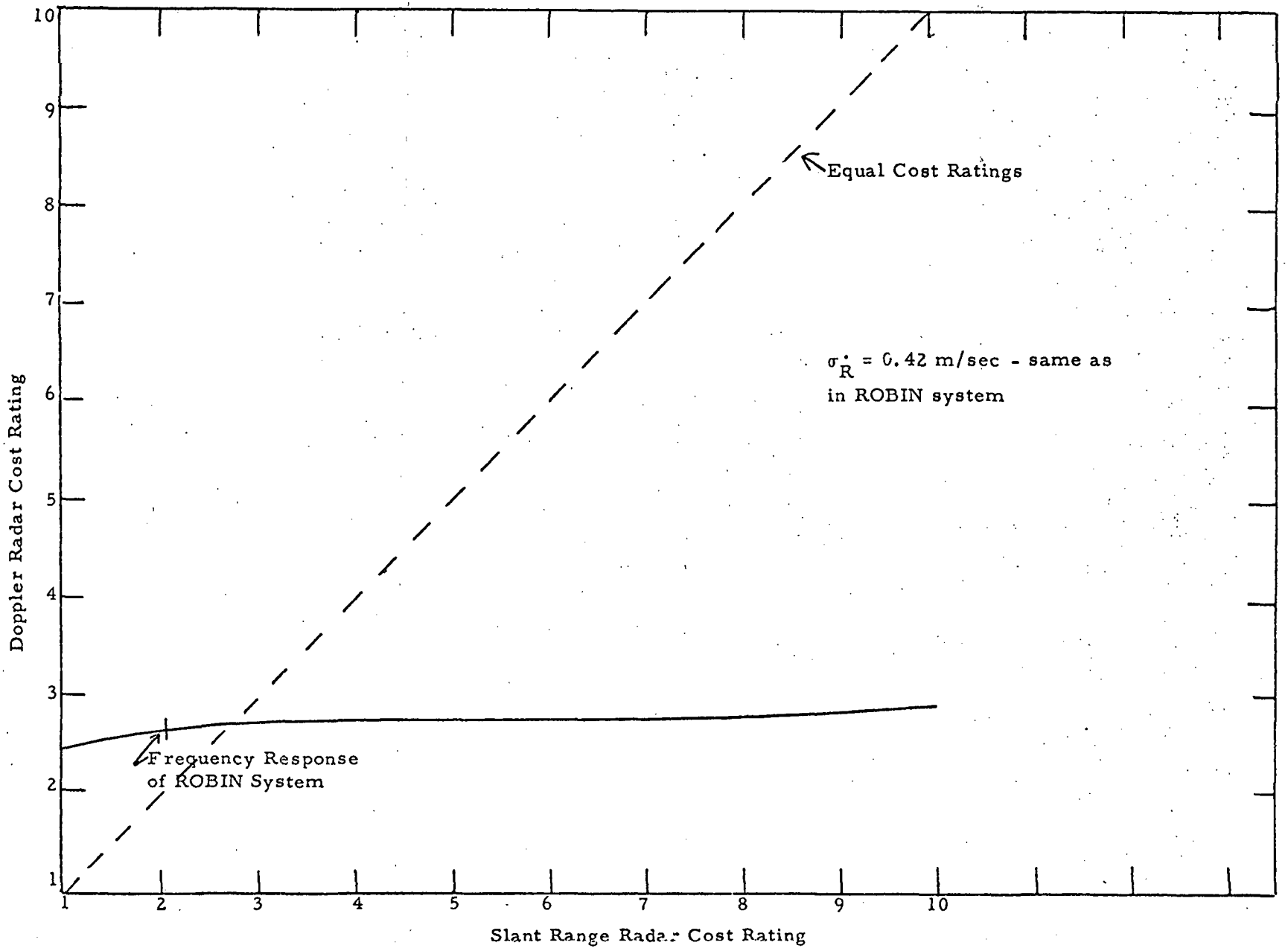

Figure 3. Equivalent Doppler and Slant Range Radars at Fixed Noise Error in $\dot{R}$.

TABLE 5

$\sigma_{\dot{R}}$ = .42 m/sec (High Altitude ROBIN Program)

Time Constant Both Radars	Slant Range Radar			Equivalent Doppler Radar		
Δt seconds	σ_R meters	N	Cost Rating	Q	$\sigma_{\dot{R}_D}$ m/sec	Cost Rating
0.5	$1/\sqrt{5}$	4	10	3	1.6	2.9
0.5	$5/\sqrt{5}$	11	3	8	2.7	2.8
0.5	$15/\sqrt{5}$	23	1	17	3.9	2.5

Comparison of Angular (A and E Radars to Angular Rate ($\dot{A}$ and $\dot{E}$) Radars

The steps (a) through (f), outlined for comparative evaluation of slant range and Doppler radars, are directly applicable to the evaluation of angular and angular rate radars. Angular and angular rate radars were compared at the N value that produced the frequency response of the High Altitude ROBIN Program and also at the various N values that provided the same noise error in $\dot{A}$ and $\dot{E}$ presently achieved with the FPS-16 radar and High Altitude Program. (i.e., $\sigma_{\dot{E}} = \sigma_{\dot{A}} = .0084$ mils/sec.) Tables 6 and 7 show the results which are graphically presented in Figures 4 and 5. Figure 4 shows the comparison at N = 91 which provides the frequency response of the High Altitude Program. Over the entire range of cost ratings the angular measuring radar has a lower (cheaper) cost rating than its equivalent angular rate radar. The difference in cost ratings is con-

TABLE 6
Frequency Response N Fixed

Time Constant Both Radars	Angular Radar			Error in Smoothed Angular Velocity	Equivalent Angular Rate Radar		
Δt seconds	σ_A mils	N	Cost Rating	$\sigma_{\dot{A}_{sr}} = \sigma_{\dot{A}_D}$ mils/sec	Q	$\sigma_{\dot{A}_D}$	Cost Rating
.1	.1	91	5	.0040	68	.033	10 gyro
.1	.5	91	3	.020	68	.165	5 servo
.1	1.0	91	2	.040	68	.330	4 servo
.1	2.0	91	1	.080	68	.660	1.8 servo

TABLE 7

$\sigma_{\dot{A}}$ = .0084 mils/sec

(High Altitude ROBIN Program)

Time Constant Both Radars	Angular Radar			Equivalent Angular Rate Radar		
Δt seconds	σ_A mils	N	Cost Rating	Q	$\sigma_{\dot{A}_D}$ mils/sec	Cost Rating
.1	.1	55	5	41	.054	8 servo
.1	.5	162	3	122	.092	7 servo
.1	1.0	257	2	193	.116	5 servo
.1	2.0	409	1	307	.147	4 servo

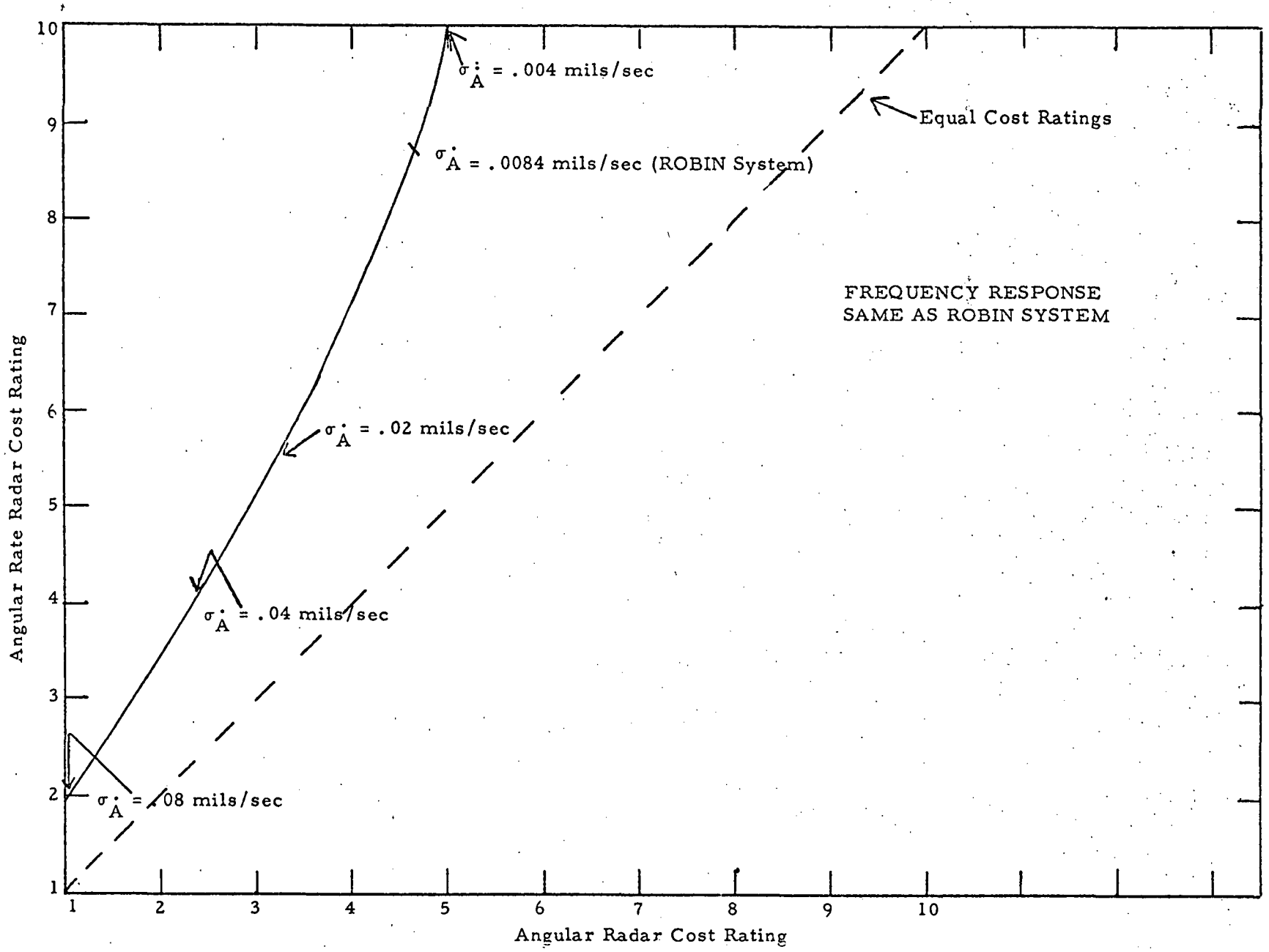

Figure 4. Equivalent Angular and Angular Rate Radars of Fixed Frequency Response.

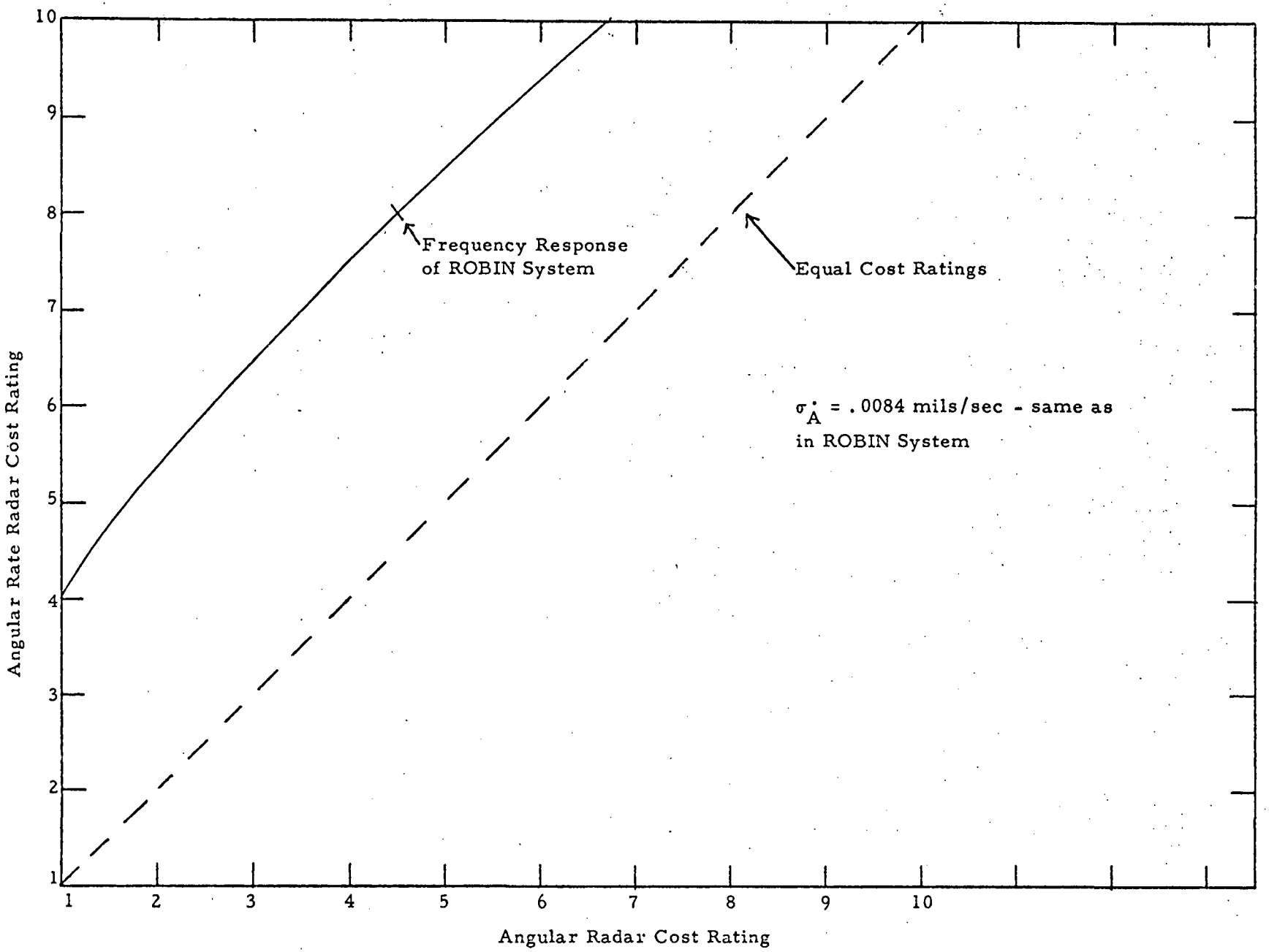

Figure 5. Equivalent Angular and Angular Rate Radars at Fixed Noise Error in $\dot{A}$.

siderable - a factor of approximately two. To achieve the accuracy attained in the High Altitude Program with an angular rate radar would require a cost rating of nearly nine as compared to an angular radar cost rating of less than five. The same results are seen in Figure 5 when the comparisons are based on the same noise error as the ROBIN system. No situation exists when the angular rate radar is superior to the angular radar. Consequently, the UDRI has discarded angular rate radars from further consideration.

Comparative Evaluation of Angular and Angular Acceleration Radars

A simple comparison can be made to show the impracticality of angular acceleration radars. For the ROBIN system the noise error in the angular acceleration is approximately

$$\sigma_{\ddot{A}} = .0015 \text{ mil/sec}^2 .$$

The noise error obtained in acceleration measurements by taking the second derivative of a quadratic fit is

$$\sigma_{\ddot{A}} = \left[\frac{720}{N^5 - 5N^3 + 4N}\right]^{1/2} \frac{\sigma_A}{\Delta t^2} \qquad \text{(Ref. 2)} \qquad (8)$$

The right hand side of Equation (8) will be equal to .0015 mils/sec^2 when $\Delta t = 0.1$, $\sigma_A = .2$ and $N = 171$. The cost rating of such an angular radar with time constant of 0.1 seconds and an RMS accuracy of .2 mils is approximately four. Next one can determine the number of points that must be averaged from an acceleration radar with a cost rating of five

(this rating is given in Table 2) to give the same noise error in acceleration. A cost rating of five corresponds to an RMS acceleration error of 1.0 mils/sec^2. Averaging Q acceleration points reduces the standard deviation of the averaged acceleration by $\sqrt{Q}$ (see Equation 3). That is,

$$\sigma_{\ddot{A}}^{*} = \frac{\sigma_{\ddot{A}}}{\sqrt{Q}} \tag{9}$$

Solving Equation (9) for the Q that makes $\sigma_{\ddot{A}}^{*}$ equal to .0015 mils/sec^2 gives

$$Q = 9628 \text{ points}$$

- obviously a few more than one would care to use. As a result of this investigation, angular acceleration measuring radars have been removed from any further consideration.

Summary

The previous discussions have led to the following results:

a) Doppler radars hold considerable promise of improving accuracy at little cost. Further evaluation of this type radar is warranted.

b) Angular rate radars are considerably more expensive than equivalent angular radars. As a result we have rejected angular rate radars from further consideration.

c) Angular acceleration radars are considerably more expensive than angular radars and can not provide the required accuracy. As a result, we have rejected angular acceleration radars from further consideration.

ERROR ANALYSIS

Error in the determination of winds and density from the ROBIN falling sphere may arise from many sources. The effects of an erroneous drag table, vertical winds, radar noise, smoothing technique, etc., all must be taken into account in estimating the accuracy of the measurements taken. In this chapter we will examine the combined effects of inaccuracy in the radar-generated coordinates (radar noise) and error introduced by the smoothing technique. Two types of radars will be considered: the devices that measure an object's position only and those which measure both position and velocity along the range direction. For brevity, we will call the former "slant range radars" and the latter "range-rate radars". The basic smoothing technique applied to the raw data from both radars is assumed to be smoothing by orthogonal polynomial fitting. A description of this method has been given by Luers (Ref. 1) so that it will be sufficient to say that orthogonal polynomial smoothing has proven to be a most desirable technique for smoothing ROBIN radar data. The majority of the discussion in this chapter will be given to the determination of noise error in the measurements of density and wind speed. Noise error originates in the noisy, unfiltered radar data and is always carried, to some extent, through the smoothing technique to the computation of the final parameters. Bias error, which is a property of the fitting polynomial(s), will also be examined in cases where methods have been devised for its measurement. Noise error and bias error may

be combined as total error in order to evaluate the overall accuracy of a particular smoothing technique.

Spherical and Rectangular Coordinates

The raw radar data of a balloon track consists of the spherical coordinates of the balloon's position: range, elevation angle, and azimuth angle, and in the case of range-rate radars, velocity along the range direction. At some point in the analysis of the radar data, a transformation must be made from the spherical coordinate system to a rectangular coordinate system in order that winds may be represented in a North-East reference frame and density associated with a particular altitude. The question has arisen as to where in the smoothing process is the best point to make this transformation. If the transformation is made on the spherical position data before any smoothing is done (assuming we have a slant range radar) the transformation equations are simple and require only the present set of the three spherical position variables. The transformation is, however, non-linear so that smoothing on the resultant rectangular coordinates could introduce some error due to "misfit" of the smoothing polynomials to the data. This misfit may or may not occur to as great a degree if smoothing were done in the spherical system. Smoothing the spherical data to obtain first velocities and then accelerations followed thereafter by transforming to accelerations in a rectangular system presents problems also. The transformation equations for spherical to rectangular acceleration are very complicated and require knowledge of previous velocities and positions (due to the non-zero

length of the smoothing interval). Identifying and saving all the necessary information to make a proper transformation of accelerations presents a non-trivial bookkeeping problem. In order to determine which method (smoothing before transforming or transforming before smoothing) should be recommended, a comparison of the noise and bias error in the rectangular accelerations computed by each method was made. The comparison was made between acceleration measurements rather than velocity because above 60 kilometers density and winds are primarily determined by acceleration measurements.

Noise error. -- Figure 6 shows the rectangular and spherical coordinate systems used in this comparison and throughout the error analysis. The rectangular system is left-handed with the x-axis positive north and y-axis positive east. The z-axis is positive upward. Range, R, is measured along a line connecting the balloon with the radar site at the origin. (It is also assumed that the rocket is launched from the origin.) Elevation, E, is measured positive counter-clockwise from the x-y plane, and azimuth is measured positive clockwise in the x-y plane from the x-axis. Although corrections for the curvature of the earth are make in the ROBIN program (Ref. 2), a flat-earth approximation is sufficient for noise and bias error analysis.

From Figure 6 it can be seen that the relationship between the spherical coordinates and rectangular coordinates is:

$$\begin{aligned} x &= R \cos E \cos A \\ y &= R \cos E \sin A \\ z &= R \sin E \end{aligned} \qquad (10)$$

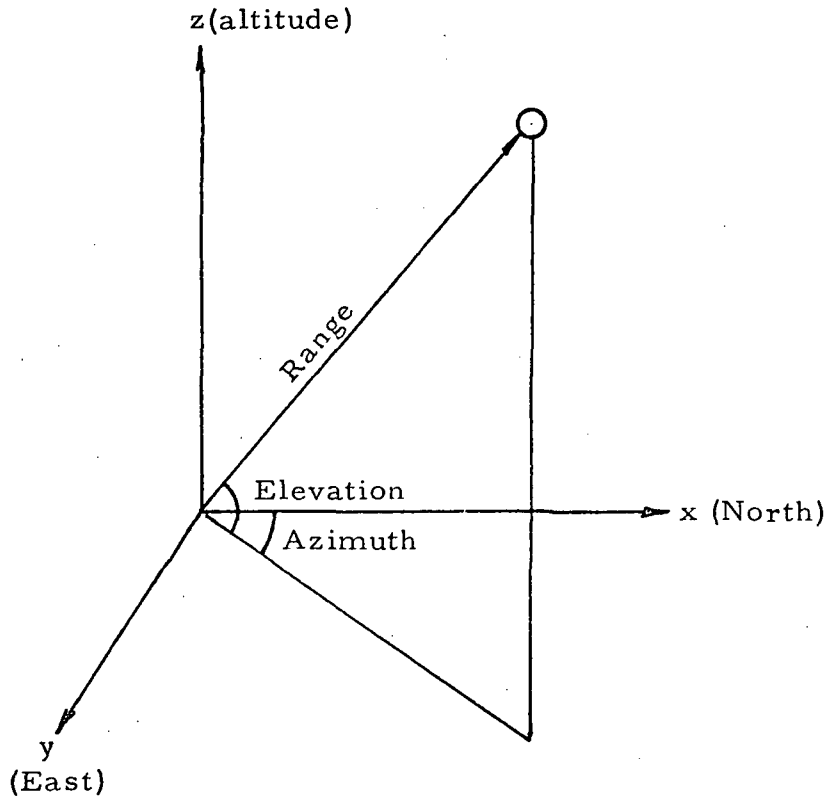

Figure 6: The Rectangular and Spherical Coordinate Systems Used in the ROBIN System.

Equations (10) are applied to the raw radar data to convert each point from R, E, A, to x, y, z representation when smoothing is done on rectangular coordinates. To find the noise error in the rectangular coordinates given the noise error in the spherical coordinates the differential error approximation may be used. Assuming noise errors in range, elevation, and azimuth of δR, δE, and δA, and ignoring second order terms, errors in x, y, and z are given by:

$$\delta x = (\cos E \cos A)\delta R - (R \sin E \cos A)\delta E - (\cos E \sin A)\delta A$$

$$\delta y = (\cos E \sin A)\delta R - (R \sin E \sin A)\delta E + (\cos E \cos A)\delta A$$

$$\delta z = (\sin E)\delta R + (R \cos E)\delta E$$

or, in a more compact notation,

$$\begin{pmatrix} \delta x \\ \delta y \\ \delta z \end{pmatrix} = [M] \begin{pmatrix} \delta R \\ \delta E \\ \delta A \end{pmatrix} \tag{11}$$

where the matrix

$$[M] = \begin{pmatrix} \cos E \cos A & -R \sin E \cos A & -R \cos E \sin A \\ \cos E \sin A & -R \sin E \sin A & R \cos E \cos A \\ \sin E & R \cos E & 0 \end{pmatrix}$$

The error variance, σ^2_i, may be written as

$$\sigma^2_i = E\left[(\delta i - E[\delta i])^2 \right]$$

where $[\delta i]$ denotes the expected value of an error in i. If the noise is truly random in nature, then the expected value of δi should be zero, or

$$\sigma_i^2 = E[(\delta i)^2] \quad .$$

In light of the above, the error variance in x, y, and z may be determined by squaring both sides of Equations (11), which yields:

$$\begin{pmatrix} \delta x^2 \\ \delta y^2 \\ \delta z^2 \end{pmatrix} = \begin{pmatrix} \cos^2 E \cos^2 A & R^2 \sin^2 E \cos^2 A & R^2 \cos^2 E \sin^2 A \\ \cos^2 E \sin^2 A & R^2 \sin^2 E \sin^2 A & R^2 \cos^2 E \cos^2 A \\ \sin^2 E & R^2 \cos^2 E & 0 \end{pmatrix} \begin{pmatrix} \delta R^2 \\ \delta E^2 \\ \delta A^2 \end{pmatrix} + [S] \quad (12)$$

where [S] represents the matrix of all the cross terms containing the factors $\delta R\,\delta E$, $\delta R\,\delta A$, and $\delta E\,\delta A$. Measurements of R, E, and A are assumed to be mutually independent so that $E(\delta R\,\delta E)$, $E(\delta R\,\delta A)$, and $E(\delta E\,\delta A) = 0$. Taking the expected value of both sides of the above expression and replacing $E[\delta x^2]$ with σ_x^2 and so forth gives:

$$\begin{pmatrix} \sigma_x^2 \\ \sigma_y^2 \\ \sigma_z^2 \end{pmatrix} = [M^2] \begin{pmatrix} \sigma_R^2 \\ \sigma_E^2 \\ \sigma_A^2 \end{pmatrix} \quad (13)$$

where

$$[M^2] = \begin{pmatrix} \cos^2 E \cos^2 A & R^2 \sin^2 E \cos^2 A & R^2 \cos^2 E \sin^2 A \\ \cos^2 E \sin^2 A & R^2 \sin^2 E \sin^2 A & R^2 \cos^2 E \cos^2 A \\ \sin^2 E & R^2 \cos^2 E & 0 \end{pmatrix}$$

The quantities σ_R^2, σ_E^2, and σ_A^2 are the noise error variances of the radar measured coordinates and are functions of the radar.

Equations (13) give the noise error variance in the rectangular position coordinates after the transformation from the radar's spherical

system. It will be shown in a later section that smoothing the rectangular coordinates to obtain rectangular accelerations results in multiplication of the position error variances by a constant dependent only upon the smoothing polynomial(s). Thus, the error variances in acceleration are given by

$$\begin{pmatrix} \sigma_{\ddot{x}}^2 \\ \sigma_{\ddot{y}}^2 \\ \sigma_{\ddot{z}}^2 \end{pmatrix} = K_1 [M^2] \begin{pmatrix} \sigma_R^2 \\ \sigma_E^2 \\ \sigma_A^2 \end{pmatrix} \tag{14}$$

where K_1 is a constant, when smoothing is done on rectangular coordinates.

To find the noise error variance in $\ddot{x}$, $\ddot{y}$, and $\ddot{z}$ when the spherical coordinates are smoothed, expressions must first be found for rectangular accelerations in terms of the corresponding spherical quantities. Differentiating Equations (10) twice yields:

$$\ddot{x} = (\ddot{R} - R\dot{E}^2 R\dot{A}^2)\cos E \cos A - (R\ddot{E} + 2\dot{R}\dot{E})\sin E \cos A$$
$$- (R\ddot{A} + 2\dot{R}\dot{A})\cos E \sin A + 2R\dot{E}\dot{A} \sin E \sin A$$

$$\ddot{y} = (\ddot{R} - R\dot{E}^2 - R\dot{A}^2)\cos E \sin A - (R\ddot{E} + 2\dot{R}\dot{E})\sin E \sin A$$
$$+ (R\ddot{A} + 2\dot{R}\dot{A})\cos E \cos A - 2R\dot{E}\dot{A} \sin E \cos A$$

$$\ddot{z} = (\ddot{R} - R\dot{E}^2)\sin E + (R\ddot{E} + 2\dot{R}\dot{E})\cos E$$

where $\ddot{R}$, $\ddot{E}$, $\ddot{A}$ and $\dot{R}$, $\dot{E}$, $\dot{A}$ are the accelerations and velocities, respectively, in the spherical system. Application of the same techniques that produced the error variances in Equations (13) gives expressions for the variances when smoothing on spherical coordinates:

$$\begin{pmatrix} \sigma_{\ddot{x}}^2 \\ \sigma_{\ddot{y}}^2 \\ \sigma_{\ddot{z}}^2 \end{pmatrix} = [M^2] \begin{pmatrix} \sigma_{\ddot{R}}^2 \\ \sigma_{\ddot{E}}^2 \\ \sigma_{\ddot{A}}^2 \end{pmatrix} + [N^2] \begin{pmatrix} \sigma_{\dot{R}}^2 \\ \sigma_{\dot{E}}^2 \\ \sigma_{\dot{A}}^2 \end{pmatrix} + [P^2] \begin{pmatrix} \sigma_R^2 \\ \sigma_E^2 \\ \sigma_A^2 \end{pmatrix} \qquad (16)$$

where

$$[M^2] = \begin{pmatrix} \cos^2 E \cos^2 A & R^2 \sin^2 E \cos^2 A & R^2 \cos^2 E \sin^2 A \\ \cos^2 E \sin^2 A & R^2 \sin^2 E \sin^2 A & R^2 \cos^2 E \cos^2 A \\ \sin^2 E & R^2 \cos^2 E & 0 \end{pmatrix} .$$

$$[N^2] = \begin{pmatrix} (\dot{E} \sin E \cos A + \dot{A} \cos E \sin A)^2 & (R\dot{A} \sin E \sin A - R\dot{E} \cos E \cos A - \dot{R} \sin E \cos A)^2 & (R\dot{E} \sin E \sin A - \dot{R} \cos E \sin A - R\dot{A} \cos E \cos A)^2 \\ (\dot{A} \cos E \cos A - \dot{E} \sin E \sin A)^2 & (R\dot{A} \sin E \cos A - R\dot{E} \cos E \sin A - \dot{R} \sin E \sin A)^2 & (\dot{R} \cos E \cos A - R\dot{A} \cos E \sin A - R\dot{E} \sin E \cos A)^2 \\ \dot{E}^2 \cos^2 E & (\dot{R} \cos E - R\dot{E} \sin E)^2 & 0 \end{pmatrix} .$$

AND

$$[P^2] = \begin{pmatrix} [(-\dot{E}^2 - \dot{A}^2) \cos E \cos A - \ddot{E} \sin E \cos A - \ddot{A} \cos E \sin A + 2\dot{A}\dot{E} \sin E \sin A]^2 & [-(\ddot{R} - R\dot{E}^2 - R\dot{A}^2) \sin E \cos A - (R\ddot{E} + 2\dot{R}\dot{E}) \cos E \cos A + (R\ddot{A} + 2\dot{R}\dot{A}) \sin E \sin A + 2R\dot{E}\dot{A} \cos E \sin A]^2 \\ [(-\dot{E}^2 - \dot{A}^2) \cos E \sin A - \ddot{E} \sin E \sin A + \ddot{A} \cos E \cos A - 2\dot{A}\dot{E} \sin E \cos A]^2 & [-(\ddot{R} - R\dot{E}^2 - R\dot{A}^2) \sin E \sin A - (R\ddot{E} + 2\dot{R}\dot{E}) \cos E \sin A - (R\ddot{A} + 2\dot{R}\dot{A}) \sin E \cos A - 2R\dot{E}\dot{A} \cos E \cos A]^2 \\ [-\dot{E}^2 \sin E + \ddot{E} \cos E]^2 & [(\ddot{R} - R\dot{E}^2) \cos E - (\ddot{R} + 2\dot{R}\dot{E} \sin E)]^2 \end{pmatrix}$$

$$\begin{pmatrix} [-(\ddot{R} - R\dot{E}^2 - R\dot{A}^2) \cos E \sin A + (R\ddot{E} + 2\dot{R}\dot{E}) \sin E \sin A - (R\ddot{A} + 2\dot{R}\dot{A}) \cos E \cos A + 2R\dot{E}\dot{A} \sin E \cos A]^2 \\ [(\ddot{R} - R\dot{E}^2 - R\dot{A}^2) \cos E \cos A - (R\ddot{E} + 2\dot{R}\dot{E}) \sin E \cos A - (R\ddot{A} + 2\dot{R}\dot{A}) \cos E \sin A + 2R\dot{E}\dot{A} \sin E \sin A]^2 \\ 0 \end{pmatrix} .$$

Note that the matrix $[M^2]$ is identical to the $[M^2]$ matrix of Equations (13) and (14). The noise error variances in the smoothed spherical velocities and accelerations can be expressed as the product of a constant and the error variances in the spherical position coordinates, in the same manner as the rectangular acceleration in Equations (14):

$$\begin{pmatrix} \sigma_{\ddot{x}}^2 \\ \sigma_{\ddot{y}}^2 \\ \sigma_{\ddot{z}}^2 \end{pmatrix} = K_1 [M^2] \begin{pmatrix} \sigma_R^2 \\ \sigma_E^2 \\ \sigma_A^2 \end{pmatrix} + K_2 [N^2] \begin{pmatrix} \sigma_R^2 \\ \sigma_E^2 \\ \sigma_A^2 \end{pmatrix} + [P^2] \begin{pmatrix} \sigma_R^2 \\ \sigma_E^2 \\ \sigma_A^2 \end{pmatrix} \qquad (17)$$

where K_1 and K_2 are constants depending only on the degree and length of the smoothing polynomial. The constant K_1 of (17) is identical to the K_1 of (14), provided of course that the same smoothing polynomials and smoothing intervals are used in each method. The R, E, and A error variances in (17) may be factored out and the matrices $K_2 [N^2]$ and $[P^2]$ combined as matrix $[Q^2]$. We can then write (17) as

$$\begin{pmatrix} \sigma_{\ddot{x}}^2 \\ \sigma_{\ddot{y}}^2 \\ \sigma_{\ddot{z}}^2 \end{pmatrix} = \left\{ K_1 [M^2] + [Q^2] \right\} \begin{pmatrix} \sigma_R^2 \\ \sigma_E^2 \\ \sigma_A^2 \end{pmatrix} \quad . \qquad (18)$$

At this point, if we reexamine (14), the expression for noise errors in acceleration when x, y, and z are smoothed, we see that the difference between predicting the noise error in acceleration when smoothing on x, y, and z rather than R, E, and A is the term

$$[Q^2] \begin{pmatrix} \sigma_R^2 \\ \sigma_E^2 \\ \sigma_A^2 \end{pmatrix} .$$

In order to determine the magnitude of the elements of $[Q^2]$ as compared to the elements of $K_1 [M^2]$, a sample trajectory was analyzed by smoothing of R, E, and A. Along with printing out the values of $\sigma_{\ddot{x}}^2$, $\sigma_{\ddot{y}}^2$, and $\sigma_{\ddot{z}}^2$, the factors

$$K_1 [M^2] \begin{pmatrix} \sigma_R^2 \\ \sigma_E^2 \\ \sigma_A^2 \end{pmatrix} \quad \text{and} \quad [Q^2] \begin{pmatrix} \sigma_R^2 \\ \sigma_E^2 \\ \sigma_A^2 \end{pmatrix}$$

were output. From this data Table 8 was prepared showing the contribution to the acceleration noise error by each of the above terms at ten kilometer altitude intervals from 60 to 100 kilometers. The smoothing of the sample trajectory was done with the 19-21 linear-cubic double polynomial filter normally used for density determination. Radar errors used were approximately

TABLE 8: A COMPARISON OF TERMS IN THE EQUATIONS FOR ACCELERATION ERROR

	Altitude (Kilometers)				
	100	90	80	70	60
Contribution to σ_{x}^{2} from					
K_1 [M^2]	.032618	.029245	.026315	.023832	.022402
[Q^2]	.000202	.000230	.000158	.000029	.000017
Contribution to σ_{y}^{2} from					
K_1 [M^2]	.032775	.029395	.026431	.023909	.022246
[Q^2]	.000203	.000232	.000166	.000029	.000015
Contribution to σ_{z}^{2} from					
K_1 [M^2]	.022408	.023543	.024461	.025183	.026591
[Q^2]	.000009	.000017	.000019	.000005	.000006

those characteristic of the AN/FPS-16 radar, a slant range radar often used in tracking the ROBIN. The standard deviation of noise error in range, σ_R, is conservatively taken as six meters and the standard deviations in elevation and azimuth, σ_E and σ_A, are assumed to be .15 mils (1.473×10^{-3} radians) each.

Examination of Table 8 quickly shows that the contribution of all the elements of the matrix $[Q^2]$ is for practical purposes negligible for all the acceleration components throughout the altitude range considered. The largest contribution from $[Q^2]$ occurs at about 90 kilometers where it may be as much as 1% of K_1 $[M^2]$ for the horizontal accelerations and .1% for the vertical acceleration. At lower altitudes the relative effect of $[Q^2]$ is less than .1% for $\sigma_{\ddot{x}}^2$ and $\sigma_{\ddot{y}}^2$ and about .02% for $\sigma_{\ddot{z}}^2$. It is apparent that the approximation made in ignoring the contribution to the noise error by the terms represented in the matrix $[Q^2]$ is quite good. One can conclude then, that there is virtually no difference in noise error variance between smoothing on the spherical coordinates R, E, and A and smoothing on the rectangular coordinates x, y, and z.

Bias error. --It has been shown above that on the basis of noise error there is little difference in smoothing on R, E, and A and smoothing on x, y, and z. Next we will consider the differences in bias error between the methods. As mentioned previously, bias error results from lack of fit of the smoothing polynomials to the actual data. A study was carried out by smoothing a computer simulated trajectory in both manners, i.e.,

smoothing on R, E, and A, and smoothing on x, y, and z. The resulting rectangular acceleration components were compared to the "true" values computed by the trajectory program. The program supplied position coordinates in REA form to a smoothing routine which used a 19-21 linear-cubic polynomial for both processes. The bias error was then computed by comparing the smoothed values of the acceleration components at a given altitude to the true value at that altitude as computed by the trajectory program. Bias error was computed as a "percent bias" by the equation:

$$\text{"\% Bias"} = \frac{\text{smoothed value - true value}}{\text{true value}} \times 100 \quad .$$

Figure 7 presents plots of the percent bias in $\ddot{x}$, $\ddot{y}$, and $\ddot{z}$ as functions of altitude. Broken lines show the bias for smoothing on R, E, and A, while bias for x, y, and z smoothing is shown by solid lines. The figure shows that while the bias error for both methods may be quite large in some cases, the difference between the two methods is no more than a few percent at most. This indicates that the difference between "lack of fit" to the data by transforming x, y, and z before smoothing and after smoothing is small and can be ignored.

Considering what small differences exist in noise and bias errors between smoothing on spherical and smoothing on rectangular coordinates, the better approach appears to be smoothing on x, y, and z. This method requires less information for the coordinate transformation as shown by comparing Equations (10) and (16), and so greatly simplifies any data analysis scheme.

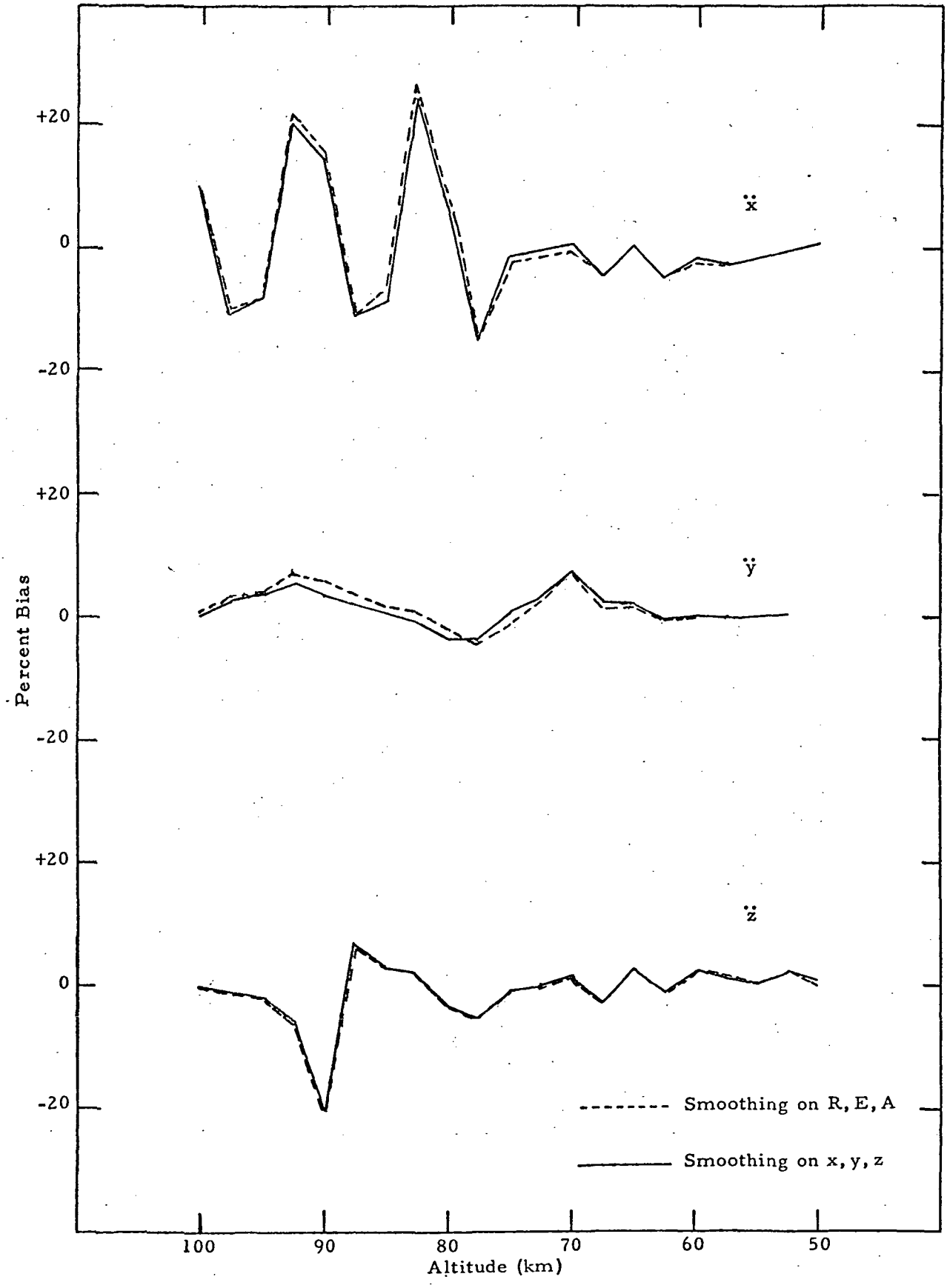

Figure 7. Bias Error in Rectangular Acceleration ($\ddot{x}$, $\ddot{y}$, and $\ddot{z}$) for Spherical and Rectangular Smoothing.

Development of Methods for the Calculation of the Noise Error in Winds and Density

Methods for computing the noise errors in wind speed and density have been developed for ROBIN systems using slant range radars and those using range-rate radars. The calculations require values of the noise error variances in the radar coordinates, parameters of the smoothing technique, and a nominal trajectory. Although temperature and pressure may also be measured by the ROBIN, their values are derived from the density measurements, so that separate studies of noise error in T and P are not required. The expressions developed should be sufficiently general as to be applicable to virtually all radars and smoothing techniques presently used in ROBIN experiments. We will first present the error analysis for slant range radar systems and then examine the alterations necessary to apply the analysis to range-rate systems. The presentation of the slant range radar systems is similar to that given in Reference 2. However, the following presentation takes into account the correlated errors in velocity - a point not considered in Reference 2.

Slant range radars. --Noise in the radar measurements of range, elevation, and azimuth is assumed to be a random, Gaussian process so that the mean (or expected value) of an error is zero. The size of the distribution of errors can then be described by specifying an error variance, σ^2 (or a standard deviation σ), where σ^2 is defined as the mean square error as shown in Equation (13). Let r_i represent a radar measurement of range,

elevation, or azimuth at the ith point in time of the trajectory. We assume that the radar provides a series of such points (i = 1, 2, 3, ...) spaced in time be an interval Δt. We also assume that the error in each measurement of r_i is independent of those errors preceding and following. The measurement of r_i may include some error so that we may express r_i as

$$r_i = r_i^t + \delta r_i \tag{19}$$

where r_i^t is the true value of r_i and δr_i is the error. Transforming from the radar's spherical coordinate system to a rectangular coordinate system transforms the errors in the coordinates by the relationship defined by Equation (13),

$$\begin{aligned}
\sigma_{xi}^2 &= \cos^2 E_i \cos^2 A_i \sigma_{Ri}^2 + R_i^2 \sin^2 E_i \cos^2 A_i \sigma_{Ei}^2 + R_i^2 \cos^2 E_i \sin^2 A_i \sigma_{Ai}^2 \\
\sigma_{yi}^2 &= \cos^2 E_i \sin^2 A_i \sigma_{Ri}^2 + R_i^2 \sin^2 E_i \sin^2 A_i \sigma_{Ei}^2 + R_i^2 \cos^2 E_i \cos^2 A_i \sigma_{Ai}^2 \\
\sigma_{zi}^2 &= \sin^2 E_i \sigma_{Ri}^2 + R_i^2 \cos^2 E_i \sigma_{Ei}^2 \quad .
\end{aligned} \tag{13}$$

The error variance in x, y, z position determined by Equation (13) can be used to express velocity and acceleration errors in rectangular x, y, z coordinates as follows:

Let

$$x_i = x_i^t + \delta x_i \tag{20}$$

where δx_i is the error in the measured value x_i and x_i^t is the true value of x at the i^{th} point. In smoothing x to obtain velocity, N values (points in the time series) of x are fitted by the least squares criterion with an

orthogonal polynomial of degree k. The derivative of this polynomial is taken and its value at the midpoint of the interval is taken as the x velocity. As N is always chosen to be odd, the midpoint of the interval is the point $\frac{N+1}{2}$. The velocity $\dot{x}$ at that point is then (Luers, Ref. 1)

$$\dot{x}\left(\frac{N+1}{2}\right) = A_1 P_1'\left(\frac{N+1}{2}\right) + A_2 P_2'\left(\frac{N+1}{2}\right) + \ldots + A_k P_k'\left(\frac{N+1}{2}\right) \qquad (21)$$

where

$$A_k = \frac{\sum_{i=1}^{N} P_k(i)\, x_i}{\Delta t \sum_{i=1}^{N} P_k^{\,2}(i)} ,$$

$P_k(i)$ is the k^{th} order Legendre polynomial in i,

$P_k'(i)$ is the first derivative of $P_k(i)$,

Δt is the time spacing between points,

and N is the number of points in the smoothing interval.

Substitution of $x_i^{\,t} + \delta x_i$ for x_i in (21) and a rearrangement of terms yields:

$$\dot{x}\left(\frac{N+1}{2}\right) = \sum_{i=1}^{N} \left\{ \frac{P_1(i)\, P_1'\left(\frac{N+1}{2}\right)}{\Delta t \sum_{i=1}^{N} P_1^2(i)} + \ldots + \frac{P_k(i)\, P_k'\left(\frac{N+1}{2}\right)}{\Delta t \sum_{i=1}^{N} P_k^{\,2}(i)} \right\} (x_i^{\,t} + \delta x_i) \qquad (22)$$

Assuming, as we did for x, that $\dot{x}$ may be written as the sum of a true value and an error, $\dot{x} = \dot{x}^{\,t} + \delta\dot{x}$, we may substitute this expression in (22). If we then assume that the polynomial is an exact representation of the

noiseless data, the noise error in velocity in terms of the noise error in position is

$$\delta\dot{x}\left(\frac{N+1}{2}\right) = \sum_{i=1}^{N} \left\{ \frac{P_i(i)\,P'\left(\frac{N+1}{2}\right)}{N} + \ldots + \frac{P_k(i)\,P_k'\left(\frac{N+1}{2}\right)}{N} \right\} \delta x_i \quad . \qquad (23)$$

$$\Delta t \sum_{i=1} P_1^{\,2}(t) \qquad\qquad \Delta t \sum_{i=1} P_k^{\,2}(i)$$

To compute the noise error variance in velocity, we square both sides of (23) and take the expected value. Great simplification can be achieved by noting that

$$1) \quad \sum_{i=1}^{N} P_j(i)\, P_k(i) = 0 \quad \text{for } j \neq k$$

$$2) \quad P_k'\left(\frac{N+1}{2}\right) = 0 \text{ for even } k$$

$$\text{and } 3) \quad E(\delta x_j\, \delta x_k) = \text{for } j \neq k \quad .$$

The velocity noise error variance is then

$$\sigma_{\dot{x}}^{\,2}\left(\frac{N+1}{2}\right) = \left\{ \frac{\left[P_1'\left(\frac{N+1}{2}\right)\right]^2}{N} + \frac{\left[P_3'\left(\frac{N+1}{2}\right)\right]^2}{N} + \frac{\left[P_5'\left(\frac{N+1}{2}\right)\right]^2}{N} + \ldots \right\} \frac{\sigma_x^{\,2}}{\Delta t^2} \qquad (24)$$

$$\sum_{i=1} P_1^{\,2}(i) \qquad \sum_{i=1} P_3^{\,2}(i) \qquad \sum_{i=1} P_5^{\,2}(i)$$

Since fifth order polynomials are rarely, if ever, used, normally only the first two terms require evaluation. These terms may be expressed as functions of N (Ref. 2) as

$$\frac{\left[P_i'\left(\frac{N+1}{2}\right)\right]^2}{\sum_{i=1}^{N} P_i^2\ (i)} = \frac{12}{N(N^2-1)} \tag{25a}$$

and

$$\frac{\left[P_3'\left(\frac{N+1}{2}\right)\right]^2}{\sum_{i=1}^{N} P_3^2\ (i)} = \frac{7(3N^2-7)^2}{(N^2-9)(N^2-4)(N^2-1)N} \tag{25b}$$

Thus, for linear smoothing on x, y, or z to obtain velocity, Equations (24) and (25a) may be combined to give an estimate of the noise error in velocity in terms of the uncertainty in position. When cubic fitting is used, the expression of (25b) must be added.

The next step in the process of obtaining wind and density measurements is the computing of accelerations. There are two approaches: 1) taking the second derivative of the polynomial fitted to the position points, or 2) fitting a new polynomial to the velocity points and taking the first derivative of this polynomial. Both methods present desirable features. Using one fitting polynomial and taking second derivatives for acceleration is a simple and relatively fast process. (Obviously the order of the polynomial must be greater than one if non-zero accelerations are to be obtained.) "Double smoothing", in contrast to "single smoothing" described above, entails fitting a new polynomial to the velocity points provided by the differentiation of the first function. The advantage to double smoothing lies in minimizing

the lack of fit (bias error) between the data and the smoothing polynomials. Bias error has been discussed in detail in Reference 2 where it is noted that the basic justification for double smoothing is that two odd order smoothing polynomials can usually be chosen so that the bias error is less than the bias resulting from taking the second derivative of an even order polynomial. Double smoothing, however, presents some complications in the computation of noise error, as we shall see below.

For single smoothing an error in acceleration arising from an error in position may be written as

$$\delta\ddot{x} = \sum_{i=1}^{N} \left\{ \frac{P_1(i)\, P_1''\left(\frac{N+1}{2}\right)}{\Delta t^2 \sum_{i=1} P_1^2(i)} + \ldots + \frac{P_k(i)\, P_k''\left(\frac{N+1}{2}\right)}{\Delta t^2 \sum_{i=1} P_k^2(i)} \right\} \delta x_i \qquad (26)$$

where $P_k''(i)$ is the second derivative of the kth order Legendre polynomial in i. Equation (26) is obtained in the same manner as was (23) except that the second derivative is now taken. Squaring both sides of (26), taking the expected value, and noting that

1) $P_j(i)\, P_k(i) = 0$ for $j \neq k$,

2) $P_k''\left(\frac{N+1}{2}\right) = 0$ for odd k,

and 3) $E(\delta x_j\, \delta x_k) = 0$ for $j \neq k$,

yields the noise error variance in acceleration,

$$\sigma_{\ddot{x}}^2\left(\frac{N+1}{2}\right) = \left\{ \frac{\left[P_2''\left(\frac{N+1}{2}\right)\right]^2}{\sum_{i=1}^{N} P_2^2(i)} + \frac{\left[P_4''\left(\frac{N+1}{2}\right)\right]^2}{\sum_{i=1}^{N} P_4^2(i)} \right\} \frac{\sigma_x^2}{\Delta t} \quad . \tag{27}$$

Since only quadratic and quartic fitting is normally used, the evaluation of the first two terms can be given as

$$\frac{\left[P_2''\left(\frac{N+1}{2}\right)\right]^2}{\sum_{i=1}^{N} P_2^2(i)} = \frac{720}{N^5 - 5N^3 + 4N} \tag{28a}$$

and

$$\frac{\left[P_4''\left(\frac{N+1}{2}\right)\right]^2}{\sum_{i=1}^{N} P_4^2(i)} = \frac{44100\,(3N^2 - 13)^2}{49N(N^2-1)(N^6 - 29N^4 + 244N^2 - 576)} \quad . \tag{28b}$$

As was the case with fitting for velocity, Equation (27) is used with (28a) for quadratic single smoothing and (28b) is added for quartic smoothing.

Double smoothing consists of using a new polynomial of a different order and/or different smoothing interval, M, to smooth the velocity points, take the derivative, and obtain accelerations. At first glance it would seem that the error variance in acceleration could be expressed by an equation similar to (24) but with $\sigma_{\dot{x}}$ replacing σ_x and $\sigma_{\ddot{x}}$ replacing $\sigma_{\dot{x}}$. However, an extra term must be added to the acceleration error equation when double smoothing is used to account for the effects of non-zero correlation of velocity errors introduced by the velocity fit. This correlation effect occurs

due to the "slide" of the filter. To obtain a sufficient number of acceleration points so that winds and density may be computed more often than every one or two kilometers, any filter used is applied to the data in a sliding manner. In single smoothing sliding goes as follows: after the N position points have been fitted and an acceleration computed and assiged to the $\left(\frac{N+1}{2}\right)$th point, the filter is moved ahead a small number, normally two, of data points and a new acceleration is determined. Thus, the time spacing between any two adjacent acceleration points is $S \cdot \Delta t$, where S is the number of points in the slide. For double smoothing, the velocity smoothing interval slides along the position data, in jumps of S points, generating velocities separated by $S\Delta t$. The acceleration interval then slides along the velocity points in jumps of one point as accelerations are computed. This procedure, as in single smoothing, results in accelerations computed at points in time separated by $S\Delta t$. A sufficient number of acceleration points are thus obtained to compute winds and densities at relatively small altitude intervals, but the slide also introduces correlation or dependence among accelerations since much of the same position data was used to compute any two nearby acceleration points. The meteorological parameters, however, are computed from a single acceleration point so that the correlation in accelerations is not a source of error in the meteorological parameters. In double smoothing, though, correlation among velocity points must be taken into account in calculating the error in acceleration. For example, in a 19-21 linear-cubic double smoothing with a slide of two, the first velocity point is obtained from the 19-point linear fit to position

points, the interval is advanced two points and the second velocity computed using two new positions and 17 of the previous position points. This process continues until 21 velocities are obtained, whereupon a cubic fit is made to yield an acceleration.

To compute the noise error in acceleration, the correlation among velocities is taken into account by the last term on the right hand side of

$$\sigma_{\ddot{x}}^2\left(\frac{M+1}{2}\right) = \left\{\frac{\left[P_1'\left(\frac{M+1}{2}\right)\right]^2}{\sum_{i=1}^{M} P_1^2(i)} + \frac{P_3'\left(\frac{M+1}{2}\right)}{\sum_{i=1}^{M} P_3^2(i)} + \cdots\right\} \frac{\sigma_{\dot{x}}^2}{\Delta t_2^2} + \sum_{i\neq j}^{M}\sum^{M} b_i b_j \rho_{ij} \frac{\sigma_{\dot{x}}^2}{\Delta t_2^2} \qquad (29)$$

where

$P_k'(i)$ is the first derivative of the kth order Legendre polynomial in i, $P_k(i)$, used for the fit to velocity,

M is the number of velocity points in the smoothing interval,

Δt_2 is the time spacing between velocity points,

$\sigma_{\dot{x}}^2$ is the error variance in velocity (as given by 24),

ρ_{ij} is the correlation coefficient for the ith and jth velocity points

and b_i, b_j are constants as defined by

$$b_i = \frac{P_1(i)\,P_1'\left(\frac{M+1}{2}\right)}{\sum_{i=1}^{M} P_1^2(i)} + \frac{P_2(i)\,P_2'\left(\frac{M+1}{2}\right)}{\sum_{i=1}^{M} P_2^2(i)} + \cdots \frac{P_k(i)\,P_k'\left(\frac{M+1}{2}\right)}{\sum_{i=1}^{M} P_k^2(i)}$$

for fitting polynomials of order k.

The complete derivation of the correlation term of (29) is presented in

Appendix C, but it should be noted that the correlation term is only a function of the degree and length of the two smoothing polynomials and the slide used in applying the filter. Thus, if these parameters are known, a number may be specified for the term which applies to any and all trajectories that will be smoothed.

Once Equations (27) and (29) have been used to determine the noise error variances in each of the rectangular components of acceleration, the noise error in wind speed (Ref. 2) in the x and y directions can be determined by

$$\sigma_{wx}^2 = \sigma_{\dot{x}}^2 + \left(\frac{\dot{z}}{\ddot{z}-g}\right)^2 \sigma_{\ddot{x}}^2 + \left(\frac{\ddot{x}}{\ddot{z}-g}\right)^2 \sigma_{\dot{z}}^2 + \left[\frac{\ddot{x}\,\dot{z}}{(\ddot{z}-g)^2}\right]^2 \sigma_{\ddot{z}}^2 \qquad (30a)$$

$$\sigma_{wy}^2 = \sigma_{\dot{y}}^2 + \left(\frac{\dot{z}}{\ddot{z}-g}\right)^2 \sigma_{\ddot{y}}^2 + \left(\frac{\ddot{y}}{\ddot{z}-g}\right)^2 \sigma_{\dot{z}}^2 + \left[\frac{\ddot{y}\,\dot{z}}{(\ddot{z}-g)^2}\right]^2 \sigma_{\ddot{z}}^2 \qquad (30b)$$

where $\sigma_{\dot{x}}^2$, $\sigma_{\dot{y}}^2$, $\sigma_{\dot{z}}^2$ are the noise error variances in the velocities $\dot{x}$, $\dot{y}$, $\dot{z}$, $\sigma_{\ddot{x}}^2$, $\sigma_{\ddot{y}}^2$, $\sigma_{\ddot{z}}^2$, are the error variances in the accelerations $\ddot{x}$, $\ddot{y}$, $\ddot{z}$, g is the acceleration due to gravity, and σ_{wx}^2 and σ_{wy}^2 the errors in the x and y winds. The noise error in density is (Ref. 2)

$$\left(\frac{\sigma_\rho}{\rho}\right)^2 = \left(\frac{\dot{x}-w_x}{V^2}\right)^2 \sigma_{wx}^2 + \left(\frac{\dot{y}-w_y}{V^2}\right)^2 \sigma_{wy}^2 + \left(\frac{2\sigma_{\dot{z}}}{\dot{z}}\right)^2 + \left(\frac{\sigma_{\ddot{z}}}{\ddot{z}-g}\right)^2 \qquad (31)$$

where $V^2 = (\dot{x}-w_x)^2 + (\dot{y}-w_y)^2 + \dot{z}^2$,

w_x and w_y are the x and y winds,

$\dot{x}$, $\dot{y}$, and $\dot{z}$ are the rectangular components of the total velocity V,

$\sigma_{\dot{z}}^2$, $\sigma_{\ddot{z}}^2$ are the noise error variances in $\dot{z}$ and $\ddot{z}$, and

σ_{wx}^2, σ_{wy}^2 are the noise error variances in x and y winds.

The noise error variance in density has been expressed as a ratio of the error in density to the computed value of density in order to simplify the expression. Note that, as usual in dealing with the ROBIN system, vertical winds are assumed not to exist.

Equations (13), (24), (27), (30), and (31) allow calculation of the noise error in wind speed and density for ROBIN tracking with slant range radars. This procedure may be used to generate tables or graphs of the noise error in a measurement as a function of altitude for given combinations of radar accuracies, sample rates, filtering techniques, etc.

To be able to apply both the above method for computing noise error for slant range radar systems and the method developed for range-rate systems, a computer program was written called RFEP (Radar-Filter Error Program). Four versions of the program were used in developing the methods and using them to evaluate radar-filter combinations, sample rates, etc. The first two versions, RFEP1 and RFEP2, are simulation programs designed to produce noise error in winds and density from randomly generated noise error in radar data. RFEP1 processes randomly generated Gaussian errors in the spherical position coordinates in identically the same manner that actual radar data would be processed. The result is the variance of the noise error in wind and density just as it appears in the ROBIN data reduction process. RFEP2 performed the same simulation for range-rate systems. With the aid of the two simulation programs, the analytic methods presented in this chapter were formulated and tested. The analytic method for slant

range radar systems derived above was coded in the third version of the error program, RFEP3, and the analytic method for range-rate systems which we will examine below, was coded in RFEP4.

Figure 8 presents an example of the comparison of the results of the simulation and analytic methods. The noise error in density for slant range radar systems (solid line) is plotted vs. altitude as computed by the analytic method of RFEP3. The noise error as computed by the simulation program is given at 5km altitude intervals. Simulation values are the result of the processing of 30 random error values in the radar coordinates. Agreement is seen to be generally good. Also shown in the figure by a broken line is the result of an earlier analytic method (Ref. 2) which does not take into account the effects of correllated velocity errors. This method consistantly predicted lower noise error than the simulation method and was thereby determined to be in error.

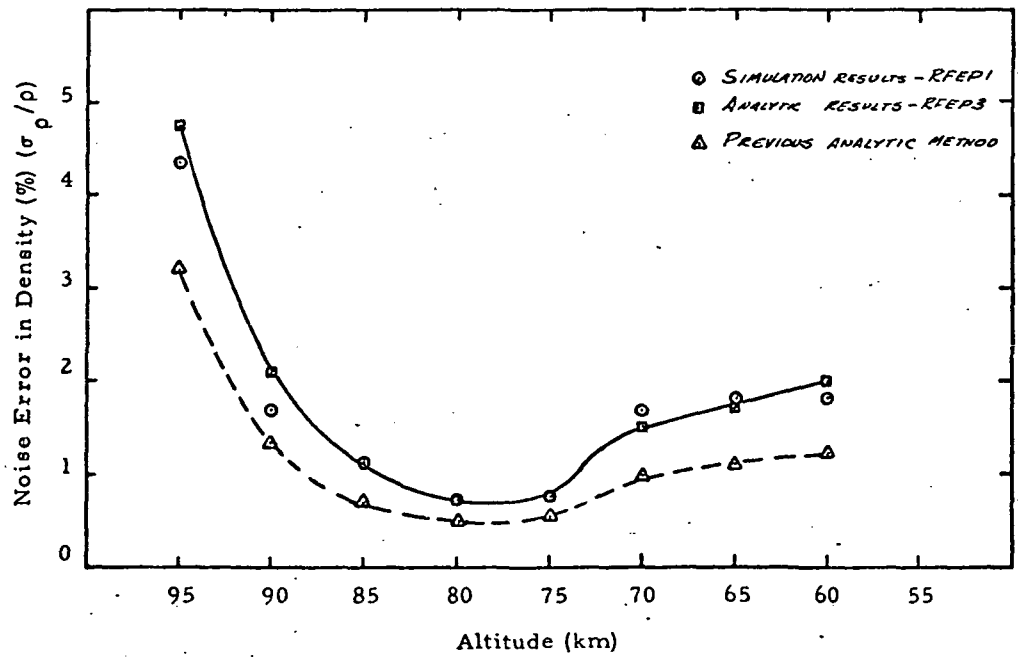

Figure 8 Noise Error in Density Computed by Analytic and Simulation Methods.

Range-rate radars. -- The raw data from a tracking by range-rate or Doppler radar consists of four quantities: range-rate, range, elevation, and azimuth ($\dot{R}$, R, E, and A) provided at points in time separated by the sampling interval Δt. At the present time there does not seem to be any generally agreed upon method for treating data from range-rate radars used to track the ROBIN balloon. The smoothing method presented here along with a noise error prediction scheme is suggested as the best utilization of of the data to obtain the meteorological parameters. The procedure of the proposed smoothing technique for range-rate radar systems begins with smoothing the values of E and A with the orthogonal polynomial technique to obtain values of $\dot{E}$ and $\dot{A}$ at the midpoint of the smoothing interval. If the length of the smoothing interval is N, then the noise error in $\dot{E}$ and $\dot{A}$ are given by

$$\sigma_{\dot{E}}^2\left(\frac{N+1}{2}\right) = \left\{\frac{\left[P_1'\left(\frac{N+1}{2}\right)\right]^2}{\sum_{i=1}^{N} P_1^2(i)} + \frac{\left[P_3'\left(\frac{N+1}{2}\right)\right]^2}{\sum_{i=1}^{N} P_3^2(i)} + \ldots\right\} \frac{\sigma_E^2}{\Delta t^2} \qquad (32a)$$

$$\sigma_{\dot{A}}^2\left(\frac{N+1}{2}\right) = \left\{\frac{\left[P_1'\left(\frac{N+1}{2}\right)\right]^2}{\sum_{i=1}^{N} P_1^2(i)} + \frac{\left[P_3'\left(\frac{N+1}{2}\right)\right]^2}{\sum_{i=1}^{N} P_3^2(i)} + \ldots\right\} \frac{\sigma_A^2}{\Delta t^2} \qquad (32B)$$

where, as in Equation (24), the first term in braces is used for linear fitting, the first two terms for cubic fitting, etc. These terms may be given in terms of N as in Equations (25a) and (25b). The smoothing on E and A data provides E and A velocities at the point (N+1)/2 which may be combined in a set of

transformation equations to find the x, y, and z velocities at (N+1)/2. The transformation equations are

$$\begin{pmatrix} \dot{x} \\ \dot{y} \\ \dot{z} \end{pmatrix} = \begin{pmatrix} \cos E \cos A & -R \sin E \cos A & -R \cos E \sin A \\ \cos E \sin A & -R \sin E \sin A & R \cos E \cos A \\ \sin E & R \cos E & 0 \end{pmatrix} \begin{pmatrix} \dot{R} \\ \dot{E} \\ \dot{A} \end{pmatrix} \quad (33)$$

which require values of R, E, and A at the point (N+1)/2 in addition to $\dot{R}$, $\dot{E}$, and $\dot{A}$. The values of R, E, and A are obtained by averaging the radar R, E, and A data and the value of $\dot{R}$ is obtained by averaging the range-rate $\dot{R}$ measurements. It was shown in a previous chapter that the number of $\dot{R}$ points to be averaged to obtain a frequency response equivalent to that of an N point linear differentiating filter is approximately (3/4)N. If we call this number of points Q, then the error variances in the averaged values of $\dot{R}$, R, E, and A (denoted by an asterisk) are:

$$\sigma_{\dot{R}}^{2*} = \sigma_{\dot{R}}^{2}/Q \quad (34a)$$

$$\sigma_{R}^{2*} = \sigma_{R}^{2}/Q \quad (34b)$$

$$\sigma_{E}^{2*} = \sigma_{E}^{2}/Q \quad (34c)$$

$$\sigma_{A}^{2*} = \sigma_{A}^{2}/Q \quad (34d)$$

Applying the differential error approximation to Equations (33), the noise errors in the rectangular components of velocity are then:

$$\begin{bmatrix} \sigma_{\dot{x}}^{2} \\ \sigma_{\dot{y}}^{2} \\ \sigma_{\dot{z}}^{2} \end{bmatrix} = [T] \begin{bmatrix} \sigma_{\dot{R}}^{2*} \\ \sigma_{\dot{E}}^{2} \\ \sigma_{\dot{A}}^{2} \\ \sigma_{R}^{2*} \\ \sigma_{E}^{2*} \\ \sigma_{A}^{2*} \end{bmatrix} \quad (35)$$

where the matrix [T] =

$$\begin{bmatrix} \cos^2 E\cos^2 A & R^2\sin^2 E\cos^2 A & R^2\cos^2 E\sin^2 A & (\dot{E}\sin E\cos A+\dot{A}\cos E\sin A)^2 & (\dot{A}R\sin E\sin A-\dot{R}\sin E\cos A-\dot{E}R\cos E\cos A)^2 & (\dot{E}R\sin E\sin A-\dot{R}\cos E\sin A-\dot{A}R\cos E\cos A)^2 \\ \cos^2 E\sin^2 A & R^2\sin^2 E\sin^2 A & R^2\cos^2 E\cos^2 A & (\dot{A}\cos E\cos A-\dot{E}\sin E\sin A)^2 & (\dot{A}R\sin E\cos A+\dot{R}\sin E\sin A+\dot{E}R\cos E\sin A)^2 & (-\dot{E}R\sin E\cos A+\dot{R}\cos E\cos A-\dot{A}R\cos E\sin A)^2 \\ \sin^2 E & R^2\cos^2 E & 0 & \dot{E}^2\cos^2 E & (\dot{R}\cos E-R\dot{E}\sin E)^2 & 0 \end{bmatrix}$$

The values of $\dot{x}$, $\dot{y}$, and $\dot{z}$ obtained from Equation (33) can now be fitted with a new polynomial and the derivative taken to yield the rectangular components of acceleration, $\ddot{x}$, $\ddot{y}$, and $\ddot{z}$. If the number of velocity points fit in this manner is M then we have values of $\ddot{x}$, etc., at (M+1)/2. The noise error in the x acceleration is

$$\sigma_{\ddot{x}}^2\left(\frac{M+1}{2}\right) = \left\{\frac{\left[P_1'\left(\frac{M+1}{2}\right)\right]^2}{M} + \frac{\left[P_3'\left(\frac{M+1}{2}\right)\right]^2}{M} + \ldots\right\} \frac{\sigma_{\dot{x}}^2}{(S\Delta t)^2} + \left\{\sum_{j\neq k}^{M}\sum \frac{b_j b_k \Phi_{jk}}{(S\Delta t)^2}\right\} \qquad (36)$$

$$\sum_{i=1} P_1^2(i) \qquad \sum_{i=1} P_3^2(i)$$

where

$$\Phi_{jk} = \left[\frac{Q-S|i-j|}{Q^2}\right]\left[\cos^2 E\cos^2 A\sigma_{\dot{R}}^{2*} + (\dot{E}\sin E\cos A + \dot{A}\cos E\sin A)^2\sigma_R^{2*} + (R\dot{A}\sin E\sin A-\dot{E}R\cos E\cos A-\dot{R}\sin E\cos A)^2\sigma_E^{2*} + (\dot{E}R\sin E\sin A-\dot{R}\cos E\sin A-\dot{A}R\cos E\cos A)^2\sigma_A^{2*}\right]$$

$$+\left[\sum_{k=1}^{N-S|i-j|} a_k a_{k+S|i-j|}\right](R^2\sin^2 E\sin^2 A\sigma_E^2 + R^2\cos^2 E\cos^2 A\sigma_A^2) \quad .$$

The first term on the right hand side of (36) is evaluated in terms of M in the same manner as Equations (32) were treated for N. The second term on the right hand side is the correction to the error variance for the effect of correlated velocities. This term may be obtained by arguments similar to those used in correcting the acceleration error term for slant range radars.

Expressions similar to (36) apply to the other rectangular acceleration errors, $\sigma_{\ddot{y}}^2$ and $\sigma_{\ddot{z}}^2$.

When the acceleration components and their noise errors have been determined, winds and density and their error variances can be found in the same manner as used with slant range radar systems, that is, the errors in wind speed and density for range-rate systems are given by Equations (30) and (31).

The above development of analytic noise error equations for range-rate systems is designed to make optimum use of the raw radar data. By placing the coordinate transformation between the determination of velocities and accelerations, we have restricted the type smoothing that can be used to double smoothing. Although detailed bias error studies of the suggested range-rate method have not been done, it is expected that double smoothing is probably most desirable in any case.

Tests of the range-rate smoothing method on data from simulated trajectories have shown that some approximations can be made that will greatly simplify the computation of the noise error. The matrix [T] that transforms the noise errors in spherical positions and velocities to errors in rectangular velocities (Equation 35), can be divided into two parts: the first three elements of each row which multiply $\sigma_{\dot{R}}^{2*}$, $\sigma_{\dot{E}}^2$, and $\sigma_{\dot{A}}^2$, and the last three elements of each row which multiply σ_R^{2*}, σ_E^{2*}, and σ_A^{2*}. Using data from a sample trajectory, the individual elements of [T] can be computed. When the elements of [T] are then multiplied by representative

values of the appropriate error variances, the contribution of each element to the error variance in $\dot{x}$, $\dot{y}$, or $\dot{z}$ can be noted. Such a comparison using typical ROBIN trajectory data shows that the contribution from the last three terms of each row of [T] is from 10^3 to 10^4 times smaller than the contribution from the first three terms. This occurs due to the fact that the values of $\dot{R}$, $\dot{E}$, $\dot{A}$ are numerically much smaller than those of R, E, and A. Thus, to a good approximation, these terms can be ignored and the matrix [T] reduced to a 3 x 3 of the first three terms of each row. This approximation further simplifies the range-rate error computations since 1) the noise error of the averaged values of R, E, and A are no longer needed (the averaged values themselves are, of course, still required in the actual data analysis) and 2) simplification of the Φ_{ij} term of Equation (36) which contains factors identical to the elements of [T]. Letting the negligible elements of [T] be zero, the Φ_{ij} for x acceleration of (36) reduces to

$$\Phi_{ij} = \left[\frac{Q-S|i-j|}{Q^2}\right](\cos^2 E \cos^2 A \sigma_{\dot{R}}^{2*}) + \left[\sum_{k=1}^{N-S|i-j|} a_k a_{k+S|i-j|}\right](R^2 \sin^2 E \cos^2 A \sigma_E^2 + R^2 \cos^2 A \sin^2 E \sigma_A^2) \quad . \quad (37)$$

Similar reductions apply to the Φ_{ij} terms for $\ddot{y}$ and $\ddot{z}$.

Summary of the methods for predicting noise error. -- At this point we may summarize the noise error expressions for slant range and range-rate radars. The equations for slant range radars are presented in Figure 9, starting with the assumed radar noise error and the filter parameters and ending with the equations for percent error in density. Figure 10 shows the same procedure for range-rate radar systems. The methods summarized

Radar Characteristics: σ_R^2, σ_E^2, σ_A^2 - Noise error variance in range, elevation, and azimuth

Δt - Sample interval = 1/(sample rate)

Filter Characteristics:

Single smoothing: N points fit with a k^{th} order polynomial, first derivative for velocity, second for acceleration

S - Slide (number of points)

Double smoothing: N points fit with a k^{th} order polynomial, first derivative for velocity, then
M velocity points fit with an L^{th} order polynomial, first derivative for acceleration

S - Slide (number of points)

Noise Error in Rectangular Position Coordinates:

$$\begin{pmatrix}\sigma_x^2\\ \sigma_y^2\\ \sigma_z^2\end{pmatrix} = \begin{pmatrix}\cos^2 E \cos^2 A & R^2 \sin^2 E \cos^2 A & R^2 \cos^2 E \sin^2 A\\ \cos^2 E \sin^2 A & R^2 \sin^2 E \sin^2 A & R^2 \cos^2 E \cos^2 A\\ \sin^2 E & R^2 \cos^2 E & 0\end{pmatrix} \begin{pmatrix}\sigma_R^2\\ \sigma_E^2\\ \sigma_A^2\end{pmatrix}$$

Noise Error in the Rectangular Velocity Components:

$$\begin{pmatrix}\sigma_{\dot x}^2\\ \sigma_{\dot y}^2\\ \sigma_{\dot z}^2\end{pmatrix} = \frac{C}{(\Delta t)^2} \begin{pmatrix}\sigma_x^2\\ \sigma_y^2\\ \sigma_z^2\end{pmatrix}$$

where $C = \dfrac{12}{N(N^2-1)}$ for linear or quadratic smoothing

$C = \dfrac{12}{N(N^2-1)} + \dfrac{7(3N^2-7)^2}{(N^2-9)(N^2-4)(N^2-1)N}$ for cubic or quartic smoothing.

Noise Error in the Rectangular Acceleration Components:

Single Smoothing:

$$\begin{pmatrix}\sigma_{\ddot x}^2\\ \sigma_{\ddot y}^2\\ \sigma_{\ddot z}^2\end{pmatrix} = \frac{C}{(\Delta t)^4} \begin{pmatrix}\sigma_x^2\\ \sigma_y^2\\ \sigma_z^2\end{pmatrix}$$

where $C = \dfrac{720}{(N^5-5N^3+4N)}$ for quadratic smoothing

$C = \dfrac{720}{(N^5-5N^3+4N)} + \dfrac{44100(3N^2-13)^2}{49N(N^2-1)(N^6-29N^4+244N^2-576)}$

for quartic smoothing

Double Smoothing:

$$\begin{pmatrix}\sigma_{\ddot x}^2\\ \sigma_{\ddot y}^2\\ \sigma_{\ddot z}^2\end{pmatrix} = \frac{C}{(S\Delta t)^2} \begin{pmatrix}\sigma_x^2\\ \sigma_y^2\\ \sigma_z^2\end{pmatrix}$$

where $C = \dfrac{12}{M(M^2-1)} + \sum_{j\neq k}^{M}\sum b_j b_k \rho_{jk}$ for linear smoothing

$C = \dfrac{12}{M(M^2-1)} + \dfrac{7(3M^2-7)^2}{(M^2-9)(M^2-4)(M^2-1)M} + \sum_{j\neq k}^{M}\sum b_j b_k \rho_{jk}$ for cubic smoothing

$$\rho_{jk} = \frac{\sum_{j=1}^{N-r} a_i a_{i+r}}{\sum_{i=1}^{N} a_i^2}, \quad r = |s(j-k)|,$$

a_i - weighting factors from the fit for velocity (N,k polynomial)

and b_j - weighting factors from the fit for acceleration (M, L polynomial)

Noise Error in the Wind Speed:

$$\sigma_{W_x}^2 = \sigma_{\dot x}^2 + \left(\frac{\dot z}{\ddot z - g}\right)^2 \sigma_{\dot x}^2 + \left(\frac{\ddot x}{\ddot z - g}\right)^2 \sigma_{\dot z}^2 + \left[\frac{\ddot x\, \dot z}{(\ddot z - g)^2}\right]^2 \sigma_{\ddot z}^2$$

$$\sigma_{W_y}^2 = \sigma_{\dot y}^2 + \left(\frac{\dot z}{\ddot z - g}\right)^2 \sigma_{\dot y}^2 + \left(\frac{\ddot y}{\ddot z - g}\right)^2 \sigma_{\dot z}^2 + \left[\frac{\ddot y\, \dot z}{(\ddot z - g)^2}\right]^2 \sigma_{\ddot z}^2$$

Noise Error in the Density (Percent):

$$\left(\frac{\sigma_\rho}{\rho}\right)^2 = \left(\frac{2\sigma_{\dot z}}{\dot z}\right)^2 + \left(\frac{\sigma_{\ddot z}}{\ddot z - g}\right)^2 + \left(\frac{\dot x - W_x}{V^2}\right)^2 \sigma_{W_x}^2 + \left(\frac{\dot y - W_y}{V^2}\right)^2 \sigma_{W_y}^2$$

where $V^2 = (\dot x - W_x)^2 + (\dot y - W_y)^2 + \dot z^2$

Figure 9

Radar Characteristics: $\sigma_{\dot{R}}^2$ - Noise error variance in the range-rate

σ_R^2, σ_E^2, σ_A^2 - Noise error variance in range, elevation, and azimuth

Δt - Sample interval = 1/(sample rate)

Filter Characteristics: N points fit with k^{th} order polynomial to elevation and range for velocities

Q range rate points averaged

S - Slide (number of points)

Noise Error in the Elevation and Azimuth Velocities:

$$\begin{pmatrix} \sigma_{\dot{E}}^2 \\ \sigma_{\dot{A}}^2 \end{pmatrix} = \frac{C}{(\Delta t)^2} \begin{pmatrix} \sigma_E^2 \\ \sigma_A^2 \end{pmatrix} \quad \text{where } C = \frac{12}{N(N^2-1)} \text{ for linear smoothing}$$

$$C = \frac{12}{N(N^2-1)} + \frac{7(3N^2-7)^2}{(N^2-9)(N^2-4)(N^2-1)N} \text{ for cubic smoothing}$$

Noise Error in the Averaged Value of Range Velocity:

$$\sigma_{\dot{R}}^{2*} = \frac{\sigma_{\dot{R}}^2}{Q}$$

Noise Error in the Rectangular Velocity Components:

$$\begin{pmatrix} \sigma_{\dot{x}}^2 \\ \sigma_{\dot{y}}^2 \\ \sigma_{\dot{z}}^2 \end{pmatrix} = \begin{pmatrix} \cos^2 E \cos^2 A & R^2 \sin^2 E \cos^2 A & R^2 \cos^2 E \sin^2 A \\ \cos^2 E \sin^2 A & R^2 \sin^2 E \sin^2 A & R^2 \cos^2 E \cos^2 A \\ \sin^2 E & R^2 \cos^2 E & 0 \end{pmatrix} \cdot \begin{pmatrix} \sigma_{\dot{R}}^{2*} \\ \sigma_E^2 \\ \sigma_A^2 \end{pmatrix}$$

Noise Error in the Rectangular Acceleration Components:

$$\begin{pmatrix} \sigma_{\ddot{x}}^2 \\ \sigma_{\ddot{y}}^2 \\ \sigma_{\ddot{z}}^2 \end{pmatrix} = \frac{C}{(S\Delta t)^2} \begin{pmatrix} \sigma_{\dot{x}}^2 \\ \sigma_{\dot{y}}^2 \\ \sigma_{\dot{z}}^2 \end{pmatrix} + \sum_{j \neq k}^{M} \sum \frac{b_j b_k}{(S\Delta t)^2} \begin{pmatrix} \phi_{jk}(\dot{x}) \\ \phi_{jk}(\dot{y}) \\ \phi_{jk}(\dot{z}) \end{pmatrix}$$

where $C = \frac{12}{M(M^2-1)}$ for linear smoothing

$$C = \frac{12}{M(M^2-1)} + \frac{7(3M^2-7)^2}{(M^2-9)(M^2-4)(M^2-1)M} \text{ for cubic smoothing}$$

b_j = weighting factors from the fit for acceleration

$$\phi_{jk}(\dot{x}) = \left[\frac{Q-r}{Q^2}\right](\cos^2 E \cos^2 A \sigma_{\dot{R}}^{2*}) + \left[\sum_{i=1}^{N-r} a_i a_{i+r}\right](R^2 \sin^2 E \cos^2 A \sigma_E^2 + R^2 \cos^2 E \sin^2 A \sigma_A^2)$$

$$\phi_{jk}(\dot{y}) = \left[\frac{Q-r}{Q^2}\right](\cos^2 E \sin^2 A \sigma_{\dot{R}}^{2*}) + \left[\sum_{i=1}^{N-r} a_i a_{i+r}\right](R^2 \sin^2 E \sin^2 A \sigma_E^2 + R^2 \cos^2 E \cos^2 A \sigma_A^2)$$

$$\phi_{jk}(\dot{z}) = \left[\frac{Q-r}{Q^2}\right](\sin^2 E \sigma_{\dot{R}}^{2*}) + \left[\sum_{i=1}^{N-r} a_i a_{i+r}\right](R^2 \cos^2 E \sigma_E^2)$$

a_i = weighting factors from the fit on E and A for velocity

and $r = S|(j-k)|$

Noise Error in the Wind Speed:

$$\sigma_{W_x}^2 = \sigma_{\dot{x}}^2 + \left(\frac{\dot{z}}{\ddot{z}-g}\right)^2 \sigma_{\ddot{x}}^2 + \left(\frac{\ddot{x}}{\ddot{z}-g}\right)^2 \sigma_{\dot{z}}^2 + \left[\frac{\ddot{x}\,\dot{z}}{(\ddot{z}-g)^2}\right]^2 \sigma_{\ddot{z}}^2$$

$$\sigma_{W_y}^2 = \sigma_{\dot{y}}^2 + \left(\frac{\dot{z}}{\ddot{z}-g}\right)^2 \sigma_{\ddot{y}}^2 + \left(\frac{\ddot{y}}{\ddot{z}-g}\right)^2 \sigma_{\dot{z}}^2 + \left[\frac{\ddot{y}\,\dot{z}}{(\ddot{z}-g)^2}\right]^2 \sigma_{\ddot{z}}^2$$

Noise Error in Density (Percent):

$$\left(\frac{\sigma_\rho}{\rho}\right)^2 = \left(\frac{2\sigma_{\dot{z}}}{\dot{z}}\right)^2 + \left(\frac{\sigma_{\ddot{z}}}{\ddot{z}-g}\right)^2 + \left(\frac{\dot{x}-W_x}{V^2}\right)^2 \sigma_{W_x}^2 + \left(\frac{\dot{y}-W_y}{V^2}\right)^2 \sigma_{W_y}^2$$

where $V^2 = (\dot{x}-W_x)^2 + (\dot{y}-W_y)^2 + \dot{z}^2$

Figure 10

in the figures allow calculation of the noise error in winds and density as a function of altitude for any combination of radar and filter of the kinds used in the ROBIN system. The propagation of the noise from its source in the raw radar data to the final determination of winds and density can be examined by these analytical techniques. Examples of the use of these methods will appear later in this report.

Noise error is not, of course, the only criterion in judging a radar-filter system. Bias error and its related phenomenon, frequency response, are also of concern, especially where determination of fine structure is important. Unfortunately, analytic expressions do not exist for the calculation of bias error and frequency response for the types of filters used on ROBIN data, so that these quantities must be computed by a simulation technique for each particular combination of radar, filter, and nominal trajectory. (Analytic expression do exist, however, for simpler types of filters. See Appendix A.) This procedure consists of smoothing a simulated trajectory with the particular filter whose frequency response is to be found and comparing the resulting wind and density structure with the "true" values used in creating the simulated trajectory. The results of this rather laborious procedure can then be combined with computations of the noise error by the methods presented above to judge the worth of a filter for a particular application.

A Comparison of Noise Error in Winds and Density for Slant Range and Range-Rate Radars

The noise error in the meteorological parameters for the two types of tracking radar has been compared by using the error prediction methods

obtained in the last section. Computations were made of the errors in density and wind speed by both methods using the same simulated trajectory. The radar errors assumed for the slant range radar were nominally those of the FPS-16. For the range-rate radar the FPS-16 errors were assumed for the errors in the R, E, and A measurements and .5 meters per second was taken as the 1 σ error of the range-rate measurement. The filters for the slant range radar system used were the 19-21 linear-cubic for density and the 51-35 cubic-cubic for winds. The filters used for the range-rate system were those that have the same frequency response as the above, i.e., the 19-21 linear-cubic with 15-point averaging and the 51-35 cubic-cubic with 39-point averaging. In computations by either method, the same slide, two, and sample rate, two points per second, were used. Table 9 summarizes the input data to the two noise error programs which were used in the comparison. The plots of noise error for both systems are presented in Figures 11 and 12 for density and North (x) wind, respectively.

Figure 11 shows, as one might expect, less noise error in density throughout the flight, for the range-rate system. Noise error in wind also shows general improvement at all altitudes for range-rate radars as shown in Figure 12. Since the filters and radar errors used in the comparison were chosen to be as similar as possible, the improvement shown in the range-rate case should reflect just the value of the added range-rate measurement (in this case with an accuracy of 0.5 meters per second). In the section of the trajectory where there is considerable motion along the slant range the improvement is most pronounced. In density, for example, a 41%

TABLE 9. --INPUT DATA TO THE COMPARISON OF NOISE ERROR FOR SLANT RANGE AND RANGE-RATE RADAR SYSTEMS

	Slant Range Radar System	Range-Rate Radar System
Radar Errors: (1 σ values)	Six Meters in Range .15 mil in Elevation and Azimuth	Six Meters in Range .15 mil in Elevation and Azimuth .5 m/sec in Range Rate
Filters:	19-21 linear-cubic for Density 51-35 cubic-cubic for Winds Slide 2	19-21 linear-cubic, 15-pt. averaging for Density 51-35 cubic-cubic, 39-pt. averaging for Winds Slide 2
Sample Rate:	$\Delta t = .5$ second	$\Delta t = .5$ second

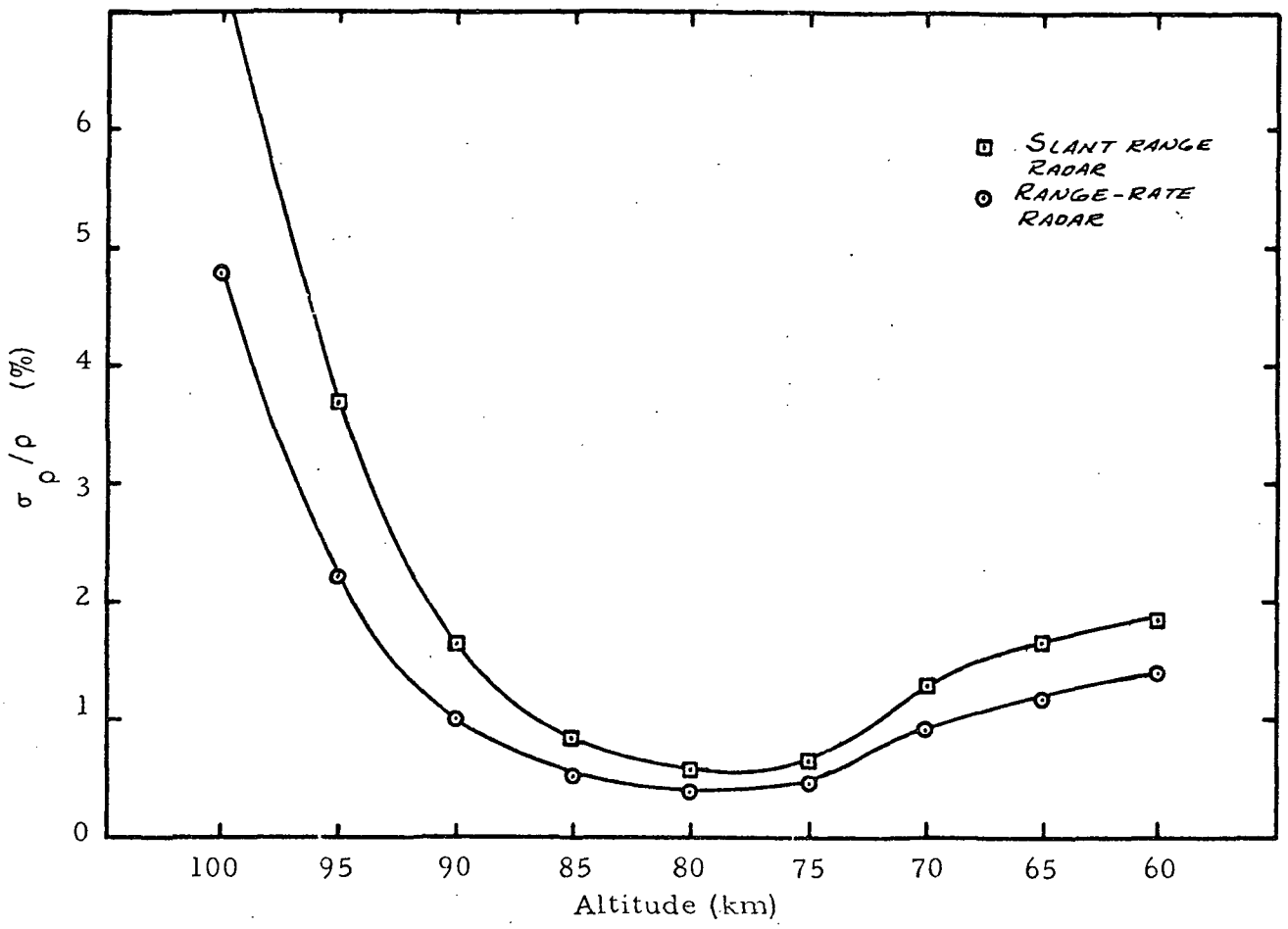

Figure 11 Noise Error in Density for Slant Range and Range-Rate Radar Tracking.

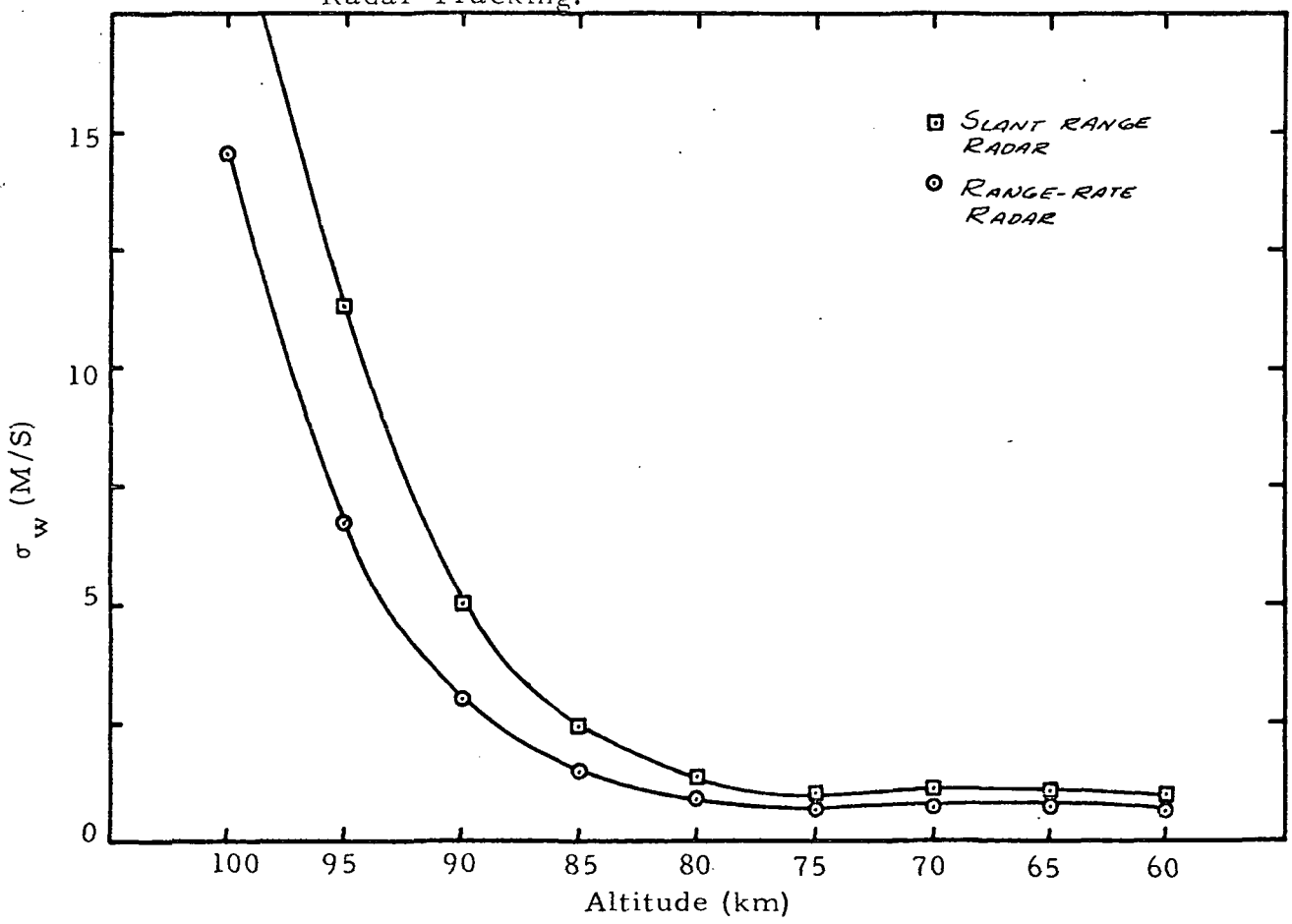

Figure 12 North Wind for Slant Range and Range-Rate Radar Tracking.

improvement is obtained at 100 and 95 kilometers by using the range-rate radar. The percentage improvement decreases at lower altitudes as the radar detects more angular motion, until at 60 kilometers, only a 22% improvement exists. The same effect appears in the North wind error where the improvement is 40% at 100 kilometers and 23% at 60 kilometers.

The increased accuracy of the range-rate radar measurement is greatest just where it is needed at the higher altitudes where slant range radar measurements become very noisy. It should be pointed out that the assumed range-rate accuracy of 0.5 meter per second used in this comparison is probably a rather conservative estimate of the accuracies that are presently available for range-rate radars. Certainly even less noise in the measurement of the range rate would result in greater advantage in the use of range-rate radars.

An Examination of the Smoothing Techniques Presently in Use with Slant Range Radar Tracking

The May 1970 High Altitude ROBIN Program (Ref. 2) was a 19-21 linear-cubic double polynomial filter to determine density and a 51-35 cubic-cubic double filter for winds. These filters were chosen for their combination of low bias and noise error over the 100 to 60 kilometer region. When the noise error for these filters was computed, the effect of correlated velocity errors for double filters was not taken into account. In order to determine what effect, if any, the added noise error would have on the choice of optimum filters for the High Altitude ROBIN, a reexamination of density filters was made. The results of the density filter study were then used to determine if a reexamination of the wind filters, a more laborious process, was required.

As we shall see, it was determined that no reexamination of wind filters was needed.

The more promising double polynomial filters considered in Reference 2 for density determination were the double filters: 41-11 cubic-linear, 19-7 linear-linear, 35-9 cubic-linear, 21-21 linear-cubic, 21-19 linear-cubic, 19-21 linear-cubic, and 31-7 linear-linear, and single filters 21 and 31 quadratic. All these filters have relatively small bias and noise error over the altitude range of interest. To determine which of these filters should be recommended, plots of the noise and bias errors as a function of altitude were made for each filter and the results compared. Figure 13 presents these plots. The computation of noise error in density for each filter was made using the technique outlined in Figure 9. For all filters the assumed radar errors were six meters in range and .15 mil in elevation and azimuth, Δt was taken as .5 seconds and a slide of two points was used. Bias error was computed by the methods described in Reference 2. The absolute value of the bias was used for convenience in preparing the plots.

An examination of Figure 13 shows that, based on the criterion of the best combination of noise and bias error over the entire altitude range, the group of filters: 19-21, 21-21, and 21-19 linear-cubic appear to be superior, the other double and single filters may be eliminated for excessive noise and/or bias over all or a major part of the altitude range. Choosing between the linear-cubic filters in the "20-20" range requires closer examination. When this is done, the 21-21 can be eliminated on the basis of slightly larger bias of the three above about 80 kilometers. The choice

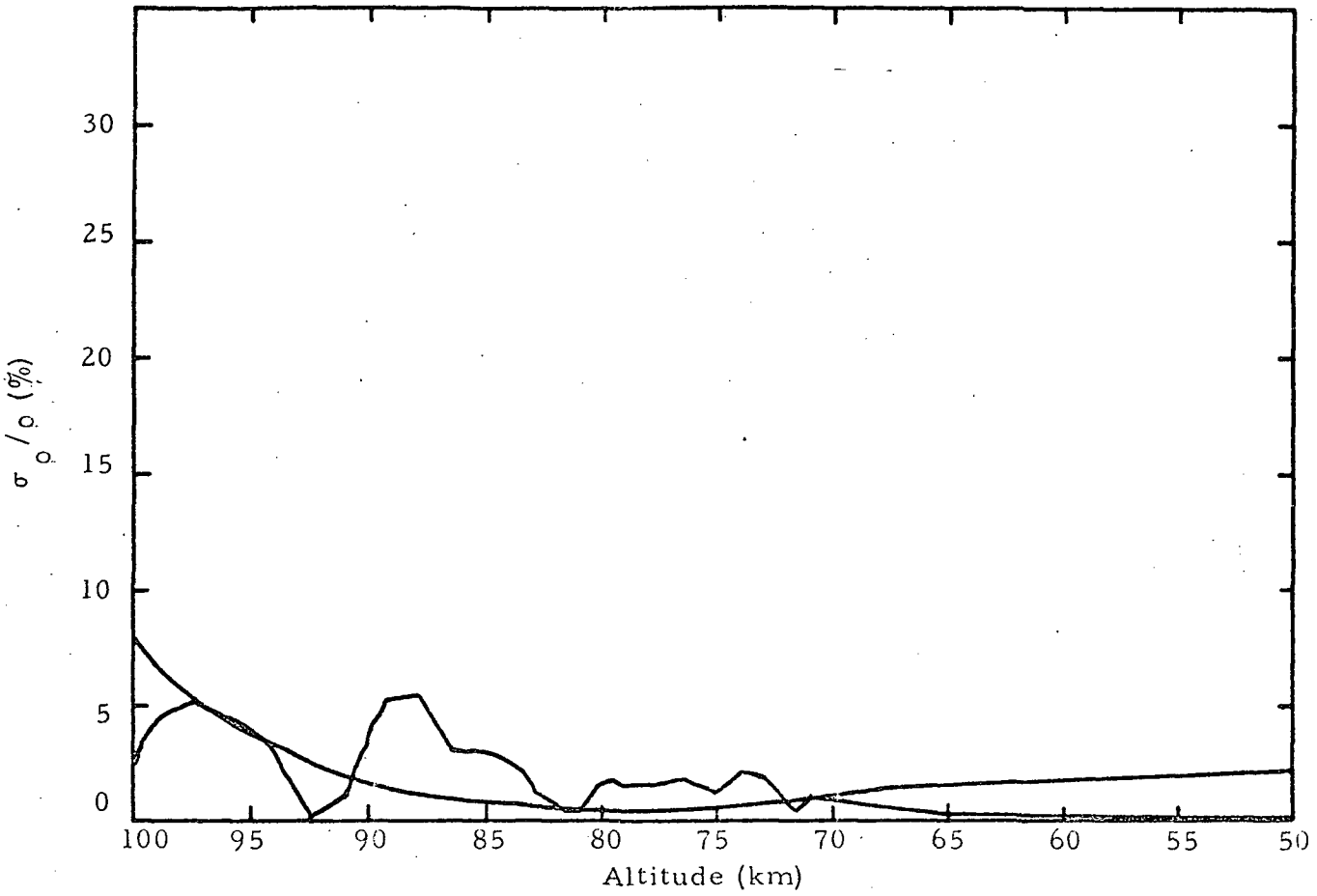

Figure 13a Noise and Bias Error in Density 19-21 Linear Cubic

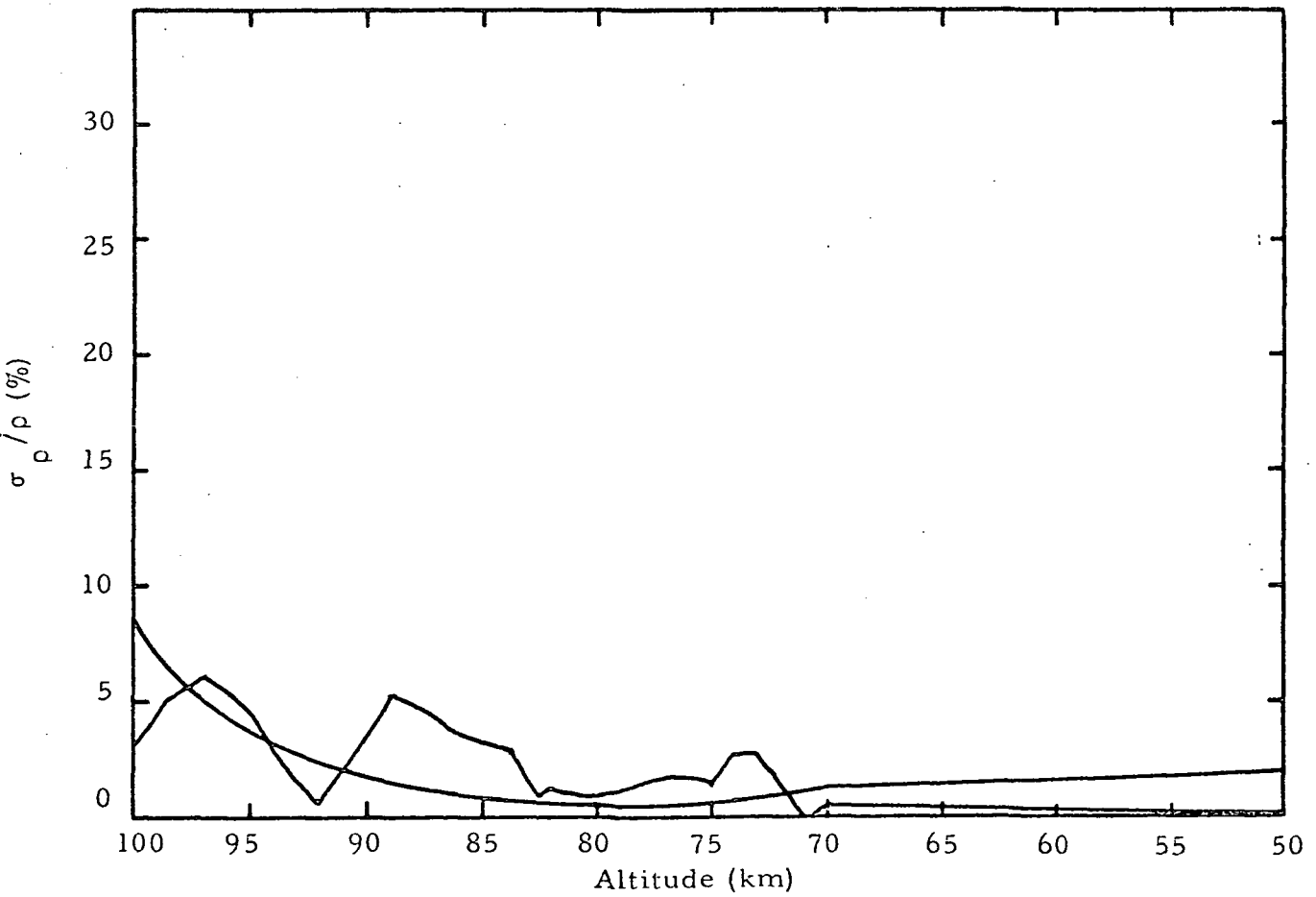

Figure 13b Noise Error and Bias Error in Density 21-19 Linear-Cubic

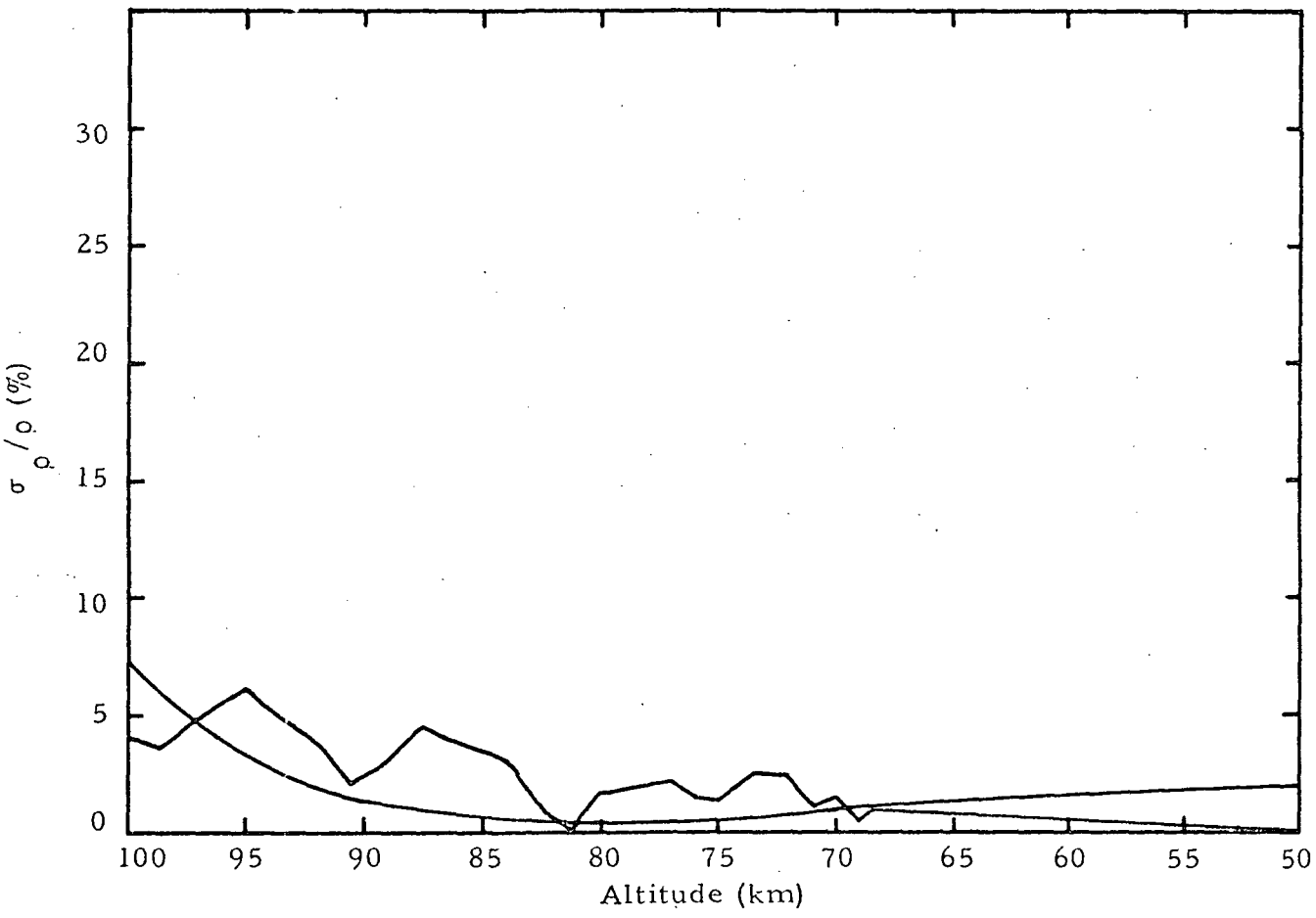

Figure 13c Noise Error and Bias Error in Density 21-21 Linear-Cubic

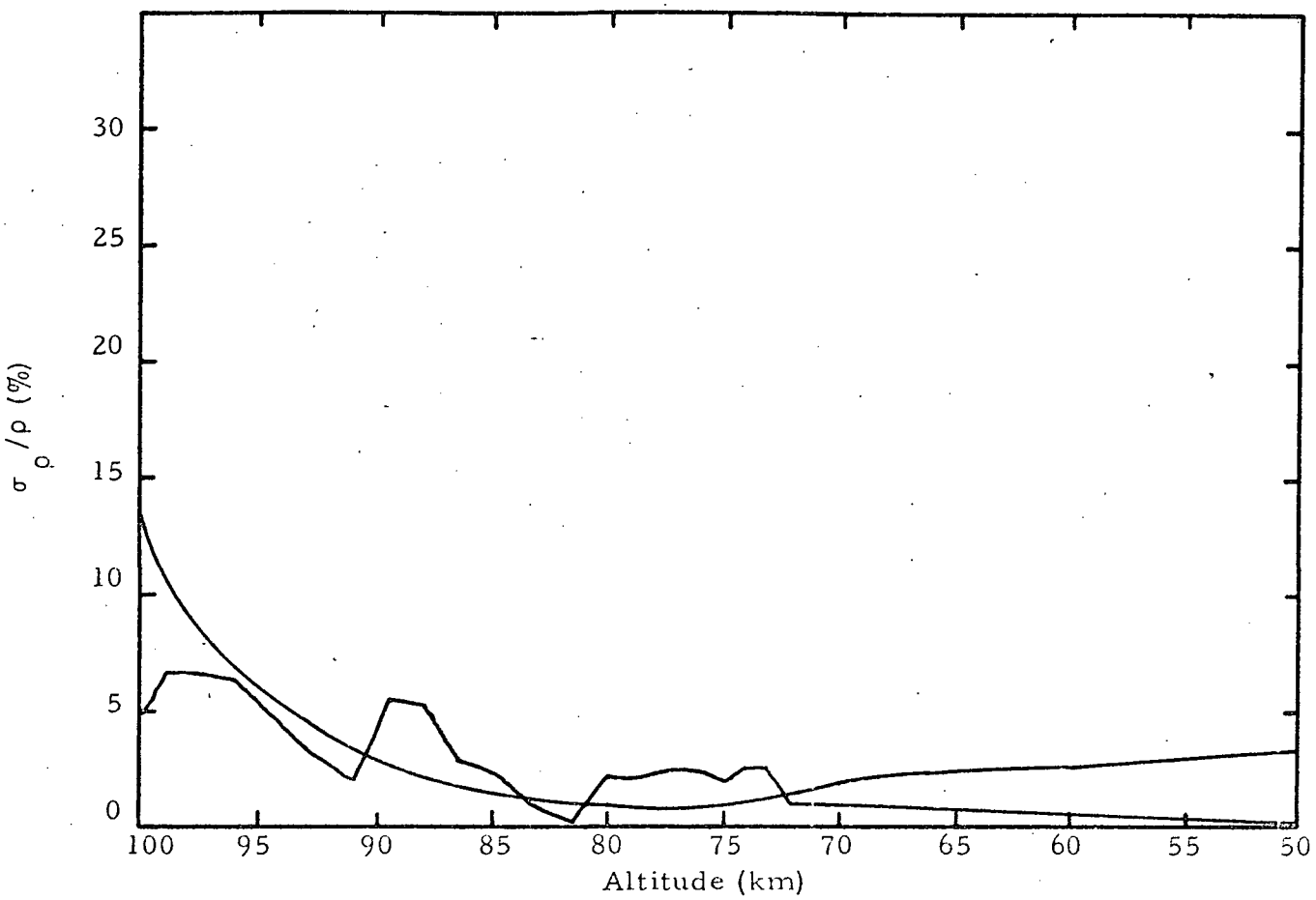

Figure 13d Noise Error and Bias Error in Density 19- 7 Linear-Linear

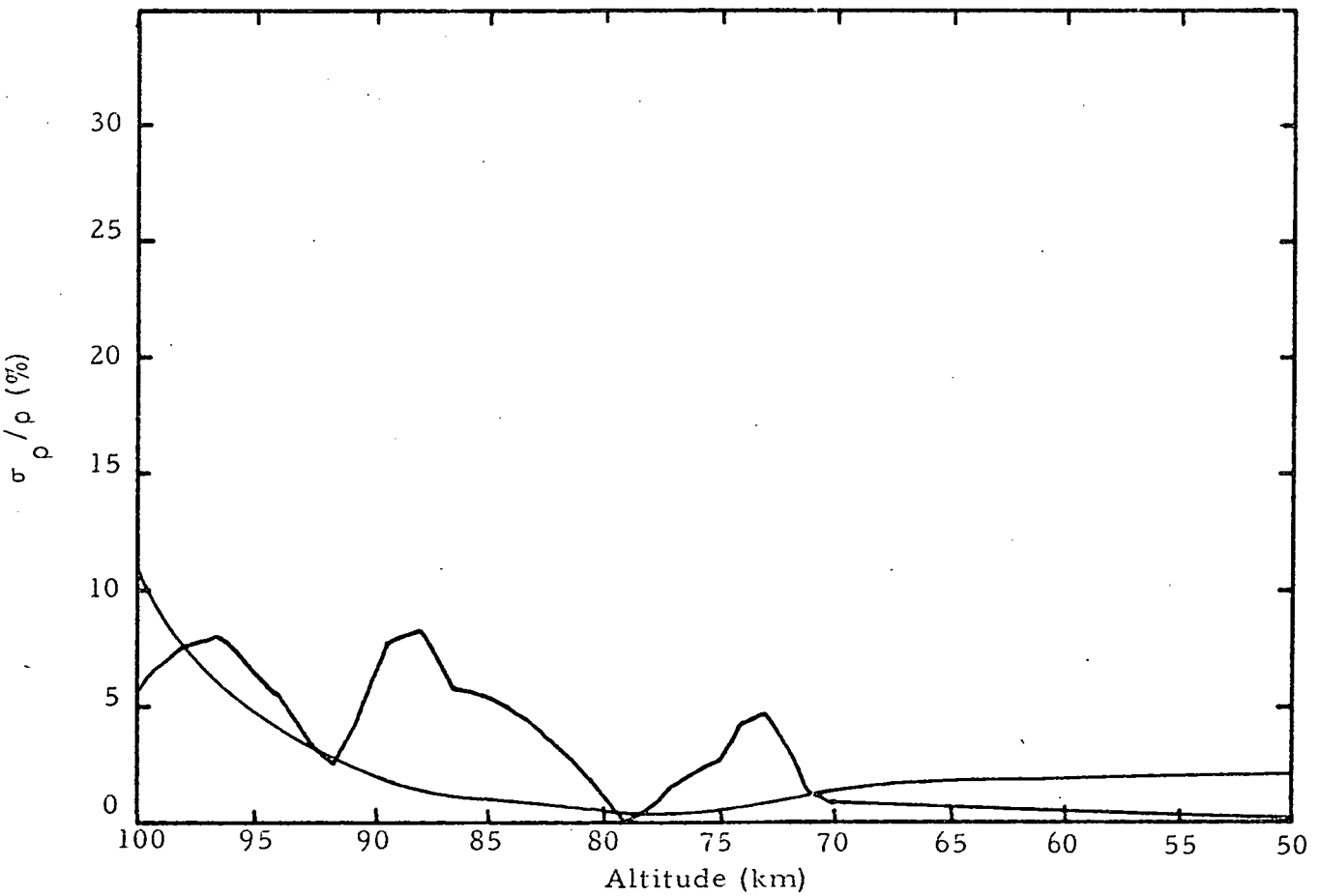

Figure 13e Noise Error and Bias Error in Density 31 Quadratic

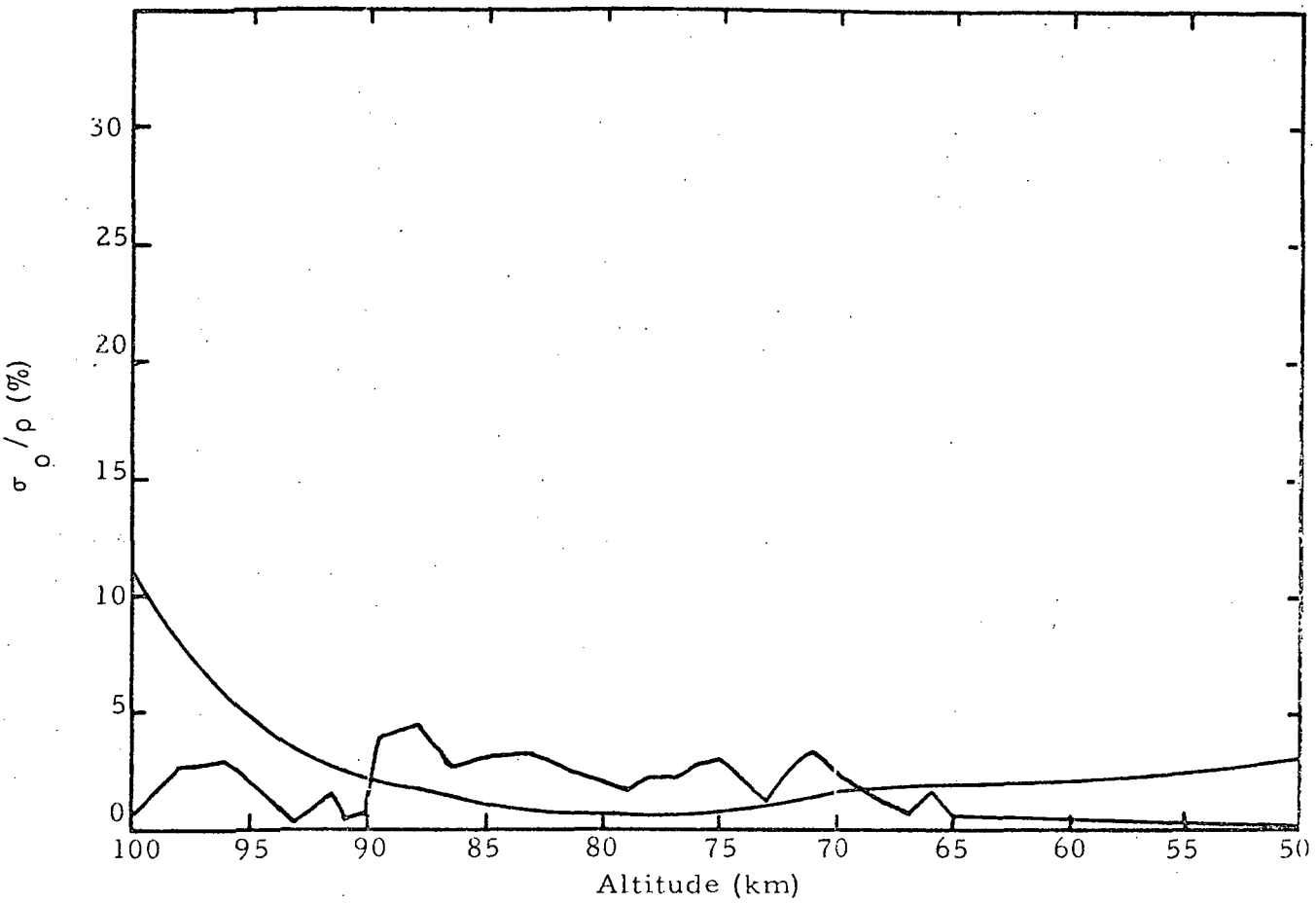

Figure 13f Noise Error and Bias Error in Density 35-9 Cubic-Linear

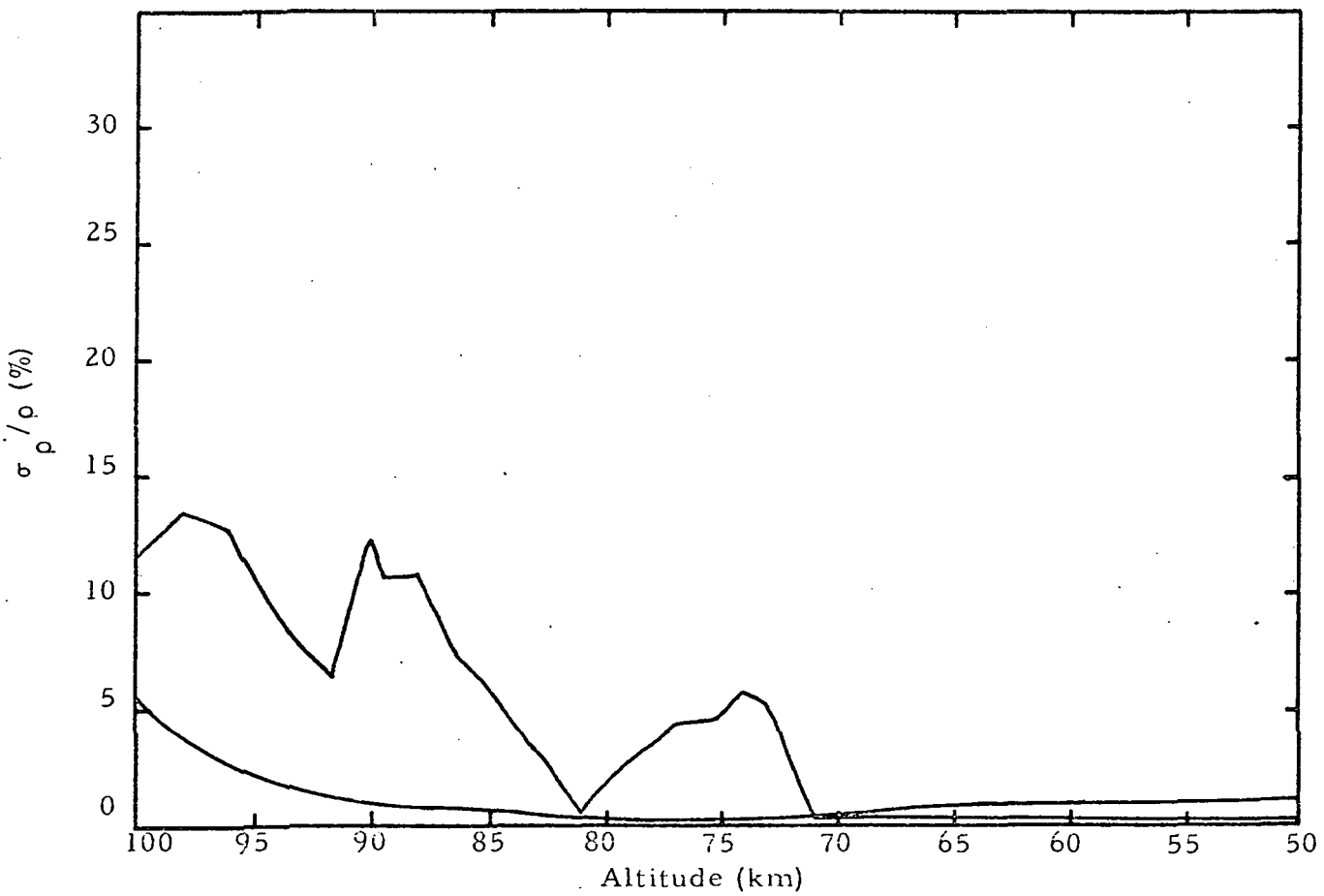

Figure 13g Noise Error and Bias Error in Density 31-7 Linear-Linear

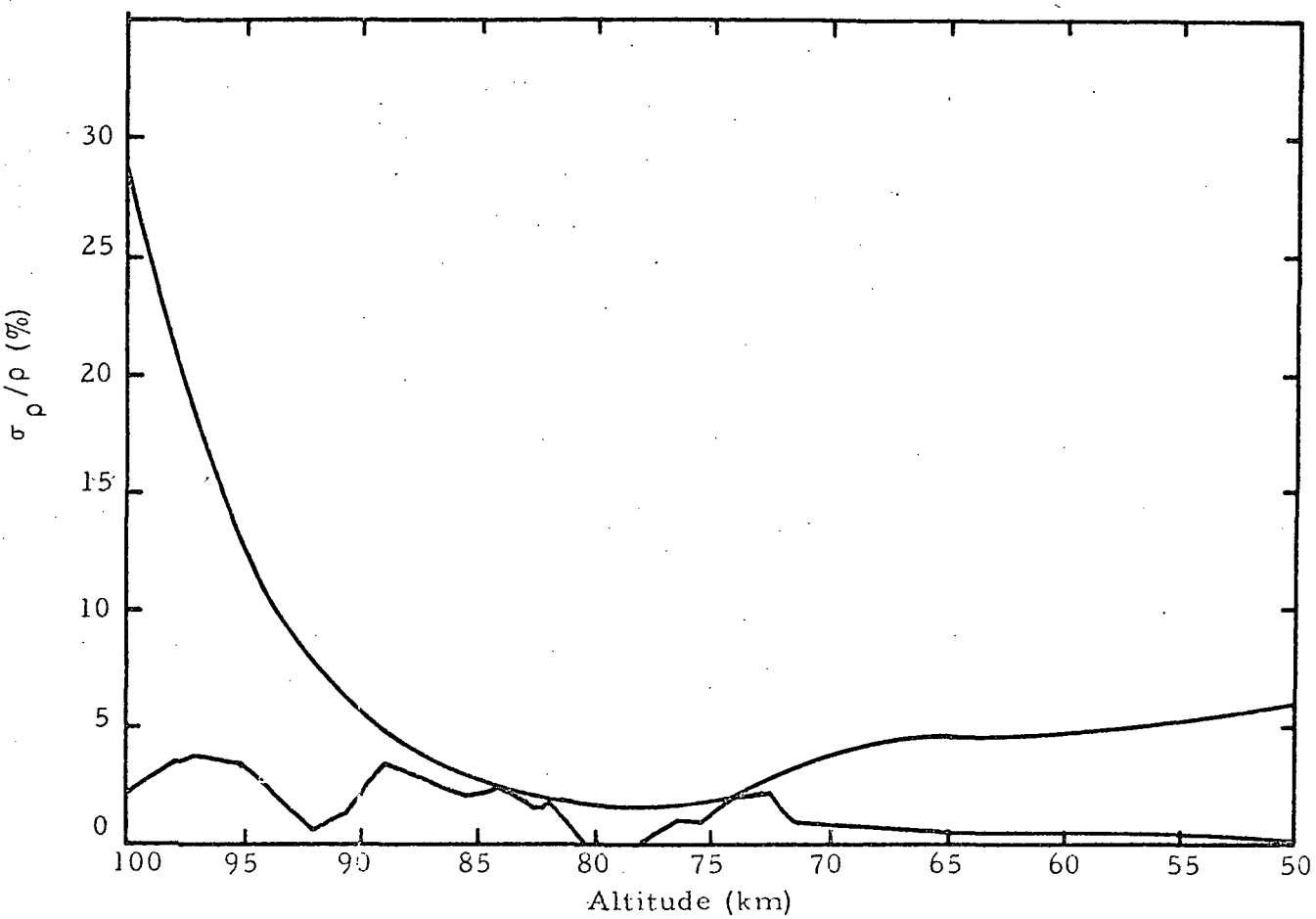

Figure 13h Noise Error and Bias Error in Density 21 Quadratic

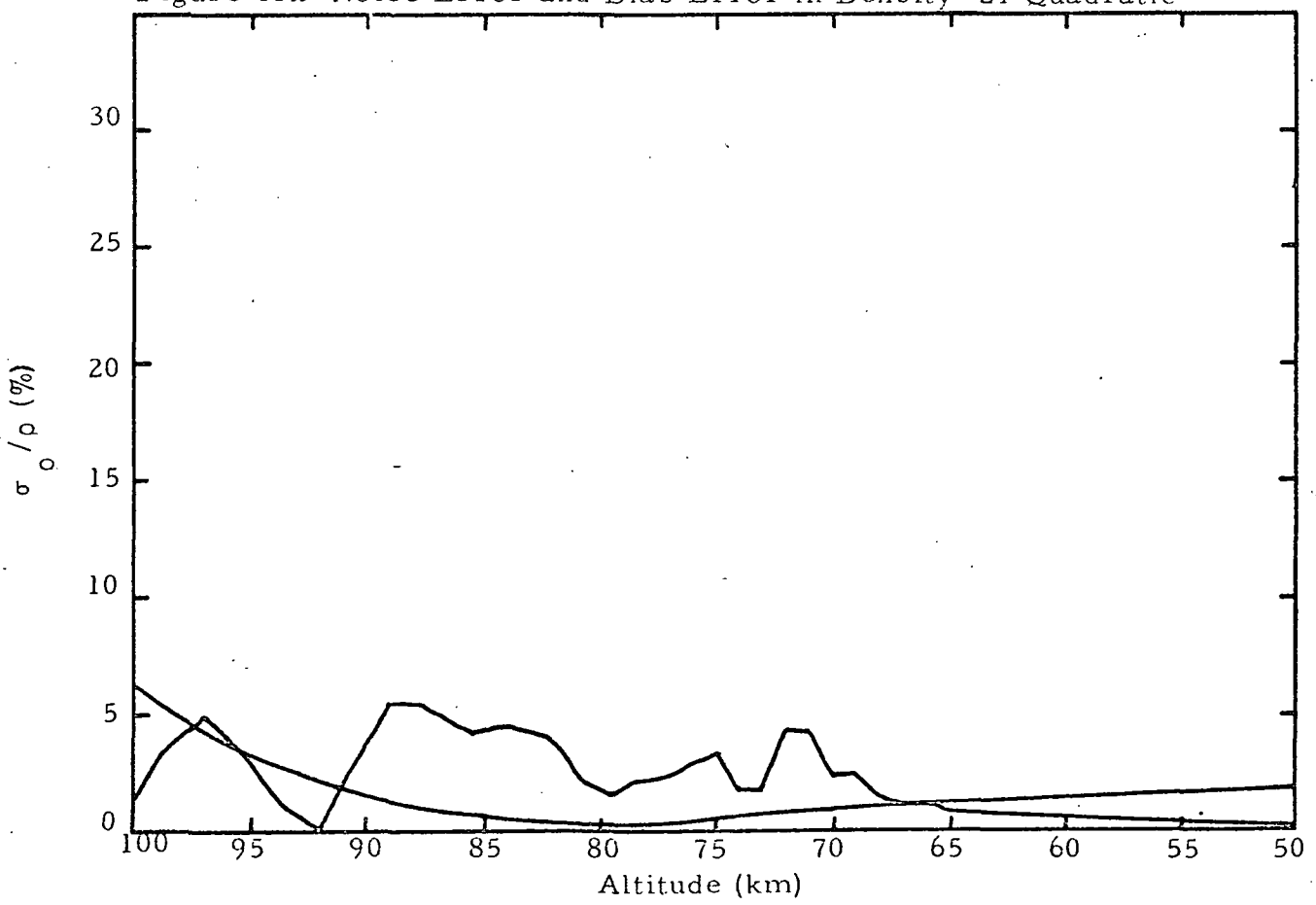

Figure 13i Noise Error and Bias Error in Density 41-11 Cubic-Linear

between the 19-21 and 21-19 is almost impossible to make as they are so evenly matched in both noise and bias. If a point by point comparison is made, however, the 19-21 shows slightly smaller bias more often for the altitude range. Based on this difference, albeit very small, the 19-21 linear-cubic double filter appears to be the best for density determination, as was previously found in Reference 2.

No new filter was found which has a better noise and bias error profile than the density filter now used in the High Altitude Program. Based on this fact and the knowledge that the effect of correlated velocity errors is most important at altitudes above about 85 kilometers where wind error computed by any filter is large, a reexamination of the wind filters was not undertaken.

THE EFFECT OF LAUNCH ELEVATION AND AZIMUTH

Much of the character of the descending section of the ROBIN trajectory is determined by the conditions at the rocket launch. The launch elevation angle primarily determines, for a given vehicle, both the altitude and downrange position at apogee. The direction of launch with respect to the wind structure, the launch azimuth, also has an effect on the trajectory of the balloon as it falls. In order to examine what influence launch elevation and azimuth have on the accuracy of wind and density measurements, error analyses were performed on theoretical trajectories generated to simulate various launch conditions. An examination of the results should suggest what launch conditions are desirable for achieving minimum noise error.

Elevation Angle

Four theoretical trajectories were generated by program THEOT, one trajectory for each of the four launch elevation angles 72^{o}, 78^{o}, 82^{o}, and 88^{o}. The launch vehicle assumed in each case was the Viper-Dart rocket. Since the program computes only the trajectory of the balloon and not that of the rocket, the position and velocity of the balloon at the release point were input for each angle. The positive downrange direction (the launch direction) was taken as North and positive crossrange direction as East. Table 10 summarizes the balloon release conditions for the four launch angles.

TABLE 10: BALLOON RELEASE CONDITIONS FOR THE STUDY OF THE EFFECTS OF LAUNCH ELEVATION ANGLE

Balloon Release Conditions (Viper Dart Vehicle)

Launch Angle	Release Position		Release Velocity	
	Altitude	Downrange	Vertical Velocity	Horizontal Velocity
72°	117000 m	80000 m	0 m/s	530 m/s
78°	126600 m	57400 m	50 m/s	360 m/s
82°	131200 m	39200 m	50 m/s	240 m/s
88°	135000 m	10000 m	52 m/s	60 m/s

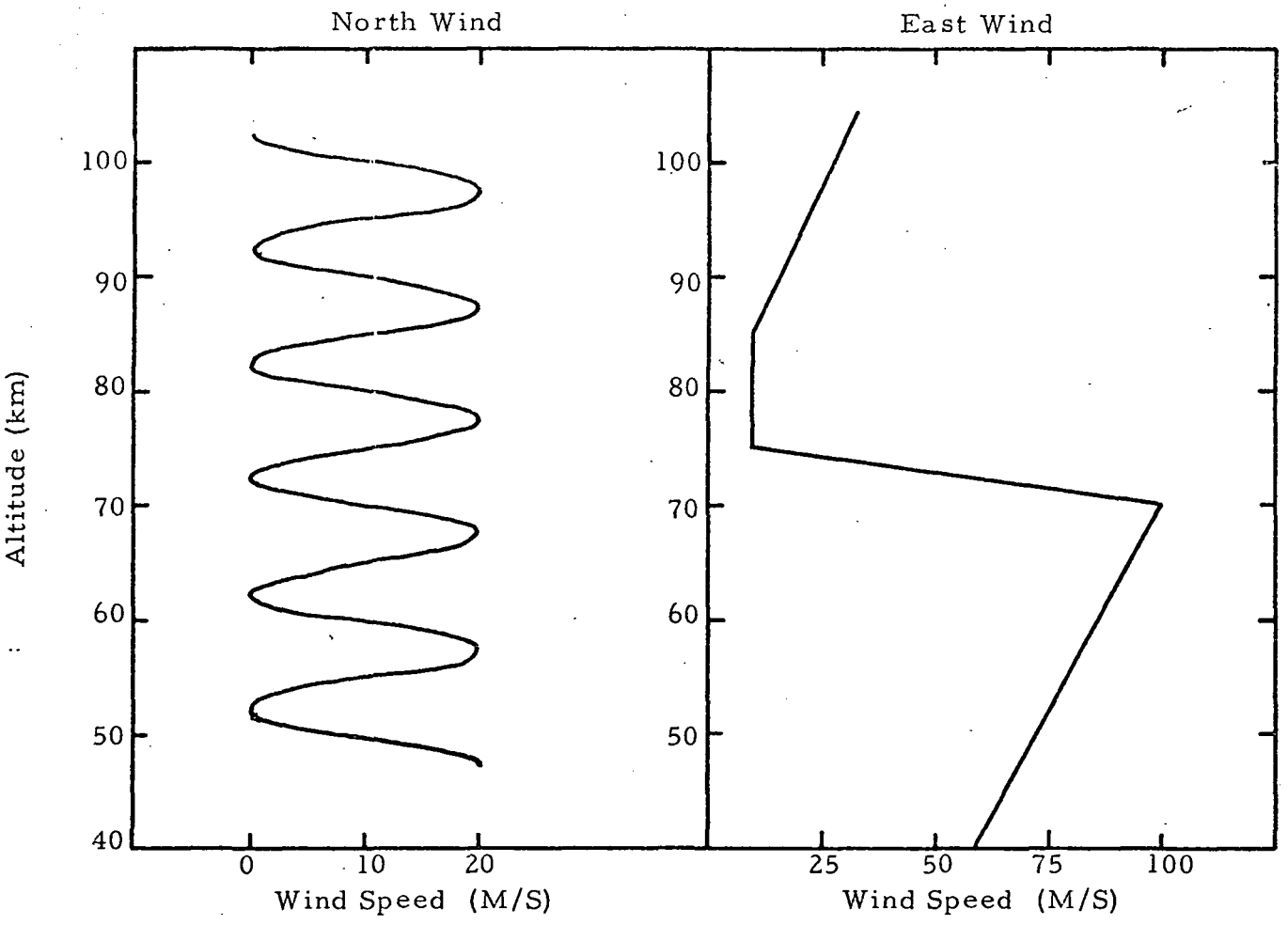

Figure 14 Assumed Wind Profiles

The above launch angle data was abstracted from information supplied by Mr. Bruce Bollermann of Space Data Corporation, manufacturers of the Viper-Dart rocket.

As the wind structure has an effect upon the resulting noise error, the same wind structure was used in each simulated flight. The wind structure used was an approximate version of the actual structure measured by Viper-Dart 12 (Ref. 2). Figure 14 presents this wind structure. The magnitude of the wind directed North is assumed to vary sinusoidily with altitude. The wavelength was taken to be ten kilometers and the amplitude ten meters per second. A constant ten meter per second North wind was added to the sinusoidal structure so that the wind speed varies between 0 and 20 meters per second. In contrast, the speed of the wind blowing East was assumed to be constructed of four linear functions of altitudes. From 60 meters per second at 40 kilometers, the East wind speed increases linearly to a maximum of 100 meters per second at 70 kilometers. A sharp decline reduces the speed to ten meters per second by 75 kilometers, after which the speed remains at that value to 85 kilometers. Above 85 kilometers the wind speed again increases so that at 100 kilometers the speed is 27.5 meters per second. This North and East wind structure was used in each of the four elevation angle trajectories and was also used in the investigation of azimuth effects.

Noise error computations for wind and density were made using the methods for slant range radars and range-rate radars coded in RFEP3 and RFEP4, respectively. The analysis of noise error for the slant range

radars was made using the 19-21 linear-cubic filter for density error and the 51-35 cubic-cubic filter for wind error.

The 19-21 linear-cubic filter with 15-point averaging was used for density in the analysis for range-rate radars. For winds the 51-35 cubic-cubic with 39-point averaging was used. The 1 σ noise errors in position coordinates for both radars were taken to be: six meters in range and .15 mils in elevation and azimuth, the nominal FPS-16 values. The noise error in the range rate for that type radar was 0.5 meter per second. In both cases a sample rate of two points per second ($\Delta t = .5$ sec) was used. The standard deviation of the noise error in each meteorological parameter was computed at each five kilometers from 60 to 100 kilometers and plotted versus altitude. Figures 15, 16, and 17 are the plots for density, North wind, and East wind, respectively for slant range radars, while Figures 18, 19, and 20 show the same plots for range-rate radars.

Slant range radars. --Figure 15 shows a rapid increase in density accuracy with increasing elevation angle. This effect is especially pronounced at the higher altitudes (85 to 100 kilometers). This is to be expected since for the greater launch elevation angles, 82^{o} and 88^{o}, the path of the balloon is closer to the radar site, and thus much of the motion at the high altitudes is along the range direction. Because accuracy of the measurement of range is independent of range (within the limits of tracking of the radar) velocity and acceleration along the range direction can be obtained with little noise error. As the elevation angles become lower, the high altitude accuracy

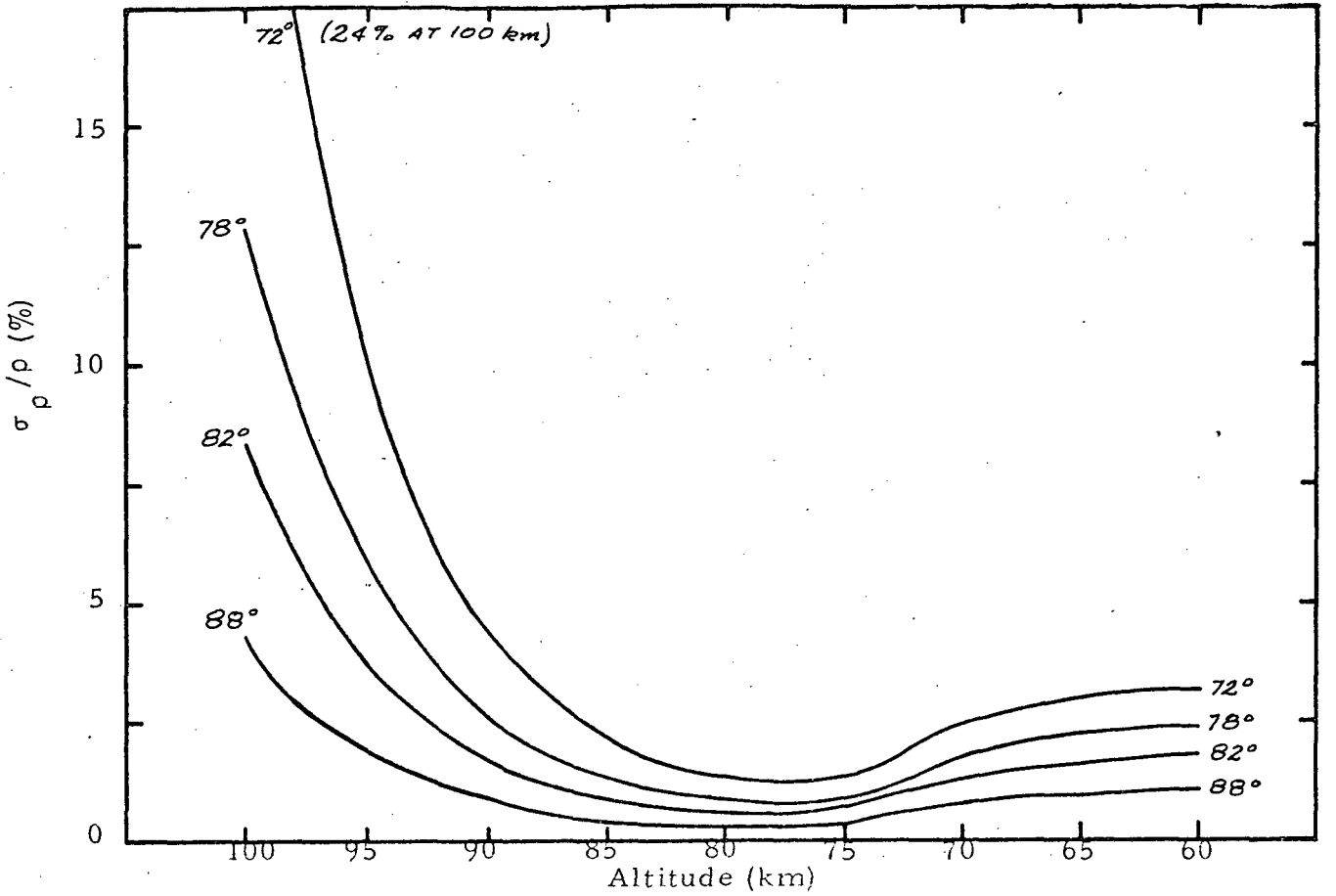

Figure 15 Noise Error in Density as a Function of Launch Elevation Angle (Slant Range Radars)

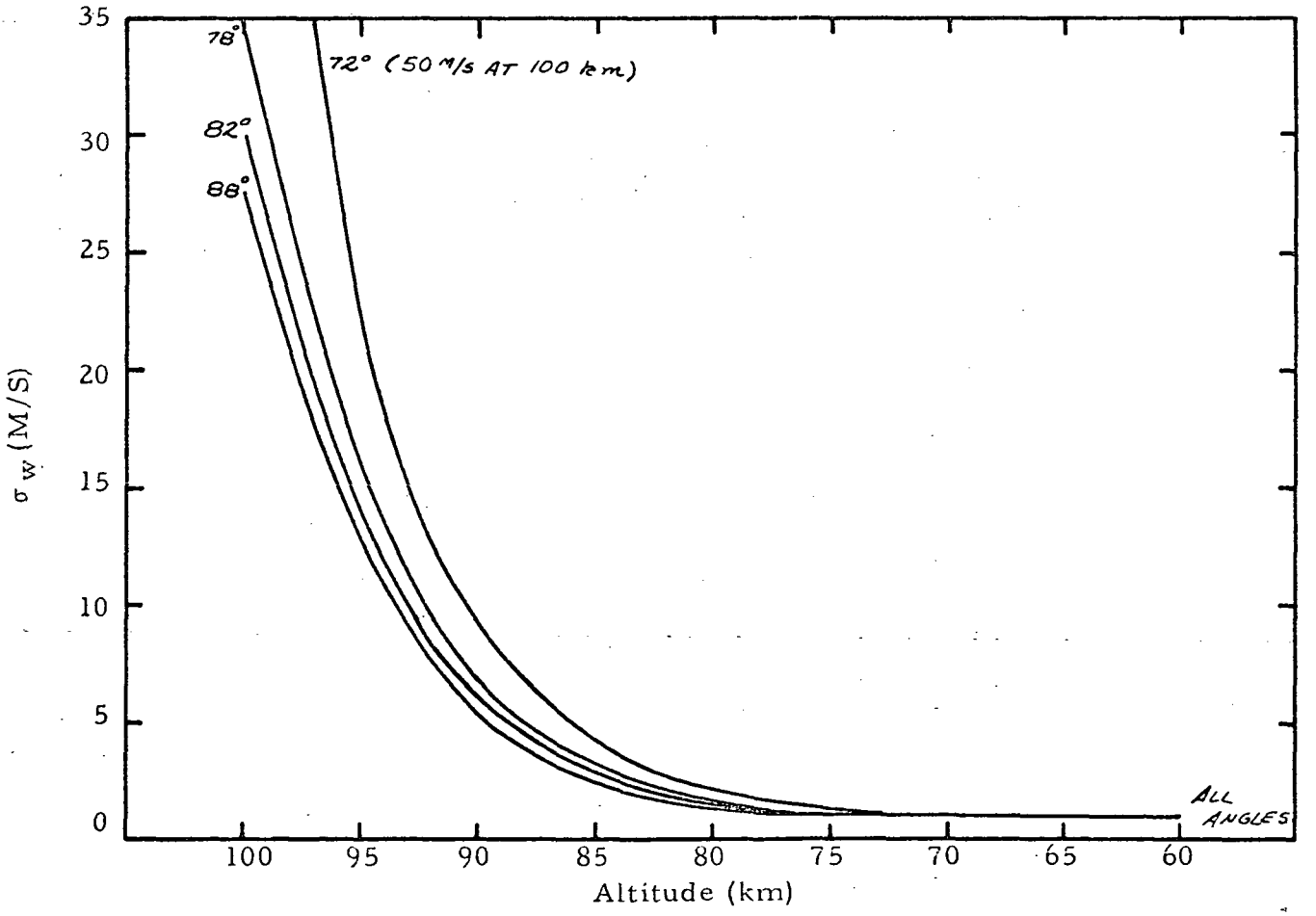

Figure 16 Noise Error in North Wind as a Function of Launch Elevation Angle (Slant Range Radars)

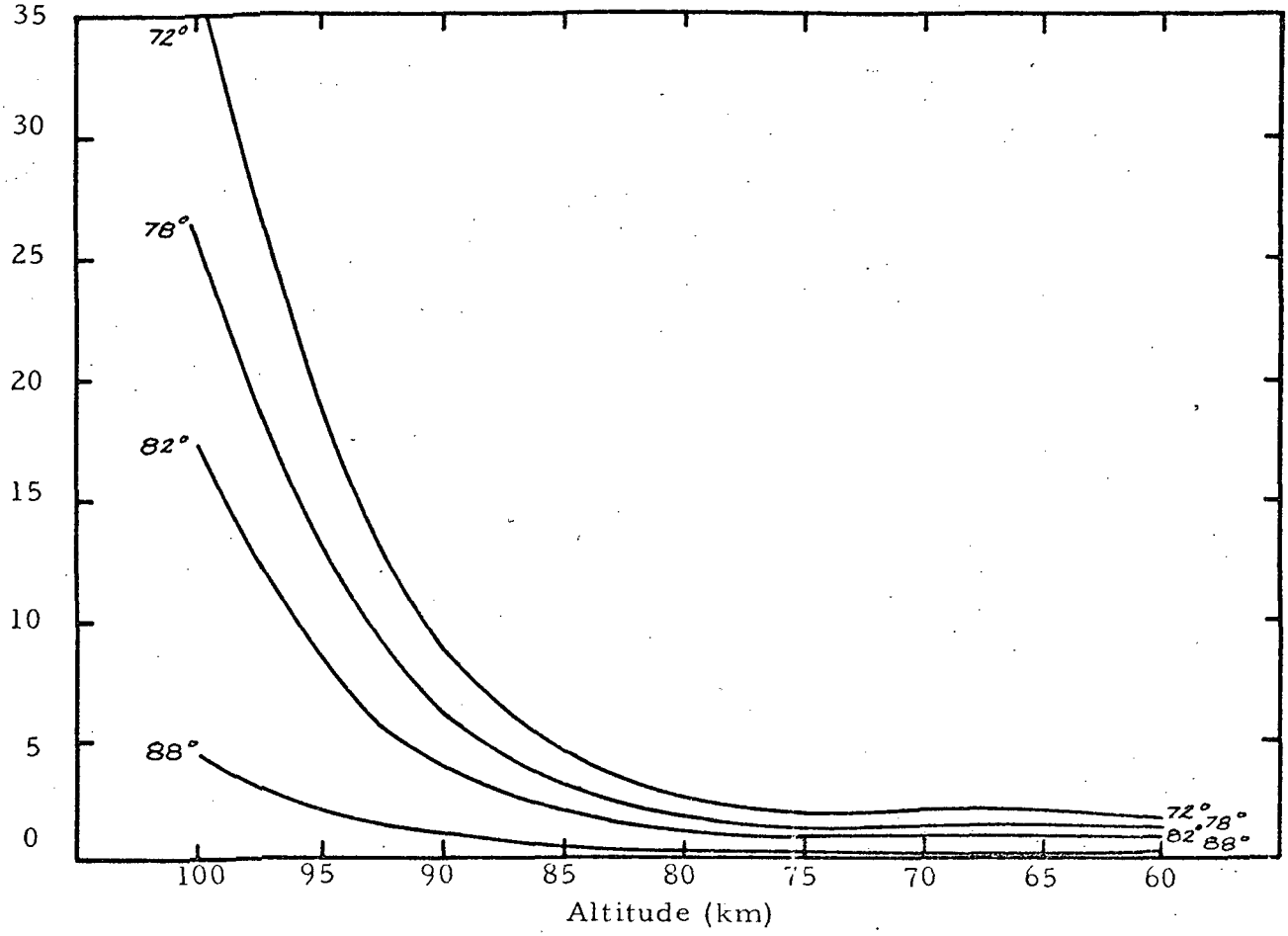

Figure 17 Noise Error in East Wind as a Function of Launch Elevation Angle (Slant Range Radars)

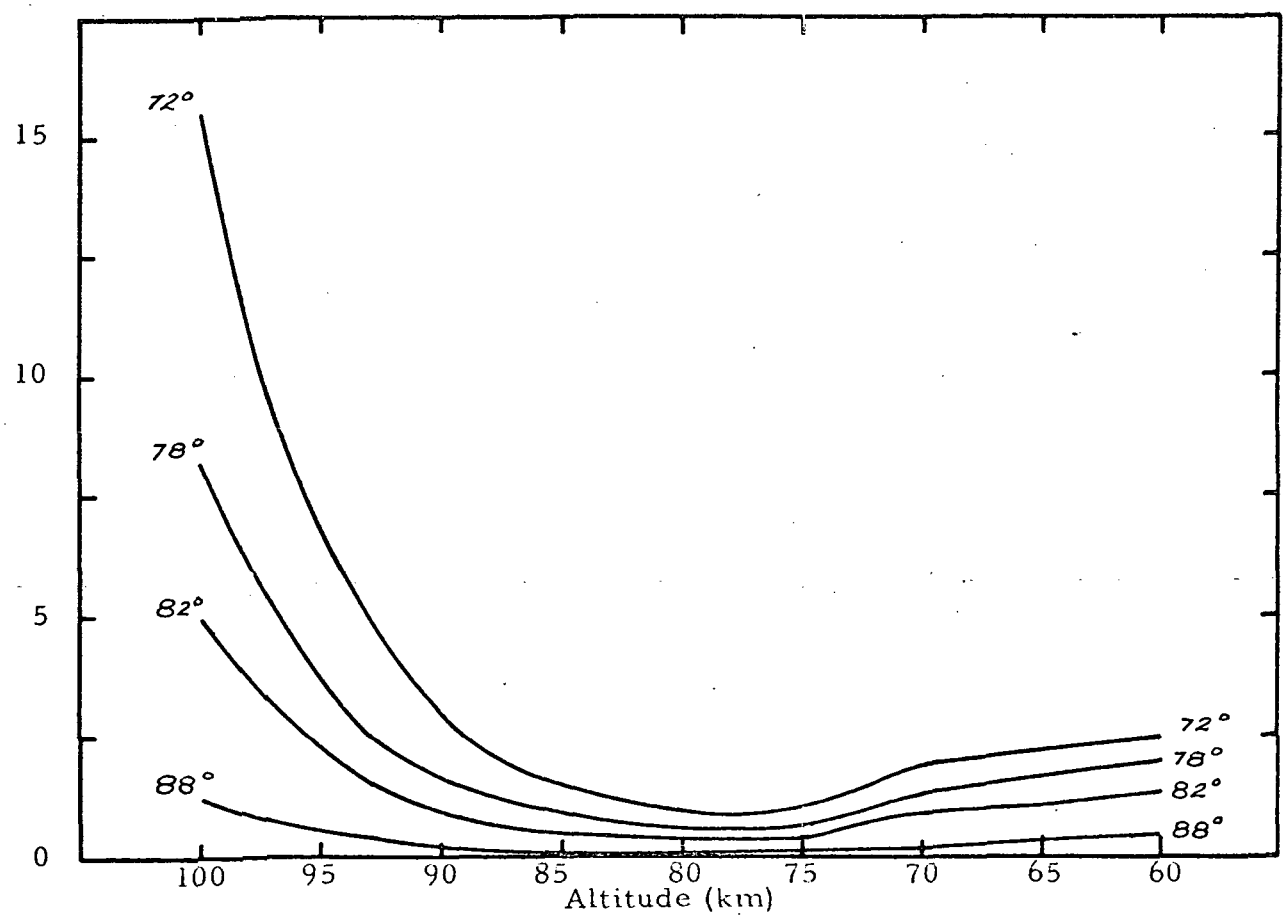

Figure 18 Noise Error in Density as a Function of Launch Elevation (Range-Rate Radars

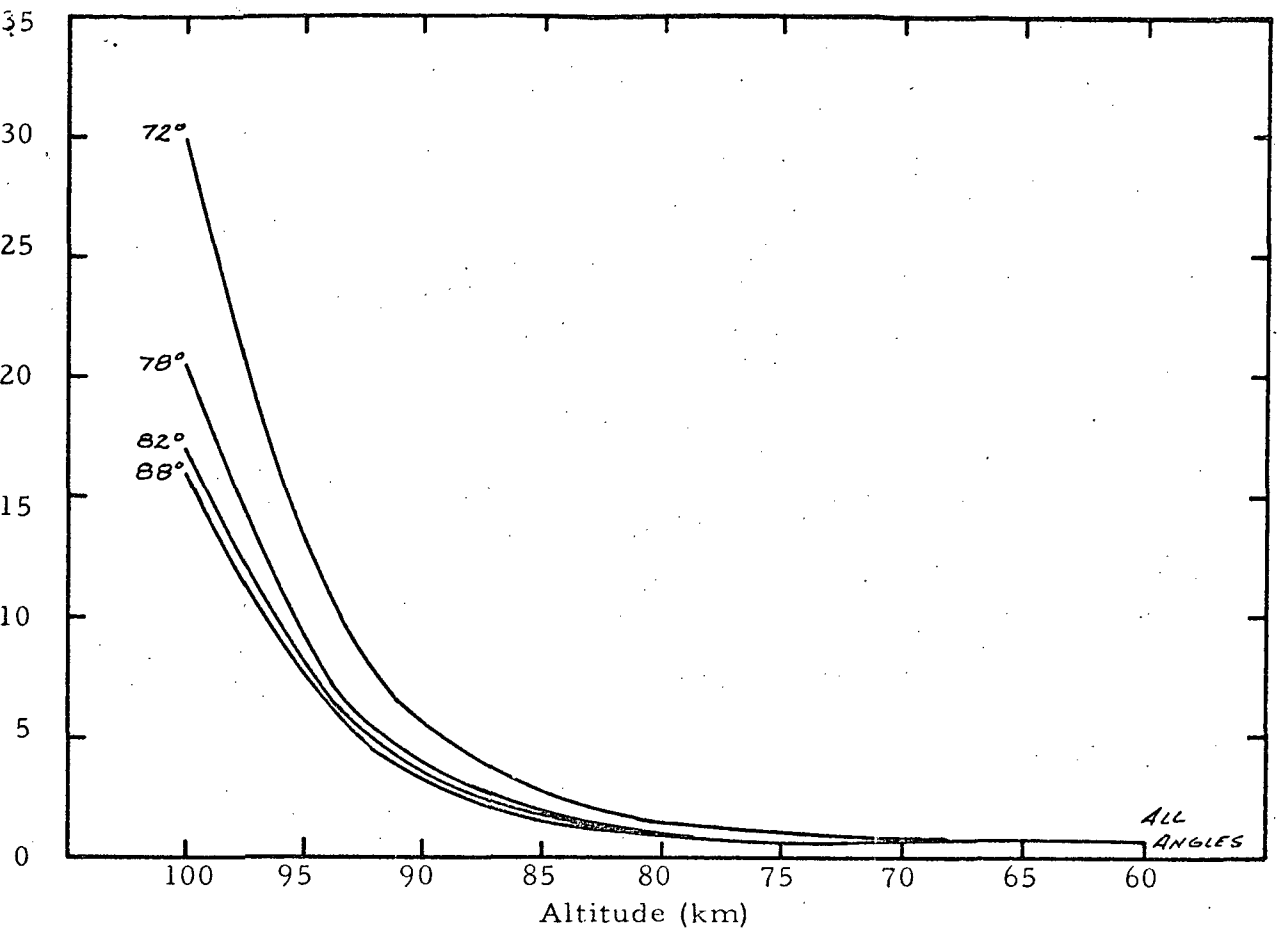

Figure 19 Noise Error in North Wind as a Function of Launch Elevation (Range-Rate Radars)

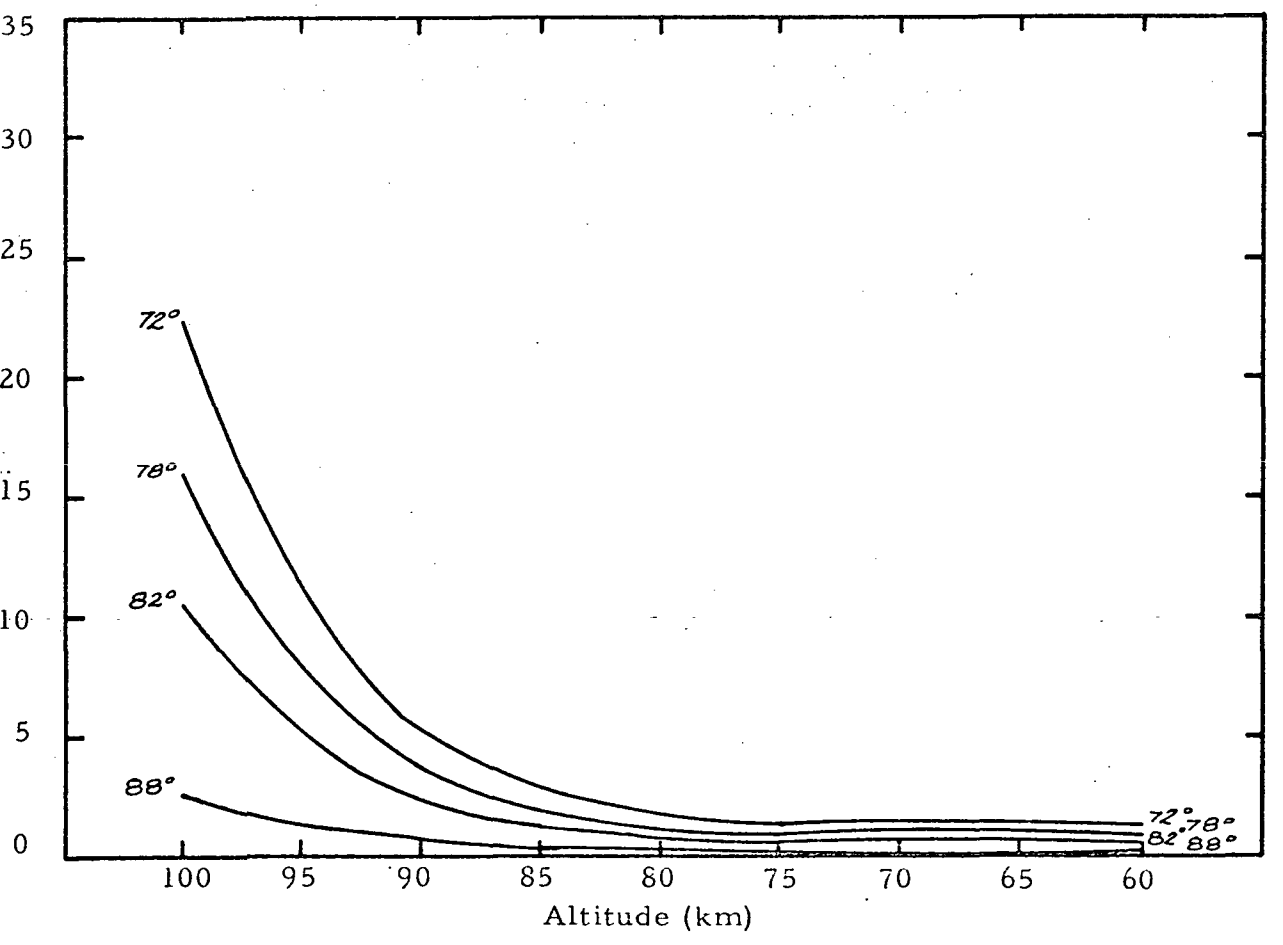

Figure 20 Noise Error in East Wind as a Function of Launch Elevation (Range-Rate Radars)

rapidly decreases. At 100 kilometers the noise error in the density is 24% for the 72^{o} launch, but only 4% for the 88^{o} launch. In these cases more of the balloon motion soon after apogee appears to the radar as angular motion. Moving to lower altitudes, the noise error for all launch angles diminishes rapidly to a minimum at about 77 kilometers. Here the 72^{o} error is less than 2% and the 88^{o} error almost 1/2%. By 60 kilometers the 72^{o} error is about 3% and the 88^{o} about 1%, so at the lower altitudes the improvement in noise error is not as great as at higher altitudes. The noise error in North, or downrange, wind speed error, Figure 16, shows much less dependence on launch elevation angle. At altitudes above 80 or 85 kilometers, the higher elevation angles do result in lower noise error, but the overall wind accuracy is so poor as to make the ROBIN-slant range-radar combination of little value as a downrange wind sensor above, say, 90 kilometers. At altitudes below 80 kilometers, downrange wind error is very low, about 1 m/sec for all four elevation angles for this wind field. The accuracy situation at high altitudes is somewhat improved in the cross-range (East) wind case. Here the three lower launch angles, 72^{o}, 78^{o}, and 82^{o}, still have wind speed errors much greater than ten meters per second at 100 kilometers, but the 88^{o} launch angle has improved the high altitude accuracy considerably, having a 1 σ error of only five meters per second at 100 kilometers. Lower altitudes, again, show better accuracy of a few meters per second for each angle.

The considerable difference in the high altitude noise errors in the North and East winds may be explained as follows. The North (downrange) wind is derived from a change in the North-South position of the ROBIN which is measured by changes in both range and elevation angle from the radar. Thus, the error in the North wind is determined by errors in range and elevation angle. Under the launch angles specified, the range error makes the larger contribution to wind error. On the other hand, the East (cross-range) wind is derived from a change in the East-West position of the ROBIN which is measured by a change in the azimuth angle of the radar. The error in the East wind, then, is determined by the error in the azimuth angle. This error is smaller than the constant six-meter error in range which composes the greater portion of the error in the North wind. Thus, the error in the East wind is less than the error in the North wind, under the assumption of a launch in the North-South direction (see Figures 16 and 17). In addition, because the error in the East wind depends upon angular errors, this wind is therefore more sensitive than the North wind to launch elevation angle.

Range-rate radars. --The effect of launch elevation angle on density error for range-rate radar systems, as shown in Figure 18, is much the same as the effect for slant range radars. Increased accuracy throughout the flight is obtained by using higher elevation angles, with the most improvement found above 85 kilometers. The curve representing the noise error for the 88^{o} launch elevation shows that error in density can be reduced to below

1% for the entire flight when this nearly perpendicular launch angle is used.

Component wind speed noise error versus altitude is plotted in Figures 19 and 20 for North (downrange) and East (crossrange) wind, respectively. The behavior with launch elevation is again similar to the slant range radar case; the major difference between them being only the overall improvement in accuracy gained by the use of range-rate tracking.

Wind Structure

To examine the effect of the magnitude of the wind field and its direction on noise errors in winds and density, trajectories were simulated using various wind structures. Three orientations were chosen of the wind structure used for the elevation angle study. The first orientation, called A, was the original orientation of the sinusoidal wind blowing North and the multi-segmented linear wind blowing East. Orientation B results from a 180° change of direction of both winds so that the sinusoidal wind is directed South and the linear wind West. Orientation C is an interchange of the two wind components, i.e., the sinusoidal wind blows East and the linear North. Figure 21 presents the three situations.

One can see from Figure 21 that if we regard orientation A as a launch with azimuth angle of 0°, orientation B is a launch with azimuth of 180°, and C is a launch with azimuth 90°. The effect of these various wind directions on noise in wind and density was examined for both slant range and range-rate radar systems using RFEP3 and RFEP4 to plot, as for the elevation angle study, the noise error versus altitude. Figures 22, 23,

and 24 show the results for slant range radars and 25, 26 and 27 for range-rate radars. In each case a launch elevation angle of 82^{o} was used.

Slant range radars and range-rate radars. --From the six figures, 22 through 27 it is readily seen that the effect of launch azimuth angle on noise error in winds and density is quite negligible. The difference between the 1 σ values for each orientation is in nearly all cases too small to appear on the scale of the plot. This result indicates that at altitudes above about 50 kilometers the magnitude and direction of the wind field has little influence on the noise error in winds.

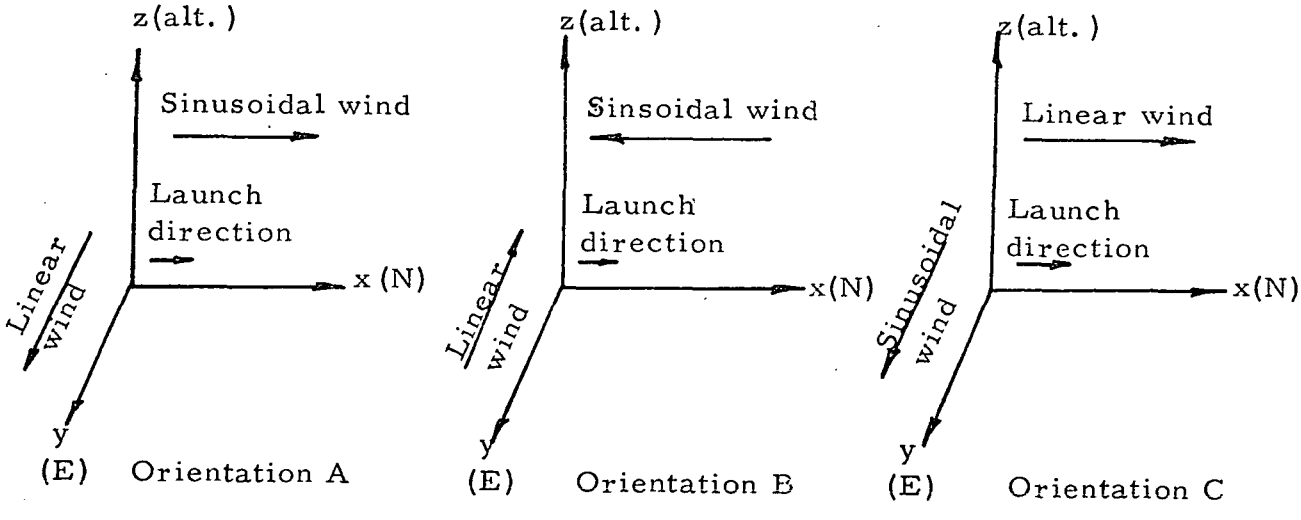

Figure 21 Wind Field Orientations for the Study of Wind Direction Effects.

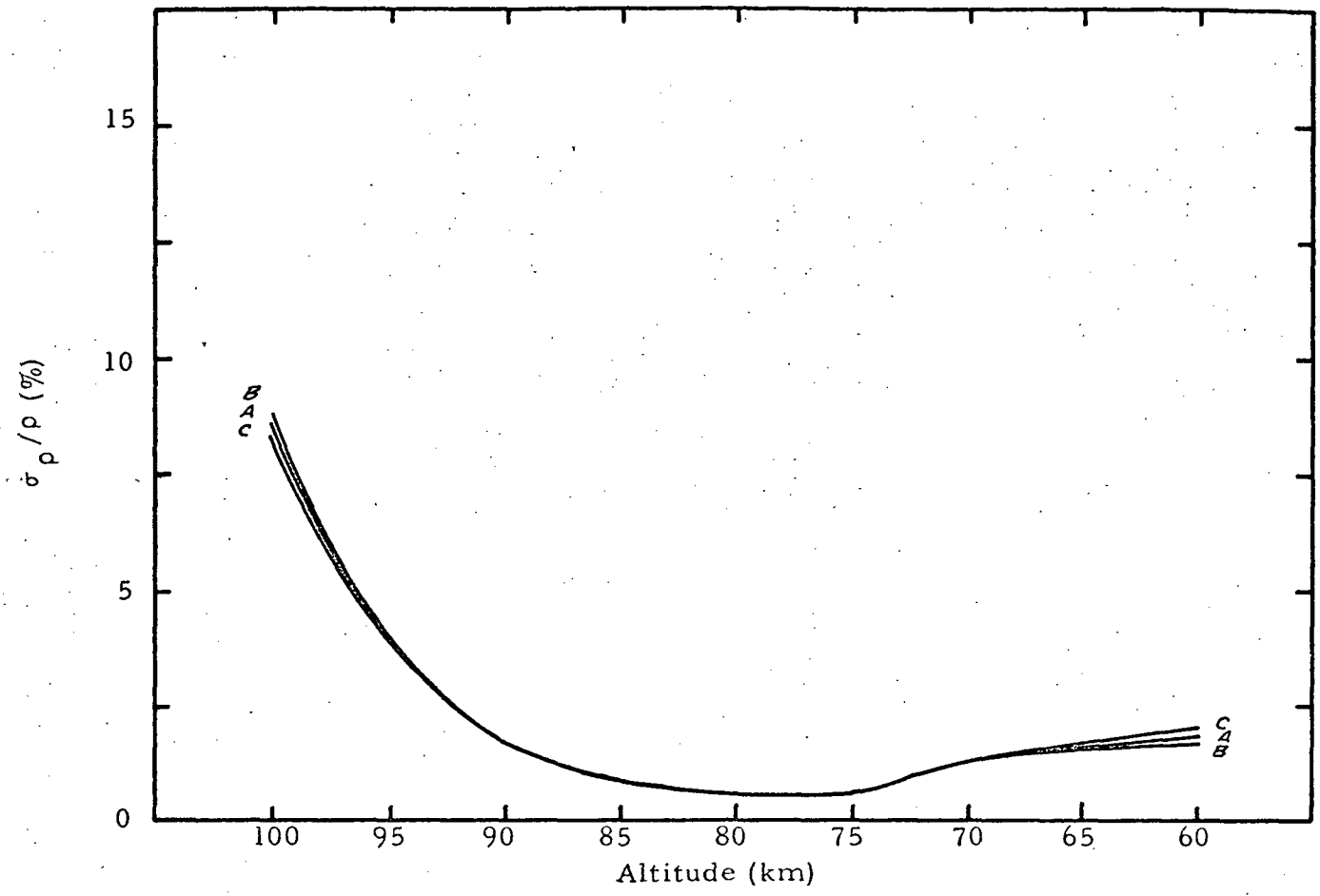

Figure 22 Noise Error in Density for Various Launch Directions (Slant Range Radars

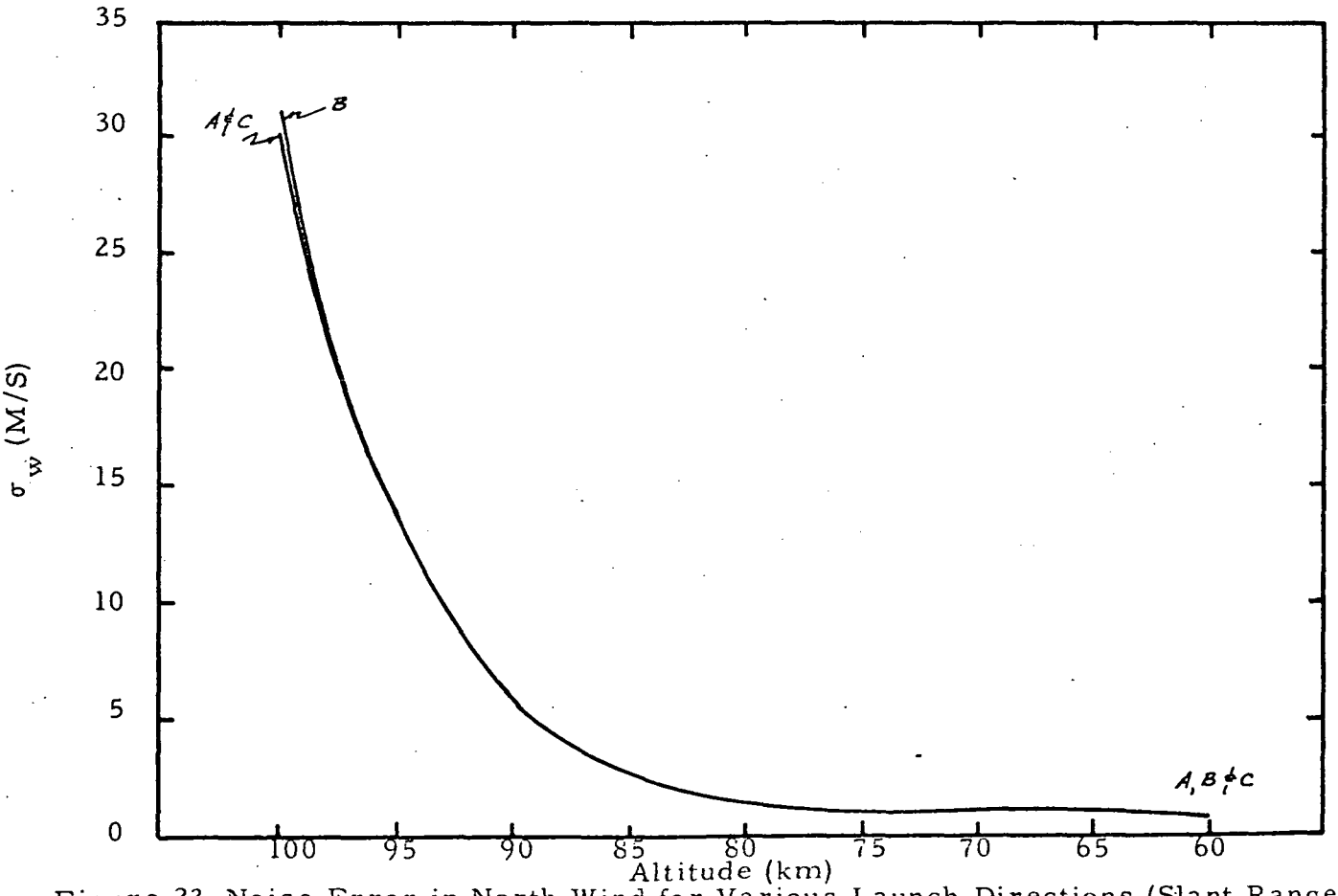

Figure 23 Noise Error in North Wind for Various Launch Directions (Slant Range Radar

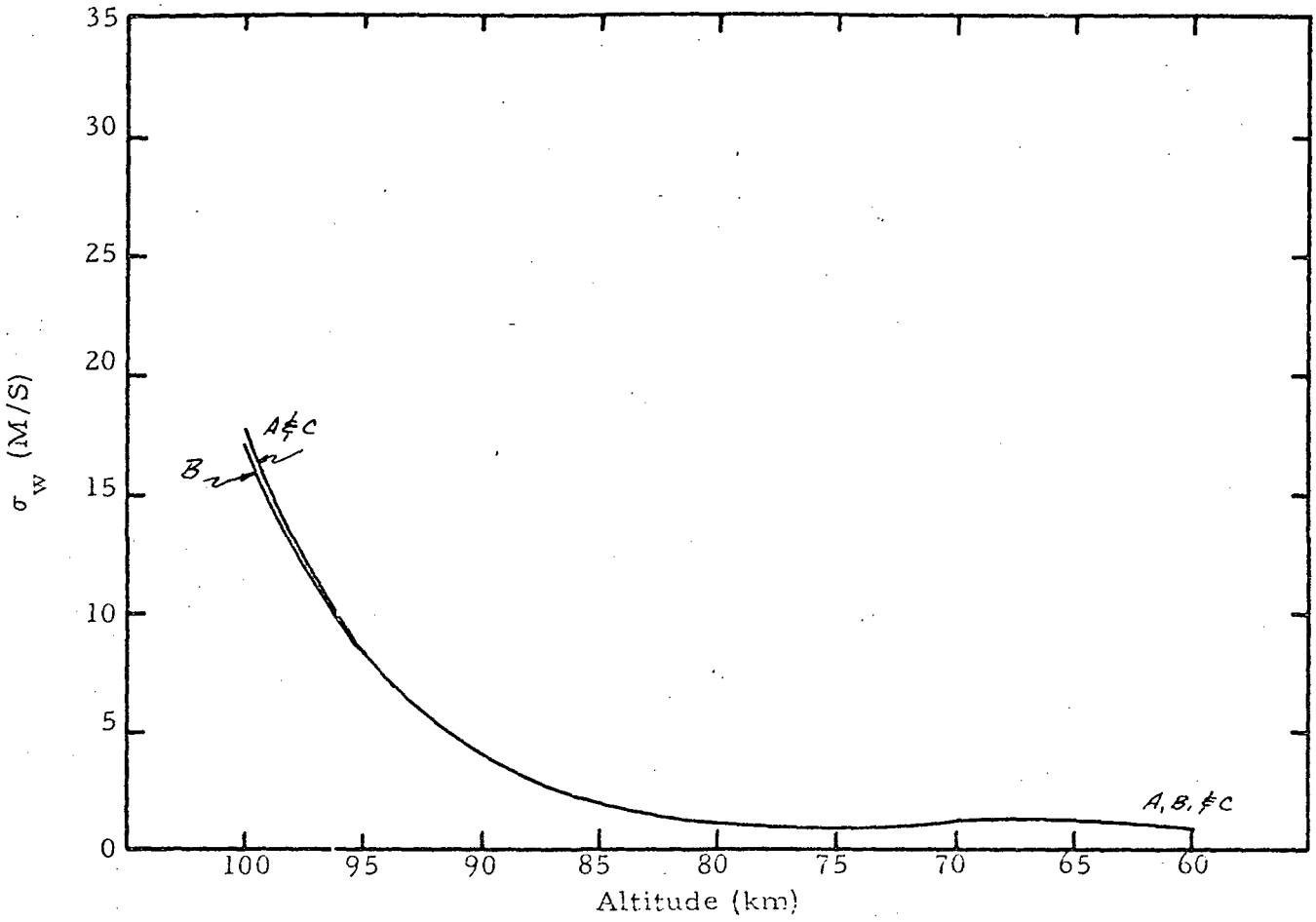

Figure 24 Noise Error in East Wind for Various Launch Directions (Slant Range Radar

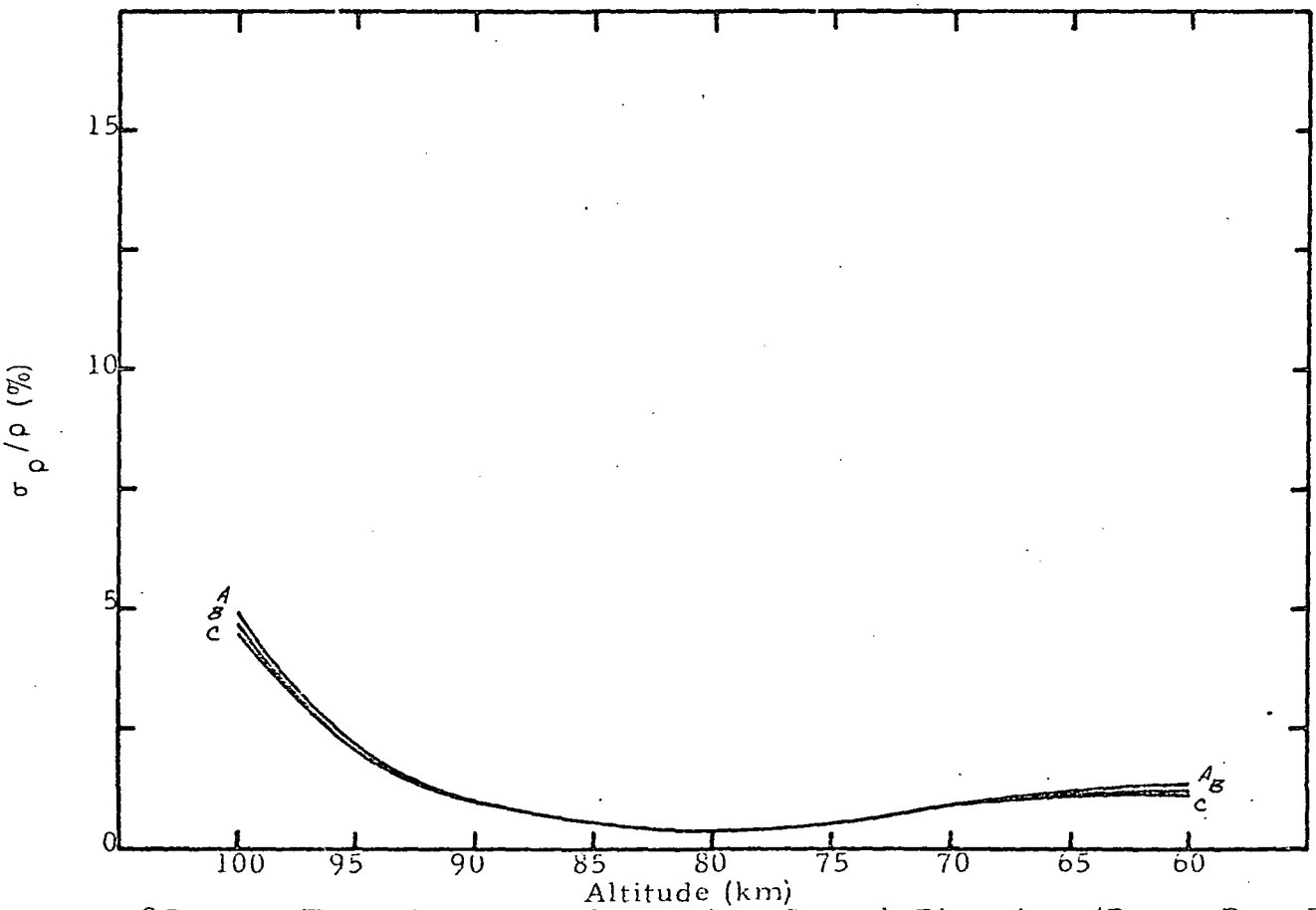

Figure 25 Noise Error in Density for Various Launch Directions (Range-Rate Radars)

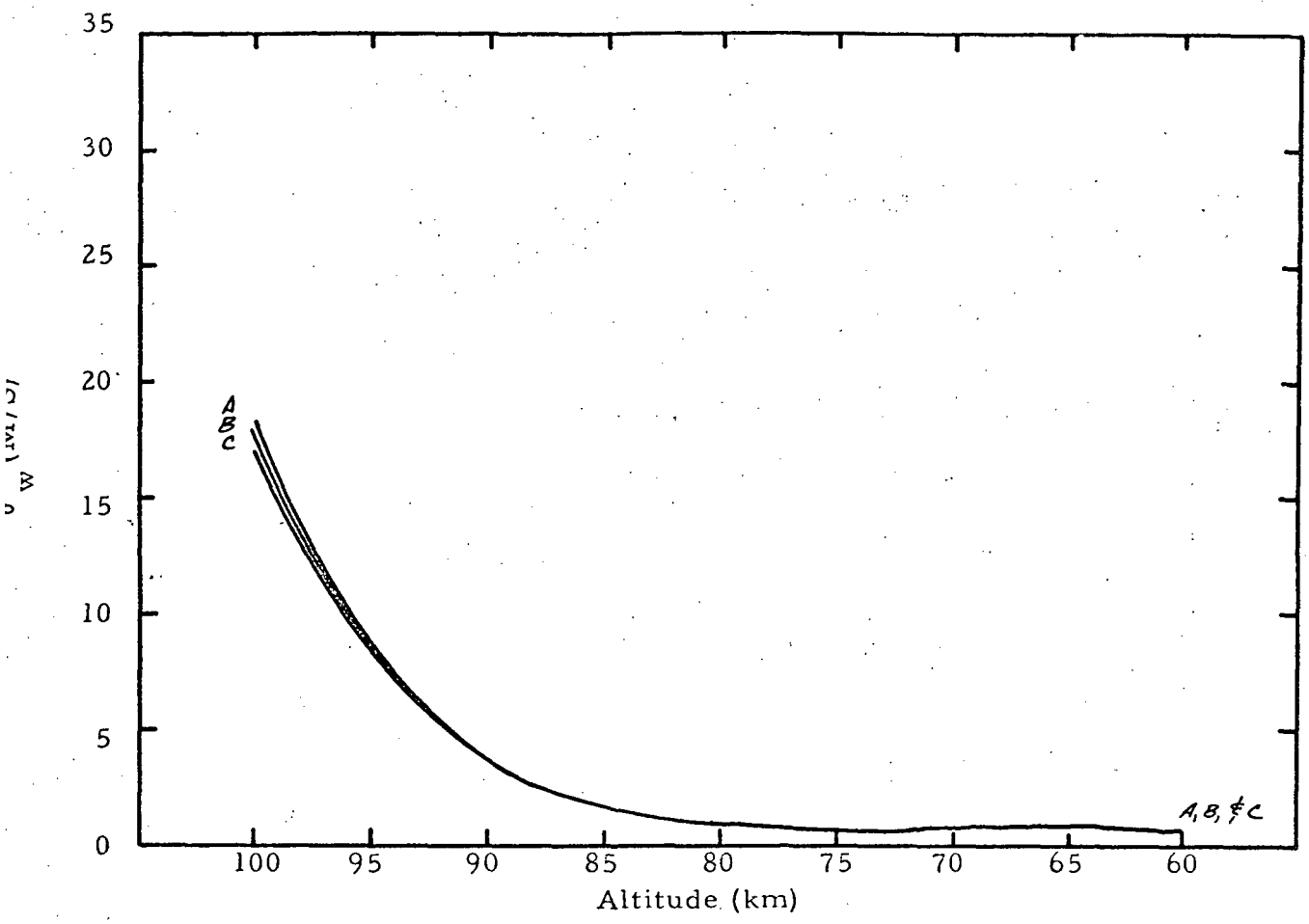

Figure 26 Noise Error in North Wind for Various Launch Directions (Range-Rate Radars)

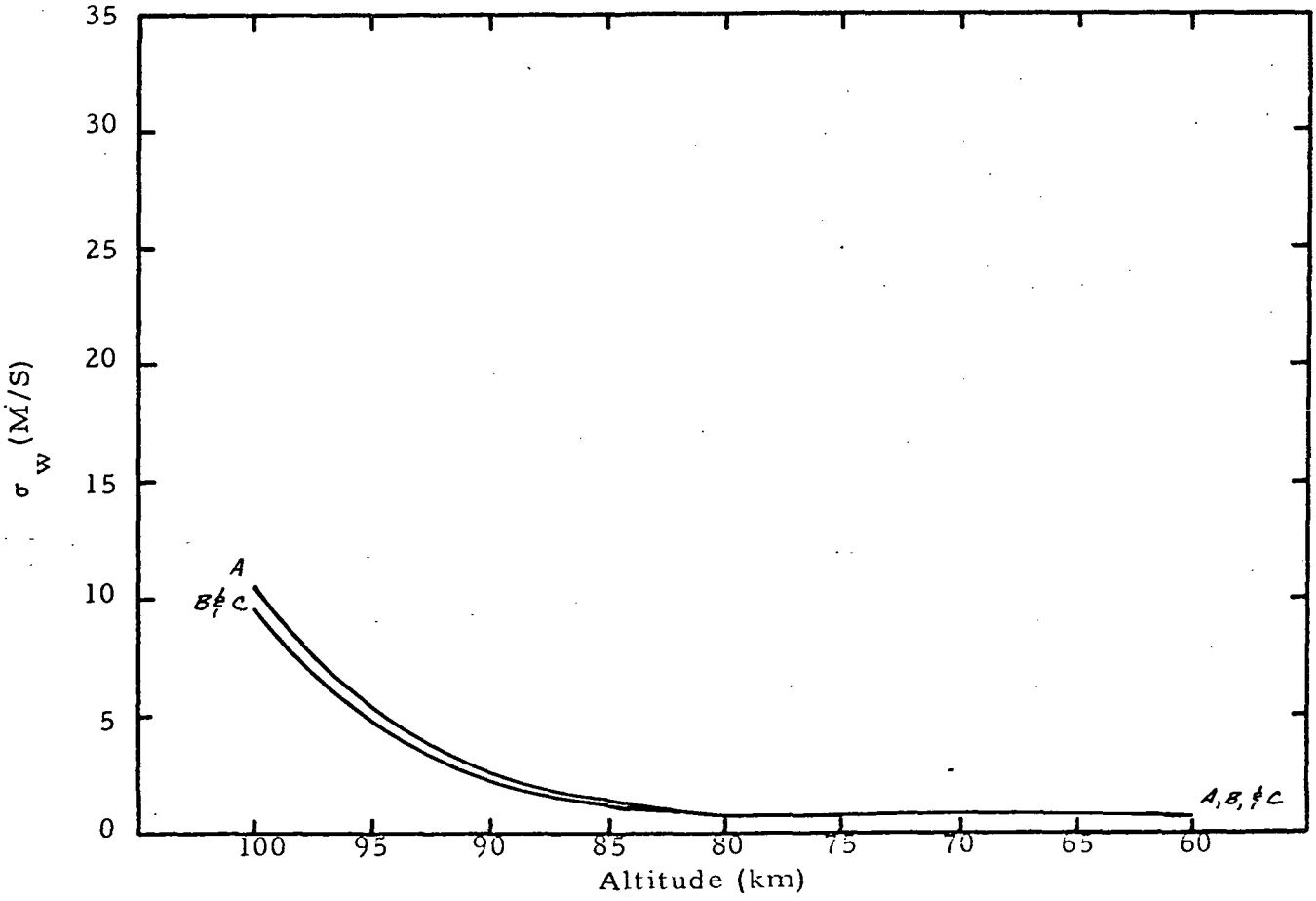

Figure 27 Noise Error in East Wind for Various Launch Directions (Range- Rate Radar)

Summary

The investigation of the effects of launch elevation, launch azimuth, and wind structure on the noise error in winds and density revealed several useful points. With regard to the elevation angle, it was found that with each radar better accuracies were achieved with launch elevations near the vertical. This fact is not surprising, as mentioned above, since higher launch elevations result in balloon descents closer to the radar, thus reducing the effects of angular error. The improvement became proportionately greater with greater elevation angles for both varieties of radar. With regard to launch azimuth, it was found that crossrange winds can be measured more accurately than downrange winds. This results because changes in downrange measurements are observed by a radar in its range and elevation measurements while the crossrange effects are observed by the azimuth of the radar. Consequently, if the east-west wind is desired to maximum accuracy, the launch should be directed in a northerly or southerly direction, and vice-versa.

CONCLUSIONS AND RECOMMENDATIONS

The study of radars, filters, and launch conditions for the ROBIN passive sphere system has revealed several heretofore unsuspected conclusions and confirmed some others which were already held. The study has shown how the present FPS-16 ROBIN system can best be utilized as well as indicating how an improved system which provides more accurate winds and densities can most economically be achieved.

A summary of the conclusions of this study and recommendations for further research are presented below:

1) Improved accuracy of the FPS-16 radar passive sphere system is most economically achieved by a Doppler measurement of range-rate. Modified FPS-16 radars that include a Doppler measurement are presently in existence. To date they have not been fully utilized to provide optimum density and wind reduction.

2) Radar measurements of angular rate, or angular acceleration are not economically feasible. It is more economical to measure angles by radar and numerically differentiate to determine angular rates and accelerations.

3) The effect of correlated errors in accelerations from double smoothing has been determined and expression derived to calculate its effect. The effect of correlated errors in acceleration was not considered in Reference 2. The resulting estimate of wind and density errors for double smoothing technique is somewhat higher than that shown in Reference

2, particularly above 80 kilometers. Nevertheless, the conclusion that the 19-21 linear-cubic provides optimum density measurements is still valid, even after including the correlated errors term.

4) With the FPS-16 tracking system both density and wind accuracy can be improved by launching at a higher elevation angle. Launching at 88 degrees improves density accuracy by a factor of three or more over a 78 degree launch. Improved wind accuracy is also significant - especially in the cross-range direction.

5) With the FPS-16 tracking system the cross-range component of winds can be measured to higher degrees of accuracy than can the down-range component.

6) The magnitude and direction of the wind profile has no significant effect upon the accuracy that can be achieved in measuring the profile.

7) There is no significant difference between wind and density accuracy resulting from smoothing on R, E, and A coordinates and smoothing on x, y, z coordinates. Since the transformation equations are simpler for x, y, z smoothing, this is the recommended smoothing procedure.

In addition to the above conclusions, the following items warrant further investigation:

a) The feasibility of installing a Doppler measurement device on all FPS-16 radars that are used for tracking passive spheres.

b) Incorporating into the High Altitude ROBIN Program an optimum filter for winds and density measurements when tracking with a Doppler radar.

c) The feasibility of using a mini-computer, on a real-time basis, to predict the trajectory of a sphere from its equations of motion and past history and then using the predicted trajectory to augment the tracking capabilities of the radar.

REFERENCES

1. "Federal Plan for Upper Air Observations Above 30 Kilometers," Washington D.C., July 1969, OFCM 69-7.

2. "A Method of Computing Winds, Density, Temperature, and the Associated Errors from the High Altitude ROBIN Sphere Using an Optimum Filter," James K. Luers, University of Dayton Research Institute, AFCRL-70-0366, July 1970.

3. "On Optimum Methods of Obtaining Wind Data from Balloon Sensors," J. Luers and N. Engler, Journal of Applied Meteorology, Vol. 6, No. 5, October 1967, pp. 816-823.

APPENDIX A

DERIVATION OF FREQUENCY RESPONSE $f(\omega, Q)$

Assuming the Doppler radar measures directly without distortion of frequencies of interest, then discounting noise, the radar output of the sinusoidal wave $R = A\sin(2\pi\omega t)$ is of the form:

$$\dot{R} = 2\pi\omega A\cos(2\pi\omega t) \quad .$$

Using moving averages, $\dot{R}_D^*$ is calculated as

$$\dot{R}_D^* = \frac{1}{Q}\sum_{i=1}^{Q} 2\pi\omega A\cos(2\pi\omega t_i) \quad . \qquad (A\text{-}1)$$

If Δt is the time spacing between data points, then Equation (A-1) can be rewritten as:

$$\dot{R}_D^* = \frac{1}{Q}\sum_{i=-\frac{Q-1}{2}}^{\frac{Q-1}{2}} 2\pi\omega A\cos(2\pi\omega i\Delta t + \beta) \qquad (A\text{-}2)$$

where β is the phase shift required so that time = 0 is on the same point of the curve previously occupied by time = $t_{\frac{Q-1}{2}}$.

By trigonometric identities, Equation (A-2) simplifies to:

$$\dot{R}_D^* = \frac{2\pi\omega A\cos\beta}{Q}\left\{\frac{\sin\frac{Q\,2\pi\omega\Delta t}{2}}{\sin\frac{2\pi\omega\Delta t}{2}}\right\} \quad .$$

The frequency response is given as the ratio of the smoothed $\dot{R}_D^*$ to the

true $\dot{R}$. The true $\dot{R}$ at the midpoint of the interval (i.e., t = 0 after the translation by β) is $\dot{R} = 2\pi\omega A \cos\beta$.

Thus,

$$f(\omega, Q) = \frac{\dot{R}_D^*}{\dot{R}} = \frac{1}{Q}\left\{\frac{\sin(Q\pi\omega\Delta t)}{\sin(\pi\omega\Delta t)}\right\} \quad . \qquad \text{(A-3)}$$

APPENDIX B

DERIVATION OF THE NOISE ERROR VARIANCE FOR DOUBLE POLYNOMIAL SMOOTHING

The double polynomial smoothing technique consists of the determination of a velocity from a linear combination of position points and the determination of an acceleration from a second linear combination of velocity points. The linear nature of this process allows one to calculate the error variances in velocity and acceleration by applying the smoothing technique directly to the assumed errors in position. Noise error in position is assumed to be normally distributed with a mean of zero, and no correlation is assumed to exist between noise error in different data points.

Let $\{\delta x_r\}$ be the set of all position errors in any of the three position coordinates. By our assumptions above, $E(\delta x_r) = 0$ for all r. So we have var $(\delta x_r) = \sigma_x^2 = E[(\delta x_r)^2]$ for all r. Also, let $\{\delta \dot{x}_j\}$ and $\{\delta \ddot{x}_p\}$ be the sets of noise errors in velocity and acceleration. We wish to determine var$(\delta \dot{x}_j)$ $= \sigma_{\dot{x}}^2$ and var $(\delta \ddot{x}_p) = \sigma_{\ddot{x}}^2$. The double polynomial smoothing technique determines members of the set $\{\delta \dot{x}_j\}$ in the following manner: For an N, M double polynomial filter with a slide of S, the first velocity error $\delta \dot{x}_1$ is formed by

$$\delta \dot{x}_1 = \sum_{i=1}^{N} a_i \delta x_i \qquad (1)$$

where $\{a_i\}$ are the weighting coefficients resulting from the Legendre polynomial fit of position points to obtain velocity. To determine $\delta \dot{x}_2$ the first

S position errors are discarded and the next S position errors (in chronological order) are added so that

$$\delta\dot{x}_2 = \sum_{i=1}^{N} a_i \delta x_{i+S} \quad . \tag{2}$$

In general,

$$\delta\dot{x}_j = \sum_{i=1}^{N} a_i \delta x_{i+(j-1)S} \qquad j = 1, M \quad . \tag{3}$$

A single acceleration error is then formed by

$$\delta\ddot{x} = \sum_{j=1}^{M} b_j \delta\dot{x}_j \tag{4}$$

where $\{b_j\}$ are the Legendre coefficients from the acceleration smoothing.

Finding $\sigma_{\dot{x}}^2$ in terms of σ_x^2:

$$\mathrm{var}(\delta\dot{x}_j) = E\left[\left(\sum_{i=1}^{N} a_i \delta x_{i+(j-1)S}\right)^2\right] = \sum_{i=1}^{N} a_i^2 E\left[\left(\delta x_{i+(j-1)S}\right)^2\right] \tag{5}$$

since $\mathrm{cov}(\delta x_i \delta x_j) = 0$ for $i \neq j$. Thus,

$$\sigma_{\dot{x}}^2 = \sigma_{\dot{x}j}^2 = \sum_{i=1}^{N} a_i^2 \sigma_x^2 \qquad \text{for all } j. \tag{6}$$

To find $\sigma_{\ddot{x}}^2$ in terms of $\sigma_{\dot{x}}^2$, we apply the definition of the variance again:

$$\sigma_{\ddot{x}}^2 = E\left[\left(\sum_{j=1}^{M} b_j \delta\dot{x}_j\right)^2\right] \tag{7}$$

But since velocity errors are correlated by the sliding nature of the smoothing, $\text{cov}(\delta\dot{x}_i\ \delta\dot{x}_j) \neq 0$ for $i \neq j$, or

$$\sigma_{\dot{x}}^2 = \sum_{j=1}^{M} b_j^2\ \sigma_{\dot{x}}^2 + \sum_{j \neq k}^{M} \sum b_j\ b_k\ \rho_{jk}\ \sigma_{\dot{x}}^2 \quad , \tag{8}$$

where $\rho_{jk} \equiv E(\delta\dot{x}_j \cdot \delta\dot{x}_k) \ / \ \sigma_{\dot{x}}^2$. (9)

To find ρ_{jk} for $j \neq k$, we may substitute (3) into (9)

$$\rho_{jk} = \frac{1}{\sigma_{\dot{x}}^2} \cdot E\left[\left(\sum_{i=1}^{N} a_i\ \delta x_{i+(j-1)S}\right)\left(\sum_{i=1}^{N} a_i\ \delta x_{i+(k-1)S}\right)\right] \tag{10}$$

$$= \frac{1}{\sigma_{\dot{x}}^2} E\left[\sum_{i=1}^{N} a_i^2\ \delta x_{i+(j-1)S} \delta x_{i+(k-1)S} + \sum_{i \neq q}^{N} \sum a_i\ a_q\ \delta x_{i+(j-1)S} \delta x_{q+(k-1)S}\right] \tag{11}$$

$$= \frac{1}{\sigma_{\dot{x}}^2}\left[\sum_{i=1}^{N} a_i^2\ E\left(\delta x_{i+(j-1)S}\ \delta x_{i+(k-1)S}\right)\right]$$

$$+ \frac{1}{\sigma_{\dot{x}}^2}\left[\sum_{i \neq q}^{N} \sum a_i a_q E\left(\delta x_{i+(j-1)S} \delta x_{q+(k-1)S}\right)\right] \tag{12}$$

The first term on the right hand side of (12) is non-zero only if j=k since any two different δx_i are not correlated. However ρ_{jk} $j = k$ are not of interest. Using the same argument, the second term is non-zero only for combinations of i, q, j, and k such that

$$i + (j-1)S = q + (k-1)S \tag{13}$$

or

$$i - q = (k-j)S \tag{14}$$

Therefore the only non-zero terms of the double summation are those in which the subscripts of the a's are different by an integral multiple of S, the particular value of this multiple depending upon the values of j and k. If, for example, $(k-j)S = 2$ the double summation term, which is ρ_{jk}, can be written out as

$$\rho_{jk} = [a_1 a_3 + a_2 a_4 + \ldots + a_{N-2} a_N] \frac{\sigma_x^2}{\sigma_{\cdot}^2 x} \quad . \quad S(k-j) = 2 \tag{15}$$

Similarly, if $(k-j)S = -2$, the expression for ρ_{jk} is

$$\rho_{jk} = [a_3 a_1 + a_4 a_2 + \ldots a_N a_{N-2}] \frac{\sigma_x^2}{\sigma_{\cdot}^2 x} \quad . \quad S(k-j) = -2 \tag{16}$$

Comparison of (15) and (16) shows that for a given S

$$\rho_{jk} = \rho_{kj} \quad . \tag{17}$$

A simpler expression for ρ_{jk} can be found by generalizing from (15), (16), and (17).

$$\rho_{jk} = \left[\sum_{i=1}^{N-c} a_i a_{i+c} \right] \frac{\sigma_x^2}{\sigma_{\cdot}^2 x} \tag{18}$$

where $c = |S(j-k)|$.

Equation (18) can be further simplified by recalling Equation (6),

$$\sigma_{\dot{x}}^2 = \sum_{i=1}^{N} a_i^2 \, \sigma_x^2 \tag{6}$$

Substituting for $\sigma_{\dot{x}}^2$ in (18), we have

$$\rho_{jk} = \frac{\sum_{i=1}^{N-c} a_i \, a_{i+c}}{\sum_{i=1}^{N} a_i^2} \qquad c = |S(j-k)| \, . \tag{19}$$

Equation (19) for ρ_{jk} may then be used with (8) to express $\sigma_{\ddot{x}}^2$ in terms of $\sigma_{\dot{x}}^2$, and $\sigma_{\dot{x}}^2$ may be found in terms of σ_x^2 by Equation (6) so that the noise error variance in acceleration for double polynomial smoothing is determined.

A great deal of labor in computing values of ρ_{jk} can be reduced by noting that $S(j-k) = S[(j+1) - (k+1)]$ so that in general $\rho_{jk} = \rho_{j+1,\, k+1}$.

APPENDIX C

RADAR ANALYSIS OF THE AN/FPS-16 TRACKING A FALLING SPHERE

Aaron S. Soltes
Raytheon Company

1. INTRODUCTION

This report describes the results of a study aimed at enabling those interested in the falling sphere upper atmospheric sensing technique to utilize the AN/FPS-16 family of tracking radars to best advantage for trajectory measurements.

It includes an error analysis of the AN/FPS-16 radar tracking a nominal ROBIN falling sphere trajectory; an evaluation of the results; and recommendations on selection of type of sphere, settings of the radar, and existing modification to the AN/FPS-16 that should be employed, if available, to improve performance.

It is shown that the AN/FPS-16 radar, when properly employed, possesses the capability for measuring falling sphere trajectories to its rated precision. However, as an occasional user of the radar rather than its operator and maintainer, the meteorologist is cautioned that the methods at his disposal for controlling the quality of his measurements are of necessity limited, and that he had best take certain precautions. Furthermore, with so many AN/FPS-16 radar configurations in the field, it was necessary for a first analysis to treat the radar and its variations in a generalized way. Comments are offered as to how the performance of particular radars may be further optimized by individual attention.

2. RADAR ERROR ANALYSIS

The AN/FPS-16 family of radars have a rated precision or instrumental error of 0.1 mrad rms in angle and 5 yds rms in range. These figures are the minimum error levels of the radar design, achievable under optimum conditions with the equipment properly maintained and calibrated, and in the absence of error components that are a function of target dynamics, echo signal strength, and external environment. In practice, the optimum conditions under which rated precision is attainable prevail in only a portion of a radar's total volume of coverage, since performance is actually dependent upon the target cross-section, range, and dynamics, and the operating environment, all of which are outside the control of the radar designer.

In order to utilize the AN/FPS-16 radar to best advantage for falling sphere trajectory measurements, it is important to evaluate its performance in the context of that tracking task, and to determine the regions and under what conditions rated performance may be expected.

There are two general categories of errors associated with a tracking radar - fixed errors, which are essentially independent of the conditions under which the radar is operated, and variable errors which depend upon the conditions of operation. In the case of falling sphere measurements, it is recognized that the meteorologist is often but an occasional user of the radar, and therefore, has little control over the fixed errors that are primarily functions of design, maintenance, calibration, and environmental conditions. He does have some options, however, which enable him to minimize the

contributions from some of the sources of variable error, and we will concentrate on them.

(A) Radar Settings

The radar design incorporates several adjustable parameters which enable the operator to adapt its characteristics to a wide range of target characteristics. This permits some latitude in matching the radar to a particular task at hand in order to minimize target-dependent errors. In order to take advantage of the adjustable radar parameters it is necessary to determine the best settings to suit the falling sphere measurement application and to supply this information to the radar operator. Failure to guide the operator may result at best in measurements that do not fully utilize the capabilities of the system, or at worst in measurements that include unnecessary errors. As a minimum, the radar settings should be recorded with the data to permit post-flight analysis and check.

(B) Radar Modifications

At some sites, there are several tracking radars available, some of which incorporate modifications that would permit better performance for falling sphere measurements. An analysis of how the various existing AN/FPS-16 modifications affect its performance provides the basis for recommendations as to which modifications to employ for falling sphere measurements.

2.1 Assumed Conditions

The parameters and conditions of the radar, sphere trajectory, and sphere radar characteristics assumed for the purposes of the analysis are stated below.

2.1.1 Parameters of Basic AN/FPS-16

The significant radar parameters vary somewhat from one source of information to the other. The set of parameters utilized here are shown in Table 2.*

2.1.2 Falling Sphere Trajectory

The nominal sphere trajectory utilized in this analysis is the "Model Balloon Trajectory"** appended in tabular form in Table 1. It is plotted in Figure 1 showing points where maxima and minima occur. The plot is in the plane of the trajectory, and to facilitate computation the radar is assumed to be located at the origin of the coordinates.

The various parameters of the sphere trajectory, including slant range (R), range rate ($\dot{R}$), range acceleration ($\ddot{R}$), elevation angle (E), angle rate ($\dot{E}$), angle acceleration ($\ddot{E}$), and altitude are plotted as functions of time in Figures 2, 3 and 4 respectively.

2.1.3 Radar Characteristics of the Spheres

Two types of inflatable spheres are commonly used for falling sphere measurements - a metalized surface reflecting sphere, and a transparent sphere containing a corner reflector.

---

* See for example, Barton, D.K., Radar System Analysis, Prentice-Hall, Inc., Englewood Cliff, N.J., page 343.

** Received from N. Engler, UDRI by letter 1/5/71.

TABLE 2

Power output (P_T)	1.0 MW peak
Pulse Width (τ)	1.0 μsec
Repetition Rates (f_r)	160 to 1707 pps
Antenna Gain (G_o)	44.5 dB (12-foot reflector)
Antenna Beamwidth (θ_o)	1.1° (19.2 mrad)
Wavelength (λ)	5.3 cm (mid-band)
Receiver Bandwidth (β)	1.6 MHz
Receiver Noise Factor ($\overline{NF}$)	11 dB
Plumbing & Duplexer-losses (L)	4 dB
Angle Tracker	
Velocity Lag Error ($1/K_V$)	0.0033 mrad/mrad/sec
Acceleration Lag Error ($1/K_A$)	0.016 mrad/mrad/sec^2
Servo Bandwidths (β_n)	0.5→ 6 Hz
Range Tracker	
Velocity Lag Error ($1/K_v$)	0.00018 m/m/sec
Acceleration Lag Error ($1/K_a$)	0.00064 m/m/sec^2
Servo Bandwidths (β_n)	1.0→10 Hz

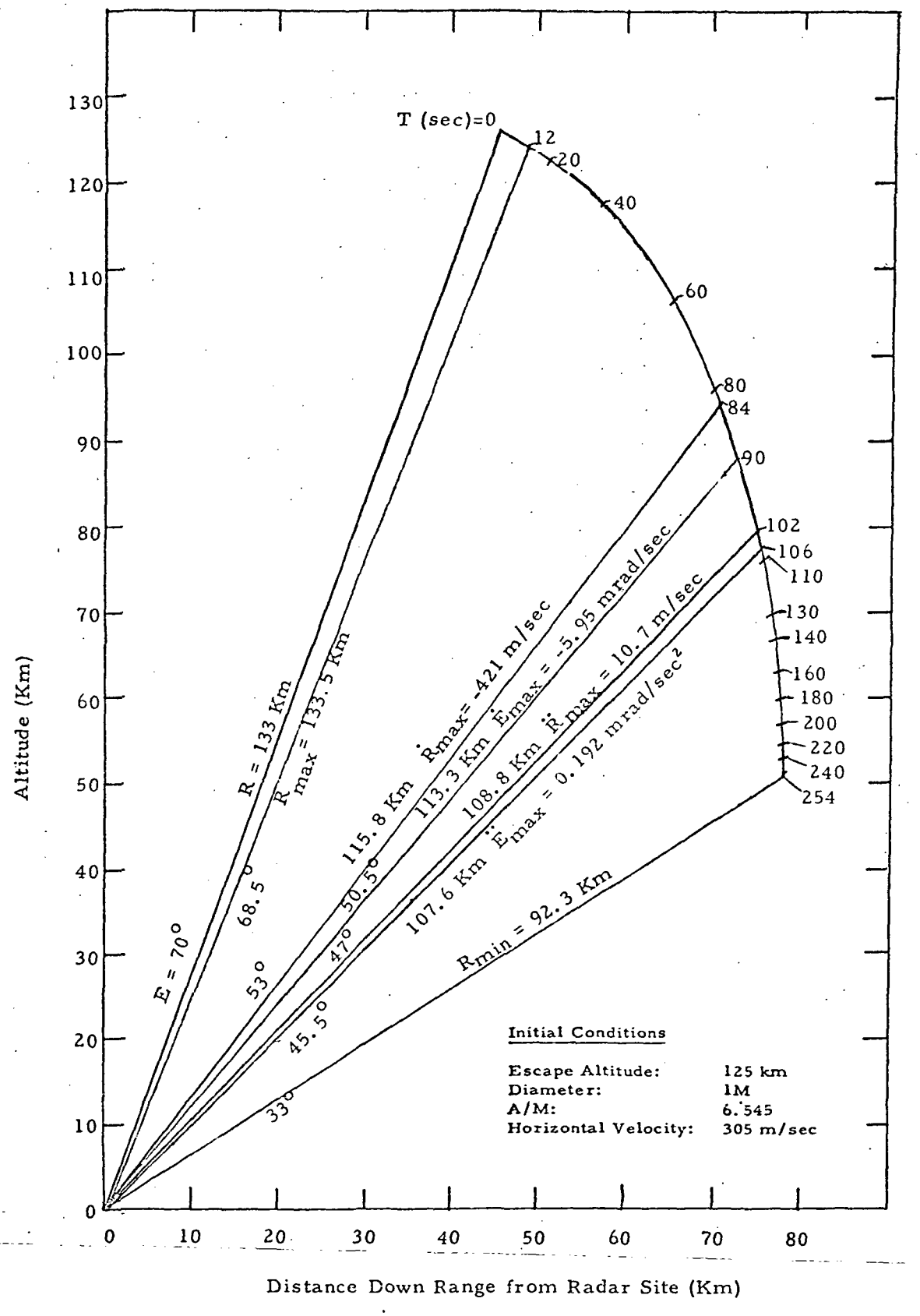

Figure 1. Model Balloon Trajectory (as observed from the origin in the plane of the trajectory).

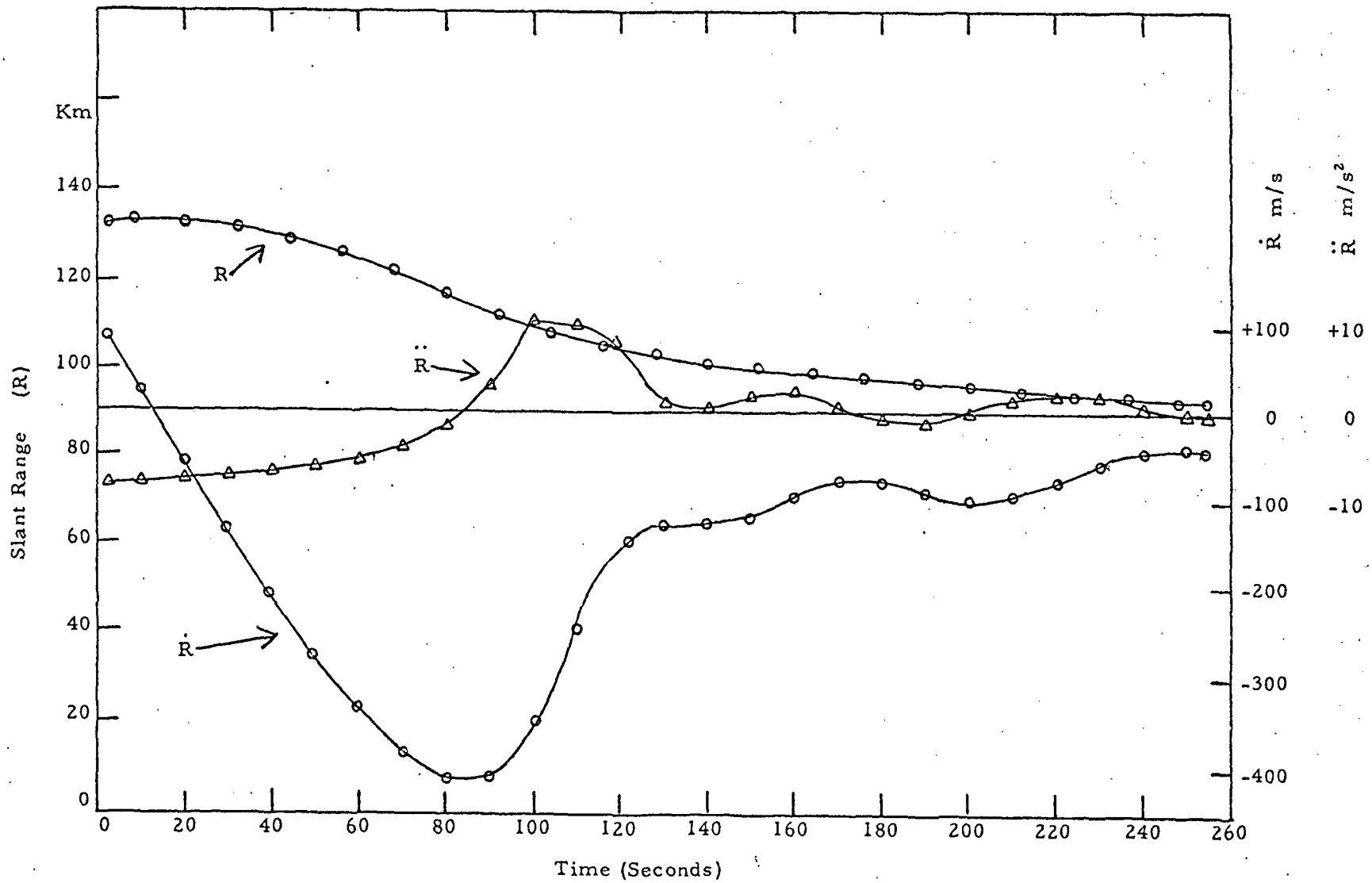

Figure 2. Slant Range, Range Rate, and Range Acceleration -vs- Time for the Model Balloon Trajectory of Figure 1.

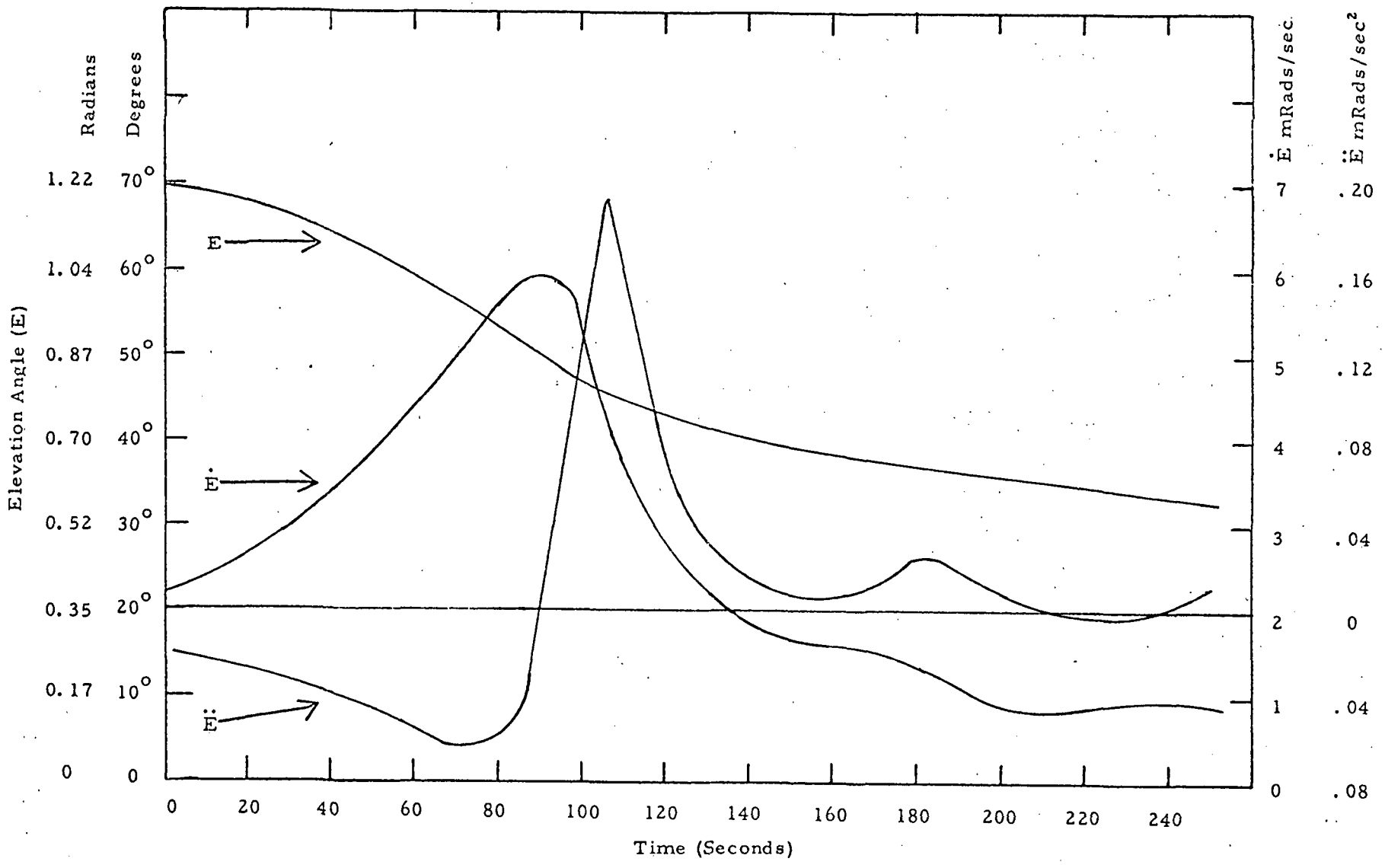

Figure 3. Elevation Angle, Angle Rate, and Angle Acceleration -vs- Time for the Model Balloon Trajectory of Figure 1.

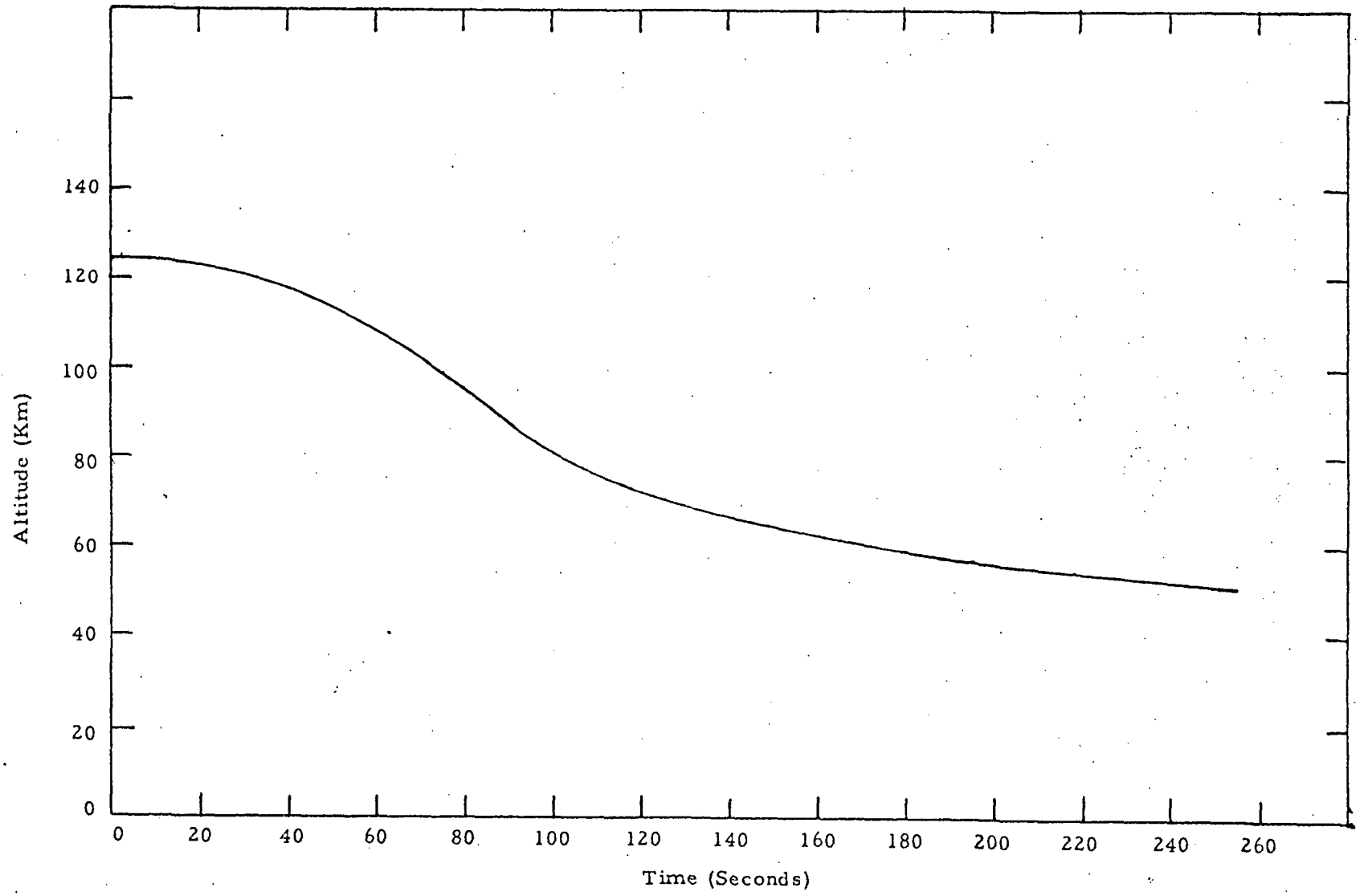

Figure 4. Altitude -vs- Time for Model Balloon Trajectory of Figure 1.

(1) A 1-meter diameter reflecting sphere has a calculated radar cross section of $\pi/4$ meter^2. This value is assumed. When, for convenience, the approximate value of 1 m^2 is used a 7% error in radar range calculations results.

(2) - ROBIN sphere with corner reflector. A 25 m^2 radar cross-section is assumed*.

2.1.4 Other Assumptions

This study is focused on those factors about which the meteorologist user has a choice, and of necessity assumes that all other sources of error, over which he has no control, are either absent or within the rated limits of the radar. Such factors include antenna alignment, bore-sighting, orthogonality, servo adjustment, data pick-offs, wind, mechanical and thermal deflections, etc.; range servo zeroing, jitter, receiver delay, servo adjustment, data read-out, etc.

It is also assumed that provision is made for refractive correction of the data; that the elevation angle of the target is sufficiently large to make multipath and residual refraction negligible; and that there is no discrete interference to degrade the measurements.

---

* See J. B. Wright, "A Summary of AFCRL Passive-Sphere Development Efforts and Experience", Proceedings of Symposium on Status of Passive Inflatable Falling Sphere Technology for Atmospheric Sensing to 100 km - NASA SP-219, Sept. 1969, p. 9.

2.2 Radar Error Sources Considered

The primary sources of radar error that have been considered are the target-dependent variable errors produced by target motion and thermal noise.

Target motion introduces dynamic lags in the angle and range servos as a function of the servo bandwidths, while thermal noise establishes the ultimate limiting factor by which the pulse width and the antenna beam width can be resolved to determine the target position coordinates. The thermal noise is evaluated in terms of the signal-to-noise-ratio (S/N) which is a function of the radar parameters in conjunction with the target radar cross-section and target range from the radar.

2.3 Radar Error Calculations

2.3.1 Preferred Settings of Console - Adjustable Parameters

Pulse Width (τ) - the pulse width is set at 1 μsec to provide an opportunity for good S/N.

PRF (f_r) With the 1 μsec pulse width, the PRF should be set as high as possible but not to exceed 1000 pps in order to provide the largest possible number of target hits per unit time without exceeding the duty cycle limit of 0.001. The maximum unambiguous range requirement of R_{max} = 133. km (see Figure 1) presents no problem, since it allows a maximum PRF of 1120 pps. The maximum available PRF not to exceed 1000 pps is f_r = 853.

Servo Bandwidths (β_n) - A time constant of 0.1 sec is desired, if it can be managed. The observation time, t_o, is established by the servo bandwidth and represents the integration time of the servo:

$$t_o = \frac{1}{2\beta_n}$$

Accordingly, a servo bandwidth of β_n = 5 Hz will be used to yield t_o = 0.1 sec.

2.3.2 Dynamic Lags

The dynamic lags produced by the maximum target dynamics are negligible compared with the fixed errors of the radar for the model trajectory and radar location of Figure 1.

From Figure 3, the maximum angle rate and acceleration occur at T = 90 secs. and T = 106 secs. respectively

$$\dot{E}_{max} = -5.95 \text{ mrad/sec. @ T} = 90 \text{ secs.}$$

$$\ddot{E}_{max} = +0.196 \text{ mrad/sec}^2 \text{ @ T} = 106 \text{ secs.}$$

Using the angle tracker lag coefficients of Table 2, the maximum angle lag errors are as follows:

Max. velocity lag error = $\dot{E}_{max}/K_V$ = 0.02 mrad

Max. acceleration lag error = $\ddot{E}_{max}/K_A$ = 0.0031 mrad.

Similarly, the maximum range rate and acceleration are, from Figure 2

$$\dot{R}_{max} = -421 \text{ m/sec } @ T = 84 \text{ secs.}$$

$$\ddot{R}_{max} = +10.7 \text{ m/sec}^2 @ T = 102 \text{ secs.}$$

Using the range tracker lag coefficients of Table 2, the maximum range lag errors are as follows:

Max. range lag error = $\dot{R}_{max}/K_v = 0.084$ meters.

Max. acceleration lag error = $\ddot{R}_{max}/K_a = 0.0075$ meters.

To investigate the possible impact of the radar-trajectory configuration of Figure 1 on the azimuth servo lags, let us assume that the trajectory is rotated 90^o around its initial point so that its plane is essentially normal to the radar line of sight. The maximum azimuth rate will occur at T = 0 secs when the horizontal velocity of the sphere is highest.

$$\dot{H} = 305 \text{ m/sec } @ T = 0 \text{ secs.}$$

$$\dot{A}_{max} = \frac{\dot{H}}{R} = \frac{305 \text{ m}}{133 \text{ km}} = 2.28 \text{ mrad/sec}$$

Max velocity lag error = $\dot{A}/K_V = 0.0076$ mrad/sec.

The azimuth angle lag is also negligible.

The total variable error remaining is that due to thermal noise.

2.3.3 Region of Optimum Accuracy Allowed by S/N

If we set the maximum angle error due to thermal noise to 0.1 mrad (so that the total error due to fixed and variable errors is $\sqrt{2}$ x 0.1 mrad),

$$\sigma_t = \frac{\theta_o}{\sqrt{2 S/N \, f_r/\beta_n}} = 0.1 \times 10^{-3}$$

and solve for the required S/N, using the values of $f_r = 853$, $\beta_n = 5$, and $\theta_o = 19.2$ mrad from Table 2 and 2.3.1 we get

$$S/N = \frac{1}{2}\left(\frac{\theta_o}{\sigma_t}\right)^2 \times \frac{\beta_n}{f_r}$$

$$= \frac{1}{2}\left(\frac{19.2 \times 10^{-3}}{0.1 \times 10^{-3}}\right) \times \frac{5}{853} = 104$$

$$= 20.2 \text{ dB}$$

The linear error at the target at the maximum range of $R_{max} = 133.5$ km (see Figure 1) due to the total elevation angle error of $\sqrt{2} \times 0.1$ mrad is

$$\sigma_z = R_{max} \times \sigma_E$$

$$= 133.5 \times 10^3 \times \sqrt{2} \times 0.1 \times 10^{-3} = 18.8 \text{ meters rms.}$$

We now evaluate the range error due to thermal noise with the same S/N, f_r and β_n

$$\sigma_{rt} = \frac{\tau}{\sqrt{S/N \, f_r/\beta_n}} = \frac{150}{\sqrt{\beta 04 \times 853/5}} \text{ meters rms}$$

$$= 1.13 \text{ meters rms.}$$

Together with an estimated fixed range error of 2 meters, this yields a total range error of

$$\sigma_{r\ total} = \sqrt{2^2 + 1.13^2} = 2.3 \text{ meters rms}$$

The next step is to substitute the parameters of the radar from Table 2 into the radar equation to determine the maximum ranges at which the two types of spheres can be tracked with a S/N of 20.2 dB.

$$R_{max} = \left[\frac{P_T G_o^2 \lambda^2 A_e}{(4\pi)^3 \, S/N \, KT \, \beta \, \overline{NF} \, L} \right]^{1/4}$$

where A_e = sphere cross section in m^2

K = Boltzmann's constant = 1.37×10^{-23} watts/deg/Hz

T = 291^o Kelvin.

For $A_e = 1\ m^2$, $R_{max} = 84$ km.

For $A_e = 25\ m^2$, $R_{max} = 188$ km.

It is seen that the basic AN/FPS-16 radar alone (Curve A of Figure 5) is not capable of accurately tracking the 1 m^2 reflecting sphere over the model balloon trajectory, Figure 1, but can perform satisfactorily with the sphere containing the corner reflector to augment the radar cross-section to 25 m^2 (Curve E of Figure 5).

2.4 Performance Improvement Calculations for Radar Modifications

There are several existing modifications to the basic AN/FPS-16 that can enhance its performance with respect to S/N. These include a 3MW transmitter, a 16-foot diameter antenna, a low-noise mixer and preamplifier, and a parametric amplifier. The range improvement factor for the same S/N (20.2 dB) is calculated below for each of these modifications.

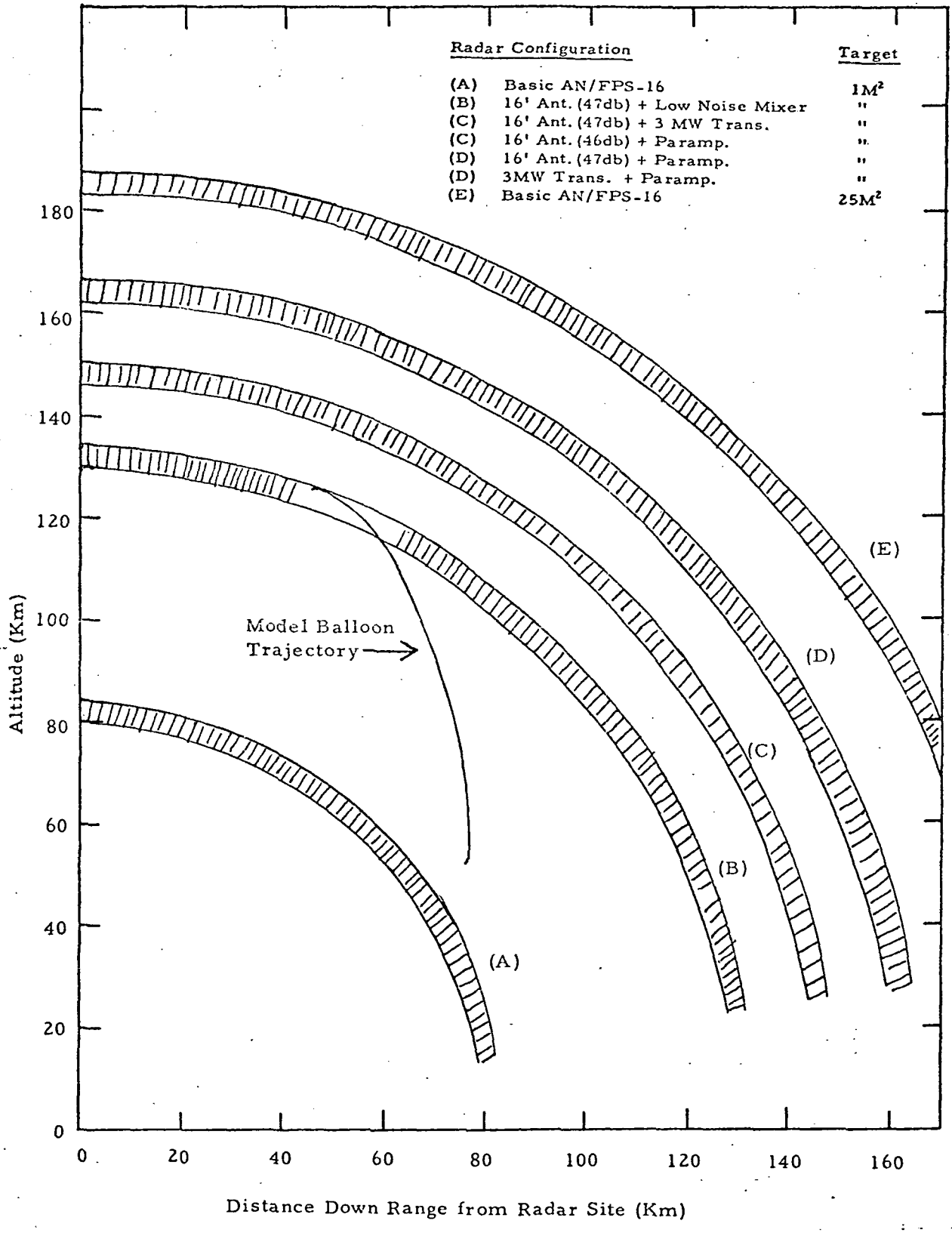

Figure 5. High Accuracy Regions of Coverage for Basic AN/FPS-16 and Combinations of Modifications when Tracking $1m^2$ and $25m^2$ Targets.

2.4.1 3MW Transmitter

Referring to the radar equation in Section 2.3, an increase in P_T from 1 MW to 3 MW yields a range improvement factor as follows

$$\frac{R(3MW)}{R(1MW)} = \left(\frac{3}{1}\right)^{1/4} = 1.32.$$

It should be noted that the higher duty cycle of 0.00167 permitted by the 3 MW transmitter offers no advantage for our purposes, since the PRF cannot be increased because of range ambiguity limitations.

2.4.2 Receiver Noise Figure Improvements

a. Low-noise Mixer and Pre-amplifier

According to the RCA catalog this mod kit reduces the system noise figure from 11 dB to 8 dB. The resulting range improvement factor is

$$\frac{R(8\ dB)}{R(11\ dB)} = (11\ dB - 8\ dB)^{1/4} = 1.19.$$

b. Parametric Amplifier

This modification improves the receiver noise figure to 4 dB* and increases the range by a factor

$$\frac{R(4\ dB)}{R(11\ dB)} = (11\ dB - 4\ dB)^{1/4} = 1.5.$$

2.4.3 Sixteen-Foot Diameter Antenna

The substitution of a 16' diameter reflector for the 12' diameter reflector of the basic AN/FPS-16 is credited with providing 46 dB

---

* See AD290-192 "Instrumentation Radar AN/FPS-16", prepared by WSMR, Aug. 1962.

or 47 dB gain, depending upon the source document. Treating both cases, the range improvement factors due to the increases in gain are

a. 47 dB Antenna Gain

$$\frac{R(47\ dB)}{R(44.5\ dB)} = (47\ dB - 44.5\ dB)^{1/2} = 1.34$$

b. 46 dB Antenna Gain

$$\frac{R(46\ dB)}{R(44.5\ dB)} = (46\ dB - 44.5\ dB)^{1/2} = 1.19$$

An additional improvement is available due to the reduction in beamwidth of the 16' antenna from 1.1^{o} to 0.8^{o}. The angular error due to thermal noise is further reduced by a factor

$$\frac{0.8^{o}}{1.1^{o}} = 0.725$$

of the value for the 12' dish.

2.4.4 Combinations of Modifications

In order for the basic AN/FPS-16 to be capable of tracking a 1 m^2 reflecting sphere over the model balloon trajectory, its maximum range capability must be augmented by a factor of at least

$$\frac{133.5\ km}{84\ km} = 1.58$$

It will be noted that none of the individual modifications described in 2.4.1 through 2.4.3 above provides sufficient improvement for the basic radar to track the 1 m^2 target. However, several combinations of the above modifications provide enough improvement to permit tracking the smaller target. These are shown in Table 3 and plotted in curves B, C, and D of Figure 5.

TABLE 3

Combination of Modifications	Combined Improvement Factor	Max. Range for 1 m^2 Target (km)
16' Ant. (47 dB) + Low Noise Mixer	1.59	134
16' Ant. (47 dB) + 3 MW Transmitter	1.77	149
16' Ant. (46 dB) + Paramp	1.78	150
3 MW Transmitter + Paramp	1.98	166
16' Ant. (47 dB) + Paramp	2.01	169

2.4.5 Digital Range Unit

A digital range unit, being completely electronic, eliminates the cyclical errors of the range resolver and some of the other problems inherent in electro-mechanical components. Although it may not provide any inherent improvement in accuracy over the analog range tracker, it requires less effort to maintain and should, therefore, be more convenient and reliable to use.

3. RECOMMENDED UTILIZATION OF RADAR-SPHERE TRAJECTORY MEASUREMENT SYSTEM

3.1 Sphere Selection

It is preferable to use the reflecting sphere rather than the sphere with a corner reflector whenever this is possible because of the following advantages:

- More uniform reflection with changes in aspect angle (less scintillation due to sphere rotation and movement).
- Mechanically simpler, easier to deploy, more reliable, and potentially less expensive.
- Less vulnerable to degradation aerodynamically and in reflection characteristics as outside pressure increases, since skin does not have to support reflector at 6 discrete points.

The corner reflector sphere (ROBIN) should, therefore, be resorted to only when inadequate S/N is available from the radar-reflecting sphere combination. As shown in Figure 5, this is true for the model balloon trajectory tracked by the Basic AN/FPS-16 alone or with only one of the radar modifications listed in 2.4 above.

However, if any of the combinations of modifications listed in Table 3 and shown in Figure 5 curves B, C, and D are available, it should be possible to track the simple 1 m^2 reflecting sphere accurately.

3.2 Console Radar Settings

It was shown in 2.3 above that the following choice of radar parameters permits accurate tracking of the model balloon trajectory at 0.1 second observation time, without degradation of accuracy due to thermal noise or dynamic lags.

Pulse Width	-	1 μsec
PRF	-	853

Servo Bandwidths - 5 Hz

Angle

Range

3.3 Radar Modifications

Combinations of the 3 MW Transmitter, 16' Antenna, Low-Noise Mixer, and Paramp Mod Kits permit the achievement of the radar range capabilities shown in Figure 5 with a 1 m^2 sphere and without thermal noise degradation of position accuracy. The 25 m^2 corner reflector sphere can provide adequate range performance with the basic radar alone, without any modifications.

As indicated in 2.4.5 above, a digital range unit should be used, if available.

3.4 Trajectory Location

It was shown in 2.3.2 that the orientation of the trajectory did not affect the angular tracking performance because at the ranges shown the angle rates are too low to introduce significant lag errors.

However, it was indicated in 2.3.3 that the position errors at the target are greater due to angle errors than range errors at the radar to target distances of Figure 1. Accordingly, it would be advantageous to locate the trajectory with respect to the radar site so that the more accurate measurement requirements are handled by the range tracker.

4.0 CONCLUSIONS

This study has identified in a general way the choices to be made by an occasional user of the AN/FPS-16 radar for Falling Sphere measurements in order to minimize errors that are within his control.

It should be emphasized that reducing such errors to negligible values in itself does not assure rated performance from the radar. The radar must be carefully maintained, calibrated and tuned in order to keep the fixed, target-dependent, instrumental errors within their advertised values. There is little that the occasional user can do to provide proper maintenance. He may, however, call for certain performance checks on the radar, or auxiliary data as part of his standard operating procedure to alert him when the radar is below par during a run. Real-time recordings of tracking error signals in 3 coordinates, for example, will enable him to correlate at a later time questionable trajectory measurements with the radar's performance at that moment.

Finally, there is the more sophisticated question of optimizing the radar parameters to obtain the data in the best form for subsequent off-line trajectory analysis. Some of the radar self-noise is not random, and hence smoothing techniques designed to improve the data in the presence of white noise may actually be counter-productive. The spectrum of the radar self-noise can depend upon the individual adjustment of the servo systems components, and hence may vary from radar to radar and from time to time. To do an effective job of matching the radar real-time smoothing, the data processing

non-real time smoothing, and the trajectory takes detailed attention to the particular radar and its components and cannot be handled satisfactorily on a generalized basis. If a particular radar should become available for detailed measurement and analysis of its servo systems, it could be made the subject of concentrated attention on the optimization of the radar-data processing interface to achieve superior performance.

TABLE 1. MODEL BALLOON TRAJECTORY

ESCAPE ALTITUDE 125000.0 DIAM 1.00 A/M 6.545

X=300.00 XDOT=215.500 Y=300.00 YDOT=215.500

TIME	RANGE	R VEL	R ACC	ELEVATION	E VEL	E ACC	AZIMUTH	A VEL	A ACC	Z.
SEC	METERS	M/S	M/S2	RADIANS	RAD/S	RAD/S2	RADIANS	RAD/S	RAD/S2	METERS
2.	133033.6	66.73	-8.20	1.221060	-0.2200E-02	-0.2083E-04	0.785399	0.1030E-05	0.5227E-06	124981.19
4.	133190.7	50.36	-8.16	1.216639	-0.2242E-02	-0.2160E-04	0.785402	0.2090E-05	0.5374E-06	124924.81
6.	133315.1	54.07	-8.12	1.212111	-0.2286E-02	-0.2240E-04	0.785407	0.3179E-05	0.5511E-06	124830.88
8.	133407.0	37.87	-8.08	1.207494	-0.2332E-02	-0.2322E-04	0.785415	0.4294E-05	0.5637E-06	124699.38
10.	133466.6	21.76	-8.03	1.202794	-0.2379E-02	-0.2407E-04	0.785424	0.5433E-05	0.5754E-06	124530.31
12.	133494.1	5.75	-7.98	1.197977	-0.2428E-02	-0.2495E-04	0.785436	0.6596E-05	0.5860E-06	124323.69
14.	133489.6	-10.17	-7.93	1.193070	-0.2479E-02	-0.2587E-04	0.785451	0.7777E-05	0.5955E-06	124079.44
16.	133453.4	-25.99	-7.88	1.188060	-0.2531E-02	-0.2681E-04	0.785468	0.8976E-05	0.6038E-06	123797.63
18.	133385.6	-41.70	-7.83	1.182943	-0.2586E-02	-0.2779E-04	0.785487	0.1019E-04	0.6111E-06	123478.25
20.	133286.6	-57.30	-7.77	1.177714	-0.2643E-02	-0.2881E-04	0.785508	0.1142E-04	0.6174E-06	123121.31
22.	133156.5	-72.78	-7.71	1.172371	-0.2701E-02	-0.2986E-04	0.785533	0.1266E-04	0.6233E-06	122726.81
24.	132995.5	-88.14	-7.65	1.166907	-0.2762E-02	-0.3095E-04	0.785559	0.1391E-04	0.6289E-06	122294.75
26.	132804.0	-103.36	-7.58	1.161321	-0.2825E-02	-0.3206E-04	0.785588	0.1518E-04	0.6349E-06	121825.13
28.	132582.1	-118.46	-7.51	1.155605	-0.2890E-02	-0.3326E-04	0.785620	0.1646E-04	0.6448E-06	121317.94
30.	132330.2	-133.41	-7.44	1.149757	-0.2958E-02	-0.3447E-04	0.785654	0.1776E-04	0.6562E-06	120773.19
32.	132048.5	-148.21	-7.36	1.143771	-0.3026E-02	-0.3572E-04	0.785691	0.1909E-04	0.6735E-06	120190.88
34.	131737.4	-162.85	-7.28	1.137642	-0.3101E-02	-0.3701E-04	0.785730	0.2045E-04	0.6966E-06	119571.06
36.	131397.2	-177.32	-7.20	1.131365	-0.3176E-02	-0.3836E-04	0.785772	0.2187E-04	0.7240E-06	118913.69
38.	131028.2	-191.63	-7.11	1.124934	-0.3255E-02	-0.3974E-04	0.785818	0.2335E-04	0.7518E-06	118218.81
40.	130630.8	-205.74	-7.01	1.118344	-0.3335E-02	-0.4118E-04	0.785866	0.2486E-04	0.7713E-06	117486.50
42.	130205.3	-219.66	-6.91	1.111589	-0.3419E-02	-0.4269E-04	0.785917	0.2642E-04	0.7733E-06	116716.69
44.	129752.2	-233.38	-6.80	1.104665	-0.3506E-02	-0.4426E-04	0.785972	0.2795E-04	0.7496E-06	115909.50
46.	129271.9	-246.87	-6.69	1.097563	-0.3596E-02	-0.4589E-04	0.786029	0.2940E-04	0.6974E-06	115064.88
48.	128764.5	-260.13	-6.57	1.090277	-0.3690E-02	-0.4758E-04	0.786089	0.3073E-04	0.6221E-06	114182.94
50.	128231.5	-273.13	-6.44	1.082801	-0.3787E-02	-0.4933E-04	0.786152	0.3189E-04	0.5425E-06	113263.69
52.	127672.4	-285.87	-6.30	1.075126	-0.3887E-02	-0.5113E-04	0.786217	0.3291E-04	0.4862E-06	112307.25

56.	126479.3	-310.48	-6.00	1.059140-0.4099E-02-0.5466E-04	0.786352	0.3491E-04	0.5670E-06	110283.00
58.	125846.4	-322.31	-5.83	1.050852-0.4210E-02-0.5642E-04	0.786423	0.3620E-04	0.7314E-06	109215.50
60.	125190.3	-333.71	-5.60	1.042319-0.4323E-02-0.5726E-04	0.786497	0.3789E-04	0.9694E-06	108111.44
62.	124511.8	-344.70	-5.39	1.033557-0.4439E-02-0.5801E-04	0.786575	0.4001E-04	0.1126E-05	106971.31
64.	123811.8	-355.25	-5.15	1.024560-0.4559E-02-0.6041E-04	0.786657	0.4223E-04	0.1043E-05	105795.50
66.	123091.2	-365.29	-4.89	1.015322-0.4681E-02-0.6205E-04	0.786744	0.4400E-04	0.6867E-06	104584.50
68.	122350.9	-374.77	-4.58	1.005835-0.4806E-02-0.6352E-04	0.786833	0.4492E-04	0.2181E-06	103338.81
70.	121592.4	-383.52	-4.26	0.996095-0.4935E-02-0.6471E-04	0.786923	0.4504E-04-0.6779E-08		102059.19
72.	120816.9	-391.77	-3.92	0.986095-0.5065E-02-0.6530E-04	0.787013	0.4530E-04	0.3999E-06	100746.44
74.	120025.7	-399.25	-3.65	0.975834-0.5195E-02-0.6494E-04	0.787105	0.4712E-04	0.1518E-05	99401.69
76.	119220.3	-406.96	-3.14	0.965314-0.5324E-02-0.6372E-04	0.787204	0.5154E-04	0.2877E-05	98026.31
78.	118402.4	-414.76	-2.64	0.954540-0.5450E-02-0.6186E-04	0.787313	0.5811E-04	0.3473E-05	96622.06
80.	117574.0	-419.40	-1.97	0.943518-0.5571E-02-0.5905E-04	0.787435	0.6434E-04	0.2424E-05	95191.25
82.	116737.8	-419.54	-1.15	0.932261-0.5685E-02-0.5520E-04	0.787567	0.6673E-04-0.2002E-06		93736.88
84.	115897.0	-420.92	-0.19	0.920784-0.5790E-02-0.4851E-04	0.787699	0.6364E-04-0.2668E-05		92262.81
86.	115055.4	-420.30	0.80	0.909113-0.5876E-02-0.3892E-04	0.787820	0.5783E-04-0.2522E-05		90774.06
88.	114217.1	-417.74	1.76	0.897294-0.5934E-02-0.1962E-04	0.787933	0.5599E-04	0.1151E-05	89277.13
90.	113385.7	-414.25	2.73	0.885384-0.5952E-02 0.1292E-05		0.788050	0.6268E-04	0.5360E-05	87779.94
92.	112565.4	-408.58	4.00	0.873517-0.5927E-02 0.2366E-04		0.788187	0.7404E-04	0.4515E-05	86291.81
94.	111751.3	-397.02	5.62	0.861724-0.5859E-02 0.4431E-04		0.788340	0.7551E-04-0.4253E-05		84823.06
96.	110979.7	-383.70	7.52	0.850109-0.5749E-02 0.6580E-04		0.788474	0.5441E-04-0.1678E-04		83384.88
98.	110228.1	-367.07	9.22	0.838758-0.5593E-02 0.9159E-04		0.788543	0.1203E-04-0.2390E-04		81989.25
100.	109513.3	-347.45	10.31	0.827776-0.5379E-02 0.1236E-03		0.788520-0.3293E-04-0.1878E-04			80648.75
102.	108839.3	-326.34	10.70	0.817249-0.5097E-02 0.1579E-03		0.788426-0.5587E-04-0.2901E-05			79375.81
104.	108207.9	-305.15	10.45	0.807428-0.4755E-02 0.1821E-03		0.788320-0.4387E-04 0.1415E-04			79181.44
106.	107618.3	-284.51	10.14	0.798291-0.4378E-02 0.1916E-03		0.788269-0.5578E-05 0.2203E-04			77072.38
108.	107069.4	-264.30	10.06	0.789915-0.4000E-02 0.1844E-03		0.788300 0.3604E-04 0.1764E-04			76050.75
110.	106560.8	-244.32	9.49	0.782272-0.3649E-02 0.1654E-03		0.788400 0.5970E-04 0.5277E-05			75114.00
112.	106092.2	-224.34	9.94	0.775290-0.3340E-02 0.1436E-03		0.788521 0.5655E-04-0.8308E-05			74256.44
114.	105663.3	-204.72	9.58	0.768885-0.3073E-02 0.1219E-03		0.788610 0.2931E-04-0.1809E-04			73471.25
116.	105272.4	-186.44	8.60	0.762967-0.2852E-02 0.9969E-04		0.788629-0.1124E-04-0.2139E-04			72750.50
118.	104915.9	-170.40	7.33	0.757451-0.2670E-02 0.8124E-04		0.788565-0.5253E-04-0.1894E-04			72094.81

122.	104265.4	-145.94	4.09	0.747340-0.2405E-02	0.4994E-04	0.788236-0.1017E-03-0.4193E-05	70881.75
124.	103998.8	-142.25	2.56	0.742623-0.2316E-02	0.3855E-04	0.788030-0.1021E-03 0.3774E-05	70325.31
126.	103722.7	-139.12	1.57	0.738063-0.2246E-02	0.3207E-04	0.787836-0.8728E-04 0.1091E-04	69790.44
128.	103453.3	-136.43	1.12	0.733635-0.2181E-02	0.3310E-04	0.787690-0.5856E-04 0.1766E-04	69269.63
130.	103168.4	-131.60	0.73	0.729339-0.2114E-02	0.3387E-04	0.787612-0.1744E-04 0.2321E-04	68762.38
132.	102926.3	-130.47	0.43	0.725179-0.2046E-02	0.3414E-04	0.787627 0.3304E-04 0.2703E-04	68267.88
134.	102666.1	-129.83	0.23	0.721154-0.1979E-02	0.3333E-04	0.787748 0.8914E-04 0.2870E-04	67785.50
136.	102406.8	-129.50	0.11	0.717262-0.1914E-02	0.3109E-04	0.787984 0.1463E-03 0.2810E-04	67314.44
138.	102147.9	-129.33	0.07	0.713494-0.1855E-02	0.2742E-04	0.788331 0.2001E-03 0.2536E-04	66853.75
140.	101859.4	-129.16	0.12	0.709836-0.1805E-02	0.2303E-04	0.788780 0.2467E-03 0.2097E-04	66402.25
142.	101631.4	-128.72	0.33	0.706270-0.1762E-02	0.1953E-04	0.789312 0.2835E-03 0.1557E-04	65958.88
144.	101374.8	-127.79	0.60	0.702783-0.1726E-02	0.1592E-04	0.789906 0.3065E-03 0.9303E-05	65523.00
146.	101120.6	-126.25	0.95	0.699360-0.1698E-02	0.1286E-04	0.790537 0.3205E-03 0.2643E-05	65094.23
148.	100870.3	-123.97	1.33	0.695989-0.1675E-02	0.1022E-04	0.791179 0.3190E-03-0.4162E-05	64672.45
150.	100625.3	-120.93	1.71	0.692656-0.1656E-02	0.8110E-05	0.791804 0.3041E-03-0.1066E-04	64257.82
152.	100387.1	-117.16	2.05	0.689360-0.1642E-02	0.6483E-05	0.792387 0.2770E-03-0.1641E-04	63850.59
154.	100157.1	-112.79	2.31	0.686069-0.1636E-02	0.5300E-05	0.792905 0.2393E-03-0.2106E-04	63451.05
156.	99936.2	-108.00	2.45	0.682838-0.1621E-02	0.4484E-05	0.793339 0.1937E-03-0.2429E-04	63059.46
158.	99725.1	-103.06	2.46	0.679606-0.1612E-02	0.4007E-05	0.793676 0.1433E-03-0.2582E-04	62675.86
160.	99523.8	-98.23	2.35	0.676389-0.1604E-02	0.3933E-05	0.793911 0.9140E-04-0.2571E-04	62300.07
162.	99332.0	-93.72	2.14	0.673188-0.1596E-02	0.4320E-05	0.794043 0.4143E-04-0.2408E-04	61931.71
164.	99148.6	-89.73	1.84	0.670006-0.1587E-02	0.5178E-05	0.794080-0.4063E-05-0.2119E-04	61570.34
166.	98972.6	-86.37	1.51	0.666844-0.1575E-02	0.6596E-05	0.794032-0.4278E-04-0.1736E-04	61215.45
168.	98802.6	-83.71	1.15	0.663708-0.1560E-02	0.8706E-05	0.793915-0.7309E-04-0.1287E-04	60866.59
170.	98637.3	-81.75	0.81	0.660607-0.1540E-02	0.1132E-04	0.793746-0.9401E-04-0.7964E-05	60523.53
172.	98475.2	-80.46	0.46	0.657552-0.1514E-02	0.1418E-04	0.793545-0.1049E-03-0.2881E-05	60186.21
174.	98314.9	-79.91	0.12	0.654554-0.1483E-02	0.1707E-04	0.793333-0.1056E-03 0.2127E-05	59854.65
176.	98155.1	-79.98	-0.19	0.651623-0.1446E-02	0.1991E-04	0.793129-0.9662E-04 0.6858E-05	59528.93
178.	97994.6	-80.65	-0.47	0.648772-0.1404E-02	0.2244E-04	0.792953-0.7864E-04 0.1105E-04	59209.20
180.	97832.2	-81.85	-0.72	0.646011-0.1357E-02	0.2431E-04	0.792820-0.5302E-04 0.1447E-04	58895.56
182.	97666.9	-83.49	-0.92	0.643346-0.1307E-02	0.2547E-04	0.792745-0.2138E-04 0.1701E-04	58588.06
184.	97497.9	-85.43	-1.06	0.640784-0.1256E-02	0.2576E-04	0.792737 0.1434E-04 0.1853E-04	58285.41

188.	97147.1	-90.06	-1.18	0.635966-0.1154E-02	0.2441E-04	0.792945	0.8976E-04	0.1050E-04	57709.96
190.	96954.6	-92.40	-1.15	0.633705-0.1107E-02	0.2274E-04	0.793161	0.1255E-03	0.1705E-04	57416.09
192.	96777.6	-94.62	-1.06	0.631536-0.1063E-02	0.2083E-04	0.793445	0.1575E-03	0.1482E-04	57135.99
194.	96586.3	-96.61	-0.92	0.629449-0.1024E-02	0.1859E-04	0.793788	0.1844E-03	0.1193E-04	56860.28
196.	96391.3	-98.26	-0.73	0.627437-0.9890E-03	0.1623E-04	0.794178	0.2049E-03	0.8487E-05	56588.64
198.	96193.5	-99.49	-0.50	0.625490-0.9588E-03	0.1390E-04	0.794602	0.2181E-03	0.4647E-05	56320.77
200.	95993.6	-100.24	-0.24	0.623599-0.9383E-03	0.1158E-04	0.795045	0.2234E-03	0.5111E-06	56056.50
202.	95792.9	-100.43	0.05	0.621754-0.9123E-03	0.9455E-05	0.795490	0.2202E-03	-0.3788E-05	55795.70
204.	95592.3	-100.03	0.36	0.619947-0.8853E-03	0.7482E-05	0.795920	0.2082E-03	-0.8169E-05	55534.38
206.	95393.2	-99.01	0.67	0.618170-0.8822E-03	0.5661E-05	0.796317	0.1877E-03	-0.1243E-04	55284.63
208.	95196.7	-97.37	0.96	0.616416-0.8727E-03	0.3876E-05	0.796645	0.1586E-03	-0.1655E-04	55034.58
210.	95004.1	-95.17	1.23	0.614677-0.8666E-03	0.2257E-05	0.796946	0.1210E-03	-0.2023E-04	54788.35
212.	94816.4	-92.46	1.47	0.612947-0.8636E-03	0.6929E-06	0.797147	0.7801E-04	-0.2347E-04	54546.03
214.	94634.5	-89.31	1.67	0.611220-0.8636E-03	-0.6812E-06	0.797255	0.2826E-04	-0.2617E-04	54307.68
216.	94459.4	-85.81	1.82	0.609491-0.8663E-03	-0.1961E-05	0.797257	-0.2612E-04	-0.2814E-04	54073.28
218.	94291.5	-82.05	1.93	0.607753-0.8713E-03	-0.3017E-05	0.797148	-0.8382E-04	-0.2946E-04	53842.77
220.	94131.3	-78.14	1.97	0.606004-0.8783E-03	-0.3927E-05	0.796921	-0.1434E-03	-0.2997E-04	53616.03
222.	93978.9	-74.14	1.96	0.604239-0.8860E-03	-0.4559E-05	0.796574	-0.2033E-03	-0.2936E-04	53392.85
224.	93834.5	-70.25	1.94	0.602456-0.8934E-03	-0.4973E-05	0.796108	-0.2624E-03	-0.2908E-04	53173.03
226.	93697.6	-66.43	1.87	0.600654-0.9005E-03	-0.5133E-05	0.795526	-0.3192E-03	-0.2770E-04	52956.32
228.	93566.6	-62.79	1.77	0.598831-0.9167E-03	-0.5029E-05	0.794833	-0.3728E-03	-0.2579E-04	52742.48
230.	93446.5	-59.38	1.63	0.596987-0.9265E-03	-0.4718E-05	0.794037	-0.4222E-03	-0.2343E-04	52531.27
232.	93330.9	-56.25	1.49	0.595125-0.9353E-03	-0.4092E-05	0.793148	-0.4664E-03	-0.2074E-04	52322.49
234.	93221.3	-53.44	1.32	0.593247-0.9426E-03	-0.3282E-05	0.792175	-0.5050E-03	-0.1774E-04	52115.95
236.	93116.9	-50.96	1.15	0.591356-0.9482E-03	-0.2195E-05	0.791132	-0.5373E-03	-0.1454E-04	51911.51
238.	93017.3	-48.82	0.98	0.589456-0.9513E-03	-0.9194E-06	0.790030	-0.5631E-03	-0.1116E-04	51709.11
240.	92921.4	-47.05	0.79	0.587552-0.9516E-03	0.4452E-06	0.788885	-0.5820E-03	-0.7671E-05	51508.72
242.	92828.3	-45.66	0.60	0.585651-0.9494E-03	0.1961E-05	0.787707	-0.5938E-03	-0.4149E-05	51310.34
244.	92738.6	-44.64	0.41	0.583757-0.9439E-03	0.3514E-05	0.786514	-0.5986E-03	-0.5865E-06	51114.01
246.	92649.9	-44.00	0.23	0.581877-0.9354E-03	0.5085E-05	0.785318	-0.5963E-03	0.2885E-05	50919.78
248.	92562.3	-43.73	0.04	0.580018-0.9237E-03	0.6591E-05	0.784133	-0.5873E-03	0.6223E-05	50727.71
250.	92474.8	-43.82	-0.14	0.578184-0.9091E-03	0.7897E-05	0.782972	-0.5714E-03	0.9416E-05	

252. 92386.0 -44.27 -0.31 0.576363-0.8010E-03 0.9346E-05 0.781851-0.5496E-03 0.1237E-04 50350.29

254. 92297.5 -45.04 -0.46 0.574618-0.8720E-03 0.1046E-04 0.780778-0.5224E-03 0.1503E-04 50169.05

NORMAL END OF JOB